Esterase 2-oligodeoxynucleotide conjugates as enzyme reporter for electrochemical detection of DNA and identification of bacterial species

A Thesis Submitted for the Degree of

Doktor der Naturwissenschaften

-Dr. Rer. Nat.-

der Fakultät für Biologie, Chemie und Geowissenschaften der

Universität Bayreuth

by

Yiran Wang

From

Zhejiang

P. R. China

Bayreuth, 2006

Die vorliegende Arbeit wurde in der Zeit von August 2003 bis November 2006 am Lehrstuhl für Biochemie der Universität Bayreuth unter der Leitung von Herrn Prof. Dr. Mathias Sprinzl angefertigt.

Vollständiger Abdruck der von der Fakultät Biologie, Chemie und Geowissenschaften der Universität Bayreuth genehmigten Dissertation zu Erlangung des Grades eines Doktors der Naturwissenschaften

- Dr. rer. nat.-

Promotionsgesuch eingericht am: 29. November 2006
Tag des Promotionskolloquiums: 8. Februar 2007

Erster Gutachter: Prof. Dr. Mathias Sprinzl
Zweiter Gutachter: Prof. Dr. Gerhard Krauss

Table of Contents

Abbreviations

APS	ammonium persulfate
BSA	bovine serum albumin
CFU	colony-forming unit
CTAB	cetyltrimethylammonium bromide
ddH$_2$O	double distilled H$_2$O
DNA	deoxyribonucleic acid
DTT	dithiolthretiol
E-Chip	Electrical Chip system
EDTA	ethylenediaminetetraacetic acid
efts	elongation factor Ts
g	gram or Earth's gravity (g=9.81 m*s^{-2})
HPLC	high-pressure liquid chromatography
IPTG	isopropyl thio-β-galactoside
kDa	kilo daltons
Ki	inhibition constant
L	liter (dm^3)
LB	Luria-Bertani medium
M	molar concentration (mol/dm^3)
μ	micro
MALDI-TOF MS	matrix assisted laser desorption ionization time-of-flight mass spectrometry
MB	molecular beacon
MBTFP	3-(4-mercaptobutylthio)- 1,1,1-trifluoro-2-propanone
mM	millimolar concentration (mmol/dm^3)
nA	nano Amper
NMR	nuclear magnetic resonance
ODN	oligodeoxynucleotide
PAGE	polyacrylamide gel electrophoresis
pAP	p-aminophenol
pAPB	p-aminophenylbutyrate
pK	negative logarithm of the dissociation constant K (-logK)
pKa	negative logarithm of the acid dissociation constant K (-logKa)
pNP	p-nitrophenol
pNPB	p-nitrophenylbutyrate
RNA	ribonucleic acid
rpm	revolutions per minute
rRNA	ribosomal RNA
S 100	supernatant after ultracentrifugation at 100 Svedberg unit
SA	streptavidin
SDS	sodium dodecyl sulfate
SSPE	saline-sodium phosphate-EDTA
sulfo-SMCC	sulfosuccinimidyl 4-(*N*maleimidomethyl)cyclohexane-1-carboxylate
TBE	Tris-borate-EDTA
TCEP	tris (2-carboxyethyl) phosphine hydrochloride
TEMED	N,*N*,*N′*,*N′*-Tetramethylethylene diamine
TFK	trifluoromethyl ketone

Tris	tris-(hydroxymethyl)-aminoethane
U	units
UV	ultra violet
v/v	volume per volume
v/w	volume per weight
X-Gal	5-bromo-4-chloro-3-indolyl-β-D-galactoside

1. Introduction

The progress of human genomic sequencing unravels genotype related diseases (Hudson, 2006). This brings a perspective for an individual therapy based on the DNA analysis. The emerged "lab-on-chip" enables a fast, robotic and cost-effective way to fulfill the so-called "point-of-care" tasks. Point-of-care diagnostic testing, or testing performed at the patient bedside, allows physicians to diagnose patients more rapidly than traditional laboratory-based testing. The capacity of current microarray technology allows processing massive data accumulation based on large numbers of genes or sequences sampled, i.e. gene transcriptional profiling, single-nucleotide polymorphism discovery, or portions of the genome resequencing (Abdullah-Sayani et al., 2006). However, clinical diagnostics do not require massive data accumulation simultaneously, but reliability, reproducibility and automated analysis (Drummond et al., 2003; Abdullah-Sayani et al., 2006). To practically realize this purpose, different disciplines, including molecular biology, electrical engineering, material science, physics and chemistry, are needed to work together to reach the aim of nucleic acids diagnostics on electrical chips, which possess characters of accurate, fast, robotic and inexpensive for patient dianostics (Drummond et al., 2003; Nebling et al., 2004).

1.1 Electrochemical detection of nucleic acids

1.1.1 Introduction of electrochemical nucleic acid biosensor

In the 1990's progress in genomics and particularly in the Human Genome Project greatly stimulated interest in new methods capable of unraveling the genetic information stored in the nucleotide sequence of DNA. Wide-scale genetic testing requires the development of easy-to-use, fast, inexpensive, miniaturized analytical devices. Traditional methods for detecting DNA hybridization, such as gel electrophoresis or membrane blots, are too slow, discontinuous and labor intensive. This increases the demand for exploitation of a new method.

The development of microfabricated devices built on silicon, glass, or plastic supports is a modern trend in biological techniques area in the last two decades, resulting in many start-up companies serving the pharmaceutical, biotechnology, and diagnostics markets. However, the idea of implementing such devices on microelectronic substrates has been introduced only

recently (Tartagni et al., 2004). Electrochemical biosensors are small devices linking specific biochemical recognition properties for a selective analysis to report the diagnosis result by means of electrical signal. And the analysis of complex DNA samples and acquisition of sequence and expression information would require the integration of multiple biosensors into arrays or chip form for parallel analysis (Service, 1998; Wang, 2000). Therefore, development of DNA sensors and the construction of a fully electronic DNA chip with electrochemical detection method has become a booming field. It is a great effort in biology, chemistry, and engineering to utilize the advantages of miniaturization for cheaper, better, and faster sample analysis. A number of terms, like electrical chip, electrochemical chip, electrochemical DNA array, electrical arrays, microelectronic chips, electrical biochips and electrical microarray are often being intermixed to describe this kind of parallel analysis device.

In brief, the common principle of such devices is the coupling of a biological recognition element with a physical transducer (Fig. 1.1). Transducing elements include optical (Piunno et al., 1995), electrochemical (Palecek et al., 2002), and microgravimetric (Zhou et al., 2001) devices, but electrochemical transducers have received considerable more attention because of its simpler, faster, and cheaper characters (Paeschke et al., 1996; Palecek et al., 2002; Gooding, 2002; Drummond et al., 2003). The first electrochemical DNA biosensor based on hybridization was developed in 1993 (Millan and Mikkelsen, 1993). Since then, the progress of semiconductor technology enables the construction of fully electrical chip, with high integration at acceptable product costs. The advantage of a fully electrical chip is the intrinsic high spatial resolution allowing highly parallel reaction and compact construction without the common expensive optical components (Drummond et al., 2003; Hintsche et al., 2005).
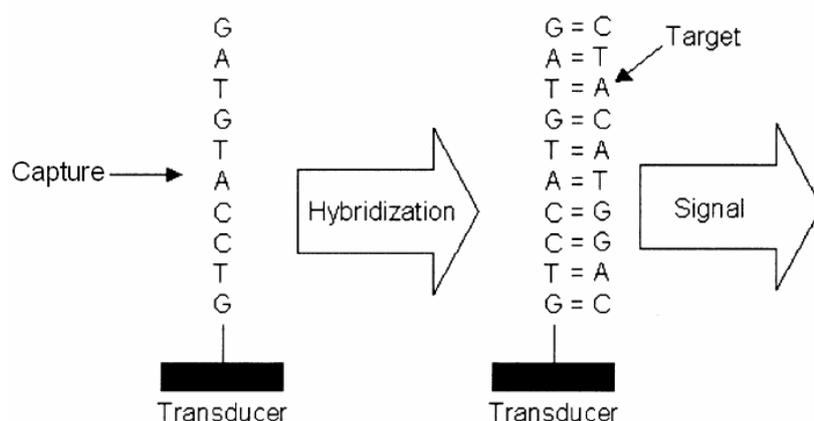
Fig. 1.1. Steps involved in the detection of a specific DNA sequence using an electrochemical DNA hybridization biosensor. Adapted from (Gooding, 2002).

1.1.2 Electrochemical biosensing of DNA hybridization

The three essential steps of functionalization of any biosensor system are capture immobilization, analyte recognition, and signal transduction and readout (Fig. 1.1) (Gooding, 2002). Electrochemical DNA hybridization biosensors commonly rely on the immobilization of ssDNA capture onto a transducer surface to recognize its complementary target sequence by hybridization. The binding of target strand to the surface-confined capture results in an electrical signal.

The term, E-Chip refers an Electrical Chip system that combines a low to middle density microelectrode arrays in silicon-technology with novel electrochemical detection. The latest system is based on an electrical chip with common electrodes (in this study) or interdigitated array (IDA) gold electrodes and a unique multiplexing 8-channel potentiostat (Paeschke et al., 1996; Hintsche et al., 2000) for direct data readout from the chip. The principle of the electrochemical biosensor is shown in Fig. 1.2. After ssDNA captures have been immobilized on sensors surface, an analyte containing target molecules is applied to each electrode position and hybridization occurs between matching DNA strands. After a washing step, an electrochemical substrate (e.g., p-aminophenylbutyrate in this study) is introduced and electrochemically redox-active compounds (in this example p-aminophenol) are produced by the enzyme (e.g., esterase in this study) bound to the target DNA strands. Applying an oxidation and a reduction potential by the order of ±100–200 mV to E1 and E2 simultaneously (Fig. 1.2c), induces a current flow between both electrodes. As schematically shown in Fig. 1.2d, an offset current is attributing to the sensor background current, substrate background and specific enzymatic hydrolysis current (Tartagni et al., 2004). Therefore, the signal to be preferably analyzed is not the current as such but its slope value, the derivative dI/dt (Nebling et al., 2004).

1.1.2.1 Sensor structure of fully integrated electrical DNA chip

The main sensing element of a fully integrated DNA chip is the electrode array. The microelectrode fingers of one of such sensor elements are illustrated in Fig. 1.2a. Chip surface is extended with additional process steps to provide sensor electrodes made of gold (Paeschke et al., 1995). The active sensor area consists of interdigitated gold electrodes (E1, E2) and a

circular compartment. Each sensor with 1 mm diameter consists of about 2 x 210 rows of 1-µm-wide gold electrodes separated by 1-µm-wide gaps. Single-stranded capture molecules are spotted and immobilized on the gold interface (Fig. 1.2b).
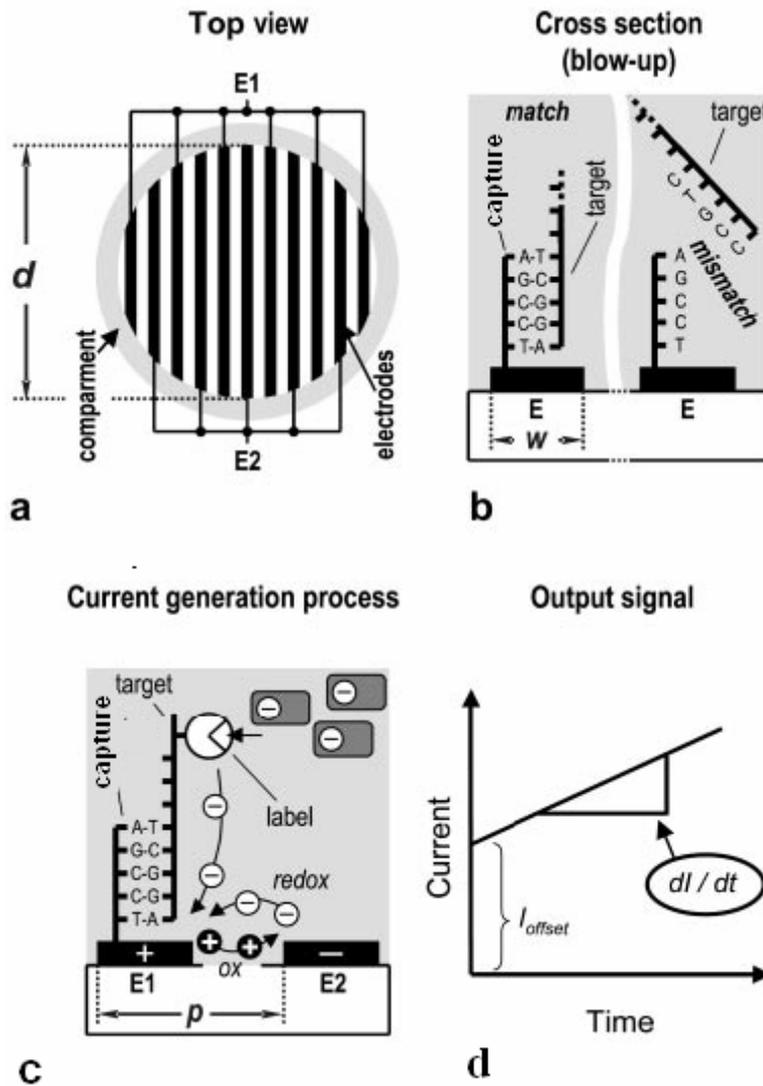
Fig. 1.2. Principle of the electrochemical biosensor. (**a**) Sensor elements with interdigitated gold electrodes. (**b**) Single-stranded captures molecules immobilized on the surface of the gold electrodes. The gray background represents the definition. Left/right: hybridization/no hybridization in case of matching/mismatching DNA strands. (**c**) Redox system and generation of electrode currents. (**d**) Schematic plot of a sensor current. Adapted from (Tartagni et al., 2004).

1.1.2.2 Capture immobilization

The most commonly capture ODN immobilization schemes includes attachment of biotin-functionalized capture ODNs to avidin-coated surfaces (Ebersole et al., 1990), self-assembling

of thiol functionalized captures onto gold transducers (Levicky et al., 1998), carbodiimide covalent binding to an activated surface (Millan et al., 1994), use of conducting polymers (Livache et al., 2003), as well as adsorptive accumulation onto carbo-paste or thick-film carbon electrodes (Wang et al., 1996). The thiol-gold self-assembling method has been particularly attractive for fabricating reproducible capture-modified surfaces with consistent hybridization efficiency (Levicky et al., 1998). Here, the capture ODN is commonly immobilized on gold by forming mixed monolayers of thiol-derivarized ODN and 6-mercapto-1-hexanol. The thiolated capture is "put upright" as a result of such co-assembly with a short-chain alkylthiol monolayer. The latter, along with a hydrophilic linker (between the thiol group and ODN), is often used for minimizing non-specific adsorption effects (Wang, 2005). However, the introduction of thiol functionalized monolayer on electrode surface was reported to have reduced the sensitivity of chip detection (Nebling et al., 2004).

1.1.2.3 DNA amplification

In the past decade, significant DNA biomarkers of therapeutic and prognostic value have been identified (Abdullah-Sayani et al., 2006). PCR DNA amplification is the main approach to prepare the biomarker DNA analyte and thus is especially important for diagnosis based on "lab-on-chip" conception.

Motorola Labs (Liu et al., 2004), the Fraunhofer institute, Siemens AG and Infineon AG (Hintsche et al., 2004) have separately constructed a fully integrated biochip embedding a microliter PCR amplification chamber. Sample preparation (including magnetic bead-based cell capture, purification and cell lysis), PCR amplification, DNA hybridization, and electrochemical detection were performed in this fully automated and miniature device. As shown in Fig. 1.3, the device is completely self-contained: no external pressure sources, fluid storage, mechanical pumps, or valves are necessary for fluid manipulation, thus eliminating possible sample contamination and simplifying device operation (Liu et al., 2004). Pathogenic bacteria detection and single-nucleotide polymorphism analysis directly from blood samples were successfully demonstrated in this microfluidic device equipped with an electrochemical electrode microarray.

In order to do faster tests, the technology of continuous flow PCR integrated on chip has been successfully developed, which enables performing PCR amplification within 2-10 min (Kopp

et al., 1998; Tillib et al., 2001; Giordano et al., 2001; Kricka and Wilding, 2003; Tartagni et al., 2004). The continuous flow PCR is realized by a time-space conversion in the PCR system- that is, by keeping temperatures constant over time at different locations in the chip and moving the sample through the individual temperature zones (Fig. 1.4). ST Microelectronics (Geneva, Switzerland) and the CEA (Grenoble, France) chose this option and developed a fully integrated silicon chip for PCR amplification coupled to analysis by hybridization on DNA captures grafted on the same silicon chip.
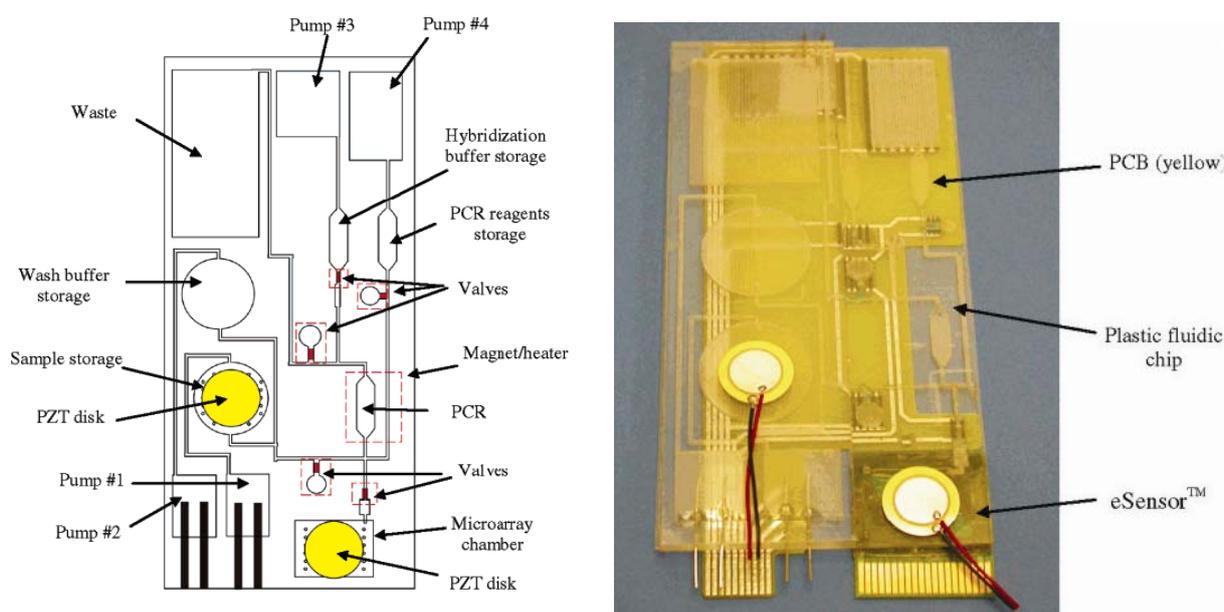
Fig. 1.3. Scheme (Left) and photograph (right) of the plastic fluidic chip integrated device. (Left) Pumps 1-3 are electrochemical pumps, and pump 4 is a thermopneumatic pump. (Right) The integrated device consists of a plastic fluidic chip, a printed circuit board (PCB), and a Motorola eSensor microarray chip. Taken from (Liu et al., 2004).
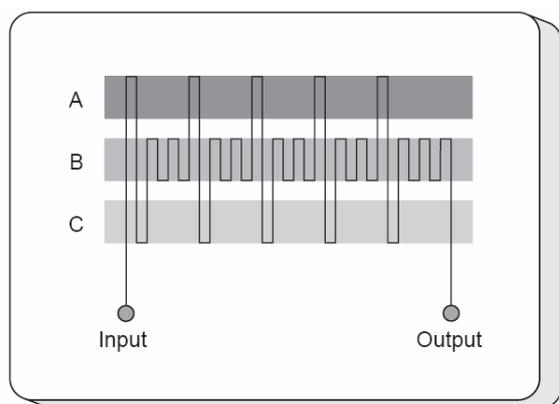
Fig. 1.4. Scheme of a chip based flow through PCR. Three well-defined zones are kept at 95 ℃, 77 ℃, and 60 ℃ by means of thermostated copper blocks. The sample is hydrostatically pumped through a single channel etched into the glass chip. The channel passing through the three temperature zones defines the thermal cycling process. Taken from (Kopp et al., 1998).

A 95 ℃ - melting
B 77 ℃ - extension
C 60 ℃ - annealing

Compared with the chamber-type DNA amplification, the attractive feature of the continuous flow microchip is that the thermal cycling process can be conducted at relatively high speeds, since it is not necessary to heat and cool the large thermal masses associated with the amplification chamber. An amplification of 500-bp DNA fragment was achieved within 2 min using the continuous flow model (Hashimoto et al., 2004).

1.1.2.4 The hybridization event

DNA hybridization relies on the selectivity of Watson-Crick base pairing. By means of hybridization, the target DNA binds specifically to the corresponding capture sequence site of biosensors (Fig. 1.5) and forms stable hybrid between strands. This transducer-solution interface hybridization event is affected by the salt concentration, temperature, capture density, secondary structure and length of target sequence, contacting time and the presence of accelerating agents (e.g. CTAB) (Levicky and Horgan, 2005; Wang, 2005). Further description about the solid-phase hybridization refers to Introduction 1.3.
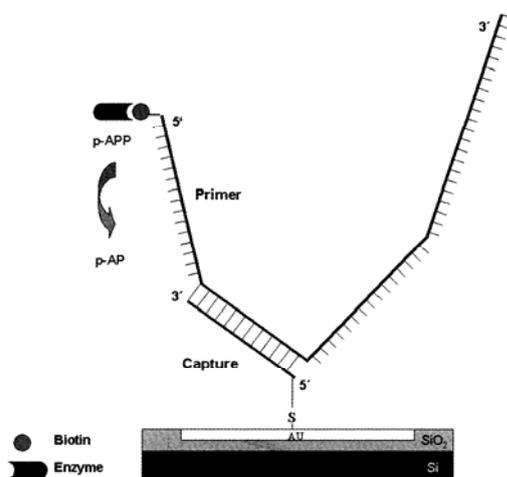
Fig. 1.5. Scheme of PCR product based detection. The biotin label is introduced through the PCR primer of the target strand. Usually the primer sequences in the hybridization scheme are designed in a way that the biotin labeling and also the enzyme conjugate are positioned in close proximity to the surface. p-APP, p-aminophenylphosphate; p-AP, p-aminophenol. Adapted from (Hintsche et al., 2005).

1.1.2.5 Electrochemical transduction of DNA hybridization

For electrochemistry-based sensors, the hybridization event is usually detected via change of current or conductivity signals based on the direct or catalyzed oxidation of nucleobases, DNA duplex mediated charge transport, as well as conductivity change and enzyme labeling.

1.1.2.5.1 Direct oxidization of nucleobases

The electroactivity of DNA was first demonstrated 40 years ago by polarographic study (Palecek, 1960). Although this method is quite simple and sensitive, its application is confined by significant background currents at the relatively high potentials required for electrochemical DNA oxidation. A two-step strategy was used to improve the signal-to-noise ration. Target DNA was hybridized with magnetic beads pre-immobilized capture ODN and then magnetically separated from the analyte pool. Afterwards, the magnetic beads enriched DNA was depurined in acid solution and the produced free guanine and adenine nucleosides are analyzed (Palecek et al., 2002). A minimal amount of 40 fmol analyte can be detected by this method.

1.1.2.5.2 Indirect oxidization of nucleobases

Among the four nucleic acid bases, the guanine moiety is the most easily oxidized and therefore is most suitable for such label free hybridization detection. In the case of low content of guanine, a greatly amplified guanine signal can be achieved by using electrocatalytic action of $[Ru(bpy)_3]^{2+}$ (Thorp, 1998).
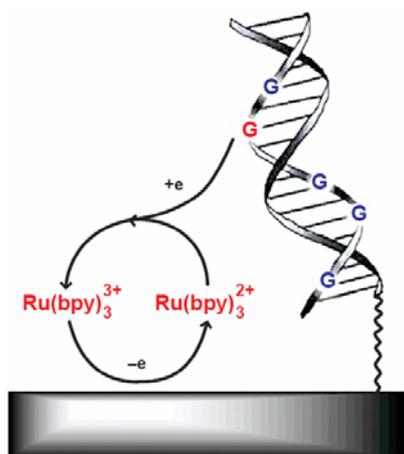
Fig. 1.6. Schematic representation of guanine oxidation mediated by a ruthenium complex in solution. The electrode is held at a potential that oxidizes the reduced metal complexes, which then come into contact with DNA. Guanine residues in DNA can reduce the metal complex, regenerating the reduced mediator. The enhanced signal thus reflects the amount of guanine available for oxidation. Adatped from (Thorp, 1998)

Some other electrochemical transduction devices rely primarily on the use of redox hybridization indicators. The indicators include DNA minor groove binder Hoechst 33258 (Nakamura et al., 2005) or dsDNA intercalator daunomycin (Marrazza et al., 2000). Some new electroactive indicators, offering better distinction between ssDNA and dsDNA have been developed to obtain higher sensitivity. Ferrocenyl naphthalene diimide binds to the DNA duplex more tightly and specifically, however shows only negligible affinity to single-stranded

capture (Takenaka et al., 2000). The method is simple with high sensitivity, but the substrate is difficult to prepare.

1.1.2.5.3 DNA-mediate charge transport

DNA-mediate charge transport takes advantage of the inherent characteristic, π-stack of duplex DNA to report on perturbations in base stacking (Boon et al., 2000). In a typical assay, as shown in Fig. 1.7, upon hybridization, the redox-active intercalator is introduced. In the electrocatalytic process, electrons flow from the electrode surface to intercalated methylene blue and reduce methylene blue into leucomethylene blue. The leucomethylene blue reduces ferricyanide in solution, so that additional electrons can flow to methylene blue and the DNA base stack is repeatedly interrogated. The current occurs only if the individual duplexes contain well-stacked base pairs; the presence of just a single intervening mismatch is sufficient to shut off the charge transport completely. If the DNA contains a mismatch, the bound methylene blue is not catalytically active and the electrochemical signal is greatly diminished. This assay is especially well suited for mutational analysis (Boon et al., 2000; Drummond et al., 2003). The mismatches discrimination relies on the change in base stacking that alters current flow, rather than depends on the thermodynamic destabilization at mismatch site. As few as 10^8 duplexes can be identified using this method at a 30 μm diameter electrode.

1.1.2.5.4 Conductivity-based detection

The deposition of silver metal onto gold nanoparticles demonstrates the ability of electrochemical methods to amplify the electrical signal (Park et al., 2002). As depicted in Fig. 1.8, in a typical approach, a sandwich assay is carried out to recruit gold nanoparticles to electrode leads mediated by target molecules. The nanoparticle labels are then developed in the silver enhancer solution, leading to the precipitation of silver metal onto the gold nanoparticles. The deposition of silver closes the electrical connection between the two flanking microelectrodes, and existence of analyte is signaled by a sharp drop in the resistance of the circuit. This method demonstrated a detection of minimal 5×10^{-13} M target DNA. The conductivity-based DNA detection method presents a straightforward approach to high-sensitivity and -selectivity, multiplexed detection of DNA (Park et al., 2002; Drummond et al., 2003).
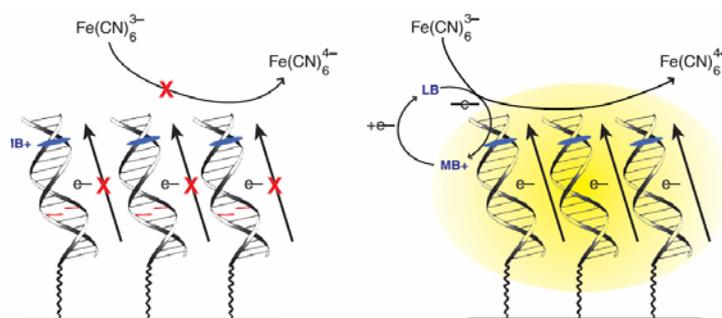
Fig. 1.7. Electrochemical assay for mismatches through DNA-mediated charge transport. On the right is shown an electrode modified with well-matched duplex DNA. Current flows through the well-stacked DNA to reduce methylene blue (MB+) intercalated near the top of the film, to leucomethylene blue (LB). LB goes on to reduce ferricyanide in solution, thereby regenerating MB+ catalytically, leading to an amplification of the hybridization signal. In the case of a DNA film containing mismatched duplexes (left), current flow through the DNA duplex is attenuated, MB+ is not reduced, and the catalytic signal is lost. Taken from (Drummond et al., 2003).
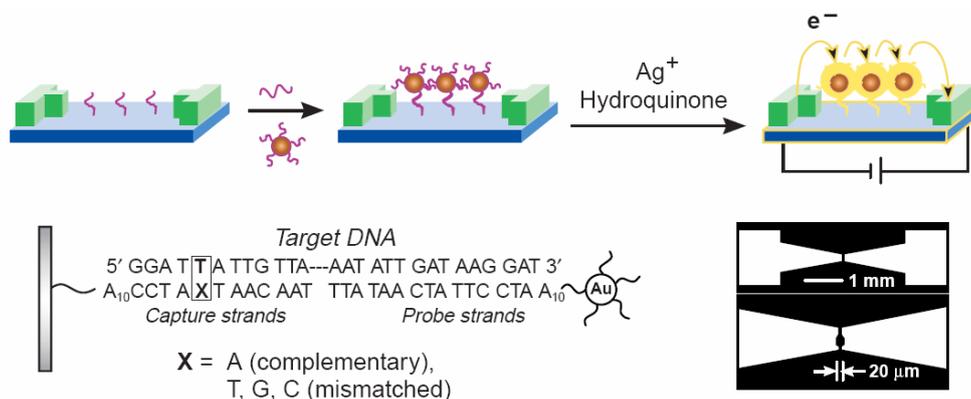
Fig. 1.8. High-sensitivity conductivity assay. Probe DNA immobilized in a small gap between two electrodes is hybridized to a portion of the unmodified target DNA. Gold nanoparticle-labeled probes are then hybridized to the unbound portion of the target, leading to the accumulation of gold in the gap. Silver metal is precipitated onto the gold nanoparticles, improving the sensitivity of the assay by lowering the resistance across the electrode gap. If the target DNA is not present, no gold nanoparticles are captured, silver is not deposited across the gap, and the circuit resistance remains high. This strategy has been extended to produce an array of electrode pairs with a different oligodeoxynucleotide capture strand in each electrode gap. Adapted from (Park et al., 2002)

1.1.2.5.5 Enzyme amplified transduction

Enzymes are highly effective catalysts, commonly enhancing reaction rates by a factor of 10^5 to 10^{17} (Cannon and Benkovic, 1998; Wolfenden et al., 1998). Enzyme labels have been widely used in electrochemical biosensor for monitoring DNA hybridization events (Nebling et al., 2004; Zhang et al., 2004). As depicted in Fig. 1.5, streptavidin-alkaline phosphatase binds to nucleic acid duplex through streptavidin/biotin interaction and subsequently produces p-

aminophenol as a measure of target DNA. The signal readout is based on electrochemical transduction of reversible redox molecules produced only at those electrode positions where affinity binding was accomplished. The enzyme converts the electrochemical inactive substrate p-aminophenylphosphate by hydrolysis into the electrochemical active form p-aminophenol (Nebling et al., 2004). The principle of redox recycling is shown in Fig. 1.9. The electrical signal can be enhanced by a factor of more than 10 through the recycling between p-aminophenol and quinoneimine, a process called redox recycling (Niwa et al., 1993).

Batch PCR amplification of DNA combined with enzyme labeling enabled Hintsche group to identify viral DNA from Epstein-Barr Virus, cytomegalovirus and herpes simplex virus (Nebling et al., 2004).

Besides the mostly used alkaline phosphatase in electrochemical detection of DNA (Gabig-Ciminska et al., 2004; Nebling et al., 2004; Hwang et al., 2005), another sensitive reporter enzyme is peroxidase (Caruana and Heller, 1999; Zhang et al., 2002; Zhang et al., 2003). In the peroxidase system, using an enzyme-labeled oligodeoxynucleotide conjugate as reporter, a single-base mismatch in an 18-base oligodeoxynucleotide was detected using a 10-µm-diameter carbon fiber electrode. Such enzymatic amplification facilitated measurement down to the zepto (1×10^{-21}) mol using 10 µl sample droplets. This great improvement was due to the utilization of a 10-µm diameter miniatured microelectrode and good performance of peroxidase-oligodeoxynucleotide conjugates (Zhang et al., 2002; Zhang et al., 2003). However, the readout is a kind of signal-off model susceptible to false-positive response.
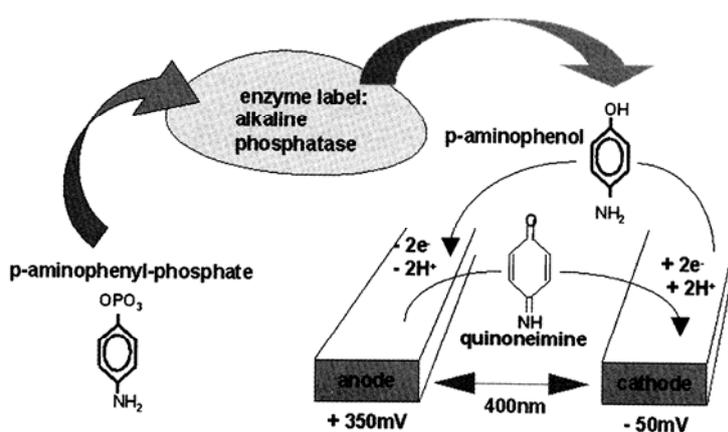
Fig. 1.9. Scheme of electrochemical redox recycling. The electrochemical inactive substrate p-APP is enzymatically hydrolyzed by alkaline phosphatase into the electrochemical active p-aminophenol, which is oxidized at the anode to quinoneimine. Subsequently, after diffusion to the cathode, quinoneimine can be reduced to p-aminophenol again and start another cycle of the redox reaction. Electrode dimensions and distances in the sub-µm range led to enhanced signal intensity. Taken from (Hintsche et al., 2005).

1.2 Esterase 2 and its potential as a reporter enzyme

The widely used alkaline phosphatase from calf intestine, being a dimeric enzyme with a molecular mass of 138 kDa, only random chemical modification is available and thus possesses more steric hindrance. Furthermore, having an optimal pH of 9.5, it exhibits only suboptimal signal response when employed as a reporter enzyme in E-Chip. In this study, esterase 2 (EST2) from *Alicyclobacillus acidocaldarius* was investigated as a novel reporter enzyme.

1.2.1 Structure and function of esterases

Esterase is a hydrolase that catalyze the hydrolysis of esters into a carboxylic acid and an alcohol. A wide range of different esterases exist that differ in their substrate specificity, protein structure, and biological function. Esterases are classified as EC 3.1.*.* in the International Enzyme Commission number classification.

Microbial esterases and lipases receive considerable attention because of their potential applications in biotechnology such as food processing, surfactant composition, detergents, paper, oil manufacture (Jaeger and Reetz, 1998; Jaeger et al., 1999; Haki and Rakshit, 2003), diagnostics (Wagaman et al., 1989; Zimmer et al., 1992; Doll et al., 1993; Van et al., 1999) and reporter protein (Agafonov et al., 2005b).

Comparison of amino acid sequence similarity has suggested that esterases, lipases and cholinesterases belong to a large family of phylogenetically related proteins. Eight subfamilies have been identified from this large family by classification of bacteria esterases and lipases based mainly on their amino acid sequences and some fundamental biological properties (Krejci et al., 1991; Hemila et al., 1994; Arpigny and Jaeger, 1999). However, merely thirteen thermostable lipases/esterases have been isolated from thermophiles and hyperthermophiles species (Haki and Rakshit, 2003). The discovered five thermostable esterases belong to a hormone sensitive lipase family, family Ⅳ of the eight subfamilies (Arpigny and Jaeger, 1999). They are esterases from *Alicyclobacillus acidocaldarius* (Hemila et al., 1994; Manco et al., 1998), *Pyrobaculum calidifontis* VA1 (Hotta et al., 2002), *Archaeoglobus fulgidus* (Manco et al., 2000), *Sulfolobus solfataricus* (Morana et al., 2002) and an uncultured archaeon (Rhee et al., 2005).

Esterases and lipases are widely present in various organisms from bacteria to higher eukaryotes. A common characteristic of these enzymes is a catalytic triad, consisting of conserved Ser, His, and Asp/Glu residues (Derewenda, 1994; Simons et al., 1997). The active site Ser is strictly conserved in all proteins, while Asp/Glu and His residues are not aligned with each other. For members of hormone sensitive lipase family, the catalytic triad is Ser, His and Asp (Fig. 1.10). In addition, most of these enzymes have a structural motif Gly-X-Ser-X-Gly, which contains the active-site Ser residue (Brenner, 1988; Derewenda and Sharp, 1993; Jaeger and Reetz, 1998; De Simone et al., 2000). The Gly-X-Ser-X-Gly pattern is also found in a serine protease (Brenner, 1988), but the tertiary structure differs from lipase and esterase (Hemila et al., 1994).

In addition, as shown in Fig. 1.10, upstream of the catalytic triad, there is another highly conserved structural motif His-Gly-Gly-Gly always found within the hormone sensitive lipase family and also in some other families, implying the specific role of this motif. This motif is involved in stabilization of the oxyanion hole, the hydrophobic binding pocket for the acyl chain of esterase's substrate (Wei et al., 1999; De Simone et al., 2000).

Fig. 1.10. Alignemt of five thermostable esterases with human hormone sensitive lipase (sequence blocks conserved in family Ⅳ) and comparison of the motif surrounding the active-site serine residue. Symbol ● is amino acid residues belong to the catalytic triad.

1.2.2 Esterase 2 from *Alicyclobacillus acidocaldarius*

Esterase 2 from *Alicyclobacillus acidocaldarius,* is a thermophilic carboxylesterase (EC 3.1.1.1), isolated and cloned from *Alicyclobacillus* (formerly *Bacillus*) *acidocaldarius* (Hemila et al., 1994), which optimally hydrolyzes p-nitrophenyl esters with straight acyl chain at 70 ℃ (De Simone et al., 2000). The 34 kDa EST2 is a thermostable, monomeric structured protein that consists of 310 amino acids (Table 1.1) (Manco et al., 1998). Solely on amino acid sequence homology and enzymatic properties, it has been classified as a member of the hormone sensitive lipase family (Fig. 1.10) (Holm et al., 1988; Hemila et al., 1994).

The structural model of EST2 from *A. acidocaldarius* exhibits a characteristic folding pattern known as the α/β-hydrolase fold and possesses Ser155, Asp252 and His282 catalytic triad (Fig. 1.11) (De Simone et al., 2000). Three-dimensional structure of EST2 shows that its catalytic triad locates on the C-terminal side of the mixed central β-sheet (Fig. 1.12). The formation of the catalytic triad by Ser155, His282 and Asp252 of EST2 has already been proven by several studies using genetic engineering mutagenesis (Hemila et al., 1994; Manco et al., 1997; De Simone et al., 2000; Agafonov et al., 2005a).

For EST2 from *A. acidocaldarius*, residues His81-Gly82-Gly83-Gly84 are involved in hydrogen bonding interactions for the stabilization of the oxyanion hole. This oxyanion hole is being hydrogen bonded by Gly83, Gly84 and Ala156 (De Simone et al., 2004).

Table 1.1 Amino acid sequence of EST2 from *Alicyclobacillus acidocaldarius*

1	MPLDPVIQQV LDQLNRMPAP DYKHLSAQQF RSQQSLFPPV KKEPVAEVRE
51	FDMDLPGRTL KVRMYRPEGV EPPYPALVYY HGGGWVVGDL ETHDPVCRVL
101	AKDGRAVVFS VDYRLAPEHK FPAAVEDAYD ALQWIAERAA DFHLDPARIA
151	VGGDSAGGNL AAVTSILAKE RGGPAIAFQL LIYPSTGYDP AHPPASIEEN
201	AEGYLLTGGM MLWFRDQYLN SLEELTHPWF SPVLYPDLSG LPPAYIATAQ
251	YDPLRDVGKL YAEALNKAGV KVEIENFEDL IHGFAQFYSL SPGATKALVR
301	IAEKLRDALA

Amino acids with shadow are the catalytical center of EST2.
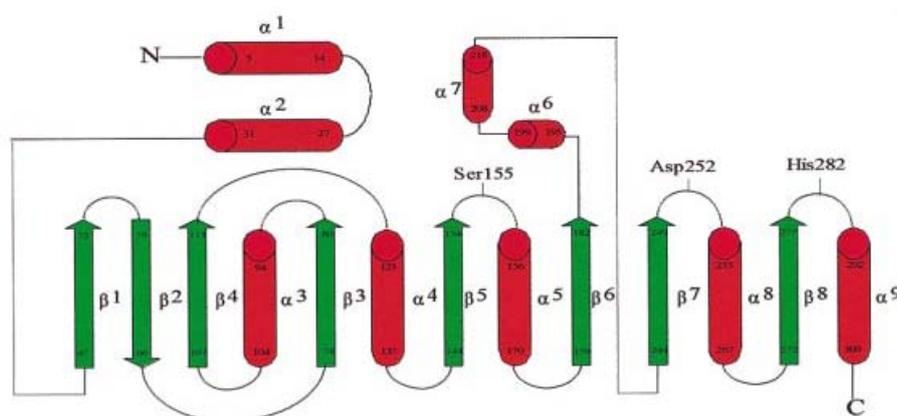
Fig. 1.11. Schematic representation of the fold showing the canonical α/β hydrolase fold. Taken from (De Simone et al., 2000).
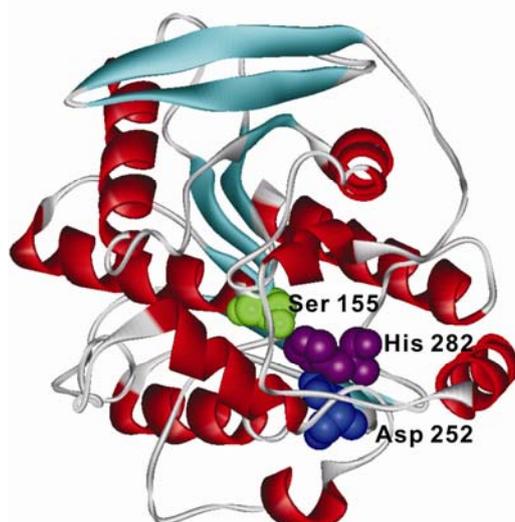
Fig. 1.12. Overall fold of EST2. Helices are shown in red, β-strands in cyan and others in gray. The residues of the catalytic triad are shown with ball symbols. From (De Simone et al., 2000).

1.2.3 Mechanism of EST2 catalysis

The mechanism of EST2 catalytic hydrolysis of p-nitrophenyl esters is based on the general procedure of the active-serine lipase catalysis (Jaeger and Reetz, 1998) and refers to the analogue chymotrypsin catalysis (Blow, 1976; Kraut, 1977). The EST2 catalysis can also be suitable simplified as a ping-pong reaction. In the event of catalysis, an ordered mechanism occurs in which several intermediates are generated. The possible catalysis process takes six steps and is summarized in Fig. 1.13.

1. As the substrate p-nitrophenyl ester enters, the ping-pong process occurs: the hydroxyl group of the Ser155 attacks the carbonyl carbon of p-nitrophenyl ester, the nitrogen of the histidine accepts the hydrogen from hydroxy of Ser155 and a pair of electrons from Ser155 hydroxy group attacks the double bond of the carbonyl.

2. The short-lived negative charge on the carbonyl oxygen of the substrate is stabilized by hydrogen bonding in the oxyanion hole. As a result, an enzyme-substrate tetrahedral intermediate is generated.

3. Instability of the negative charge on the substrate carbonyl oxygen leads to collapse of the tetrahedral intermediate; re-formation of a double bond with carbon displaces the bond between carbonyl oxygen and the oxygen group of the substrate ester linkage, breaking the ester bond and releasing of p-nitrophenol. The oxygen leaving group is protonated by His282, facilitating its displacement. The electrons that previously from

the carbonyl double bond come back from the negative oxygen to recreate the double bond, generating an acyl-enzyme intermediate.

4. An incoming water molecule is deprotonated by general base catalysis, generating a strongly nucleophilic hydroxide ion. Attack of hydroxide on the ester linkage of the acylenzyme generates a second tetrahedral intermediate, with oxygen in the oxanion hole again taking on a negative charge.

5. The bond formed in the first step between the Ser155 and the carbonyl carbon moves to attack the hydrogen that the His282 just acquired. Collapse of the tetrahedral intermediate forms the second product and the deacylation stage is closed.

6. Diffusion of the second product, carboxylic acid, from the active site regenerates free enzyme.
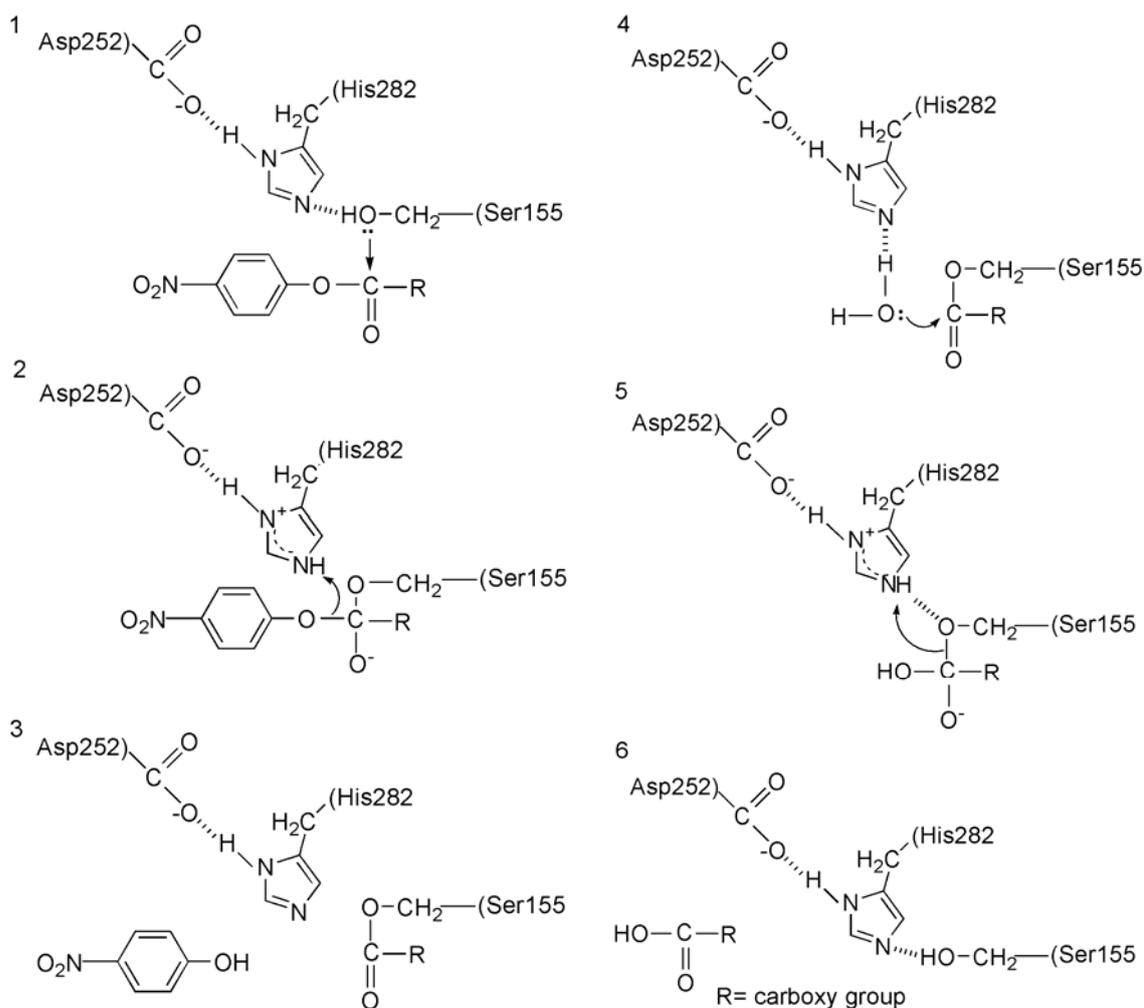
Fig. 1.13. Catalytic mechanism of hydrolytic cleavage of ester bond by EST2.

1.2.4 Trifluoromethyl ketones inhibit active-serine esterases

Esterases with serine catalytic triad are strongly inhibited by organophosphate reagents (e.g. diethyl p-nitrophenyl phosphate and diisopropyl phosphorofluoridate) (Schaffer et al., 1973; Massiah et al., 2001), carbamation reagent (e.g. eserin) (Manco et al., 1998) and trifluoromethyl ketones (TFK) (e.g. 3-alkylthio-1,1,1-trifluoro-2-propanones) (Prestwich et al., 1984).

There are extensive studies about inhibition of TFK to serine-active esterases because of the important role of acetylcholine esterase in catalytic hydrolysis of neurotransmitter acetylcholine (Brodbeck et al., 1979; Gelb et al., 1985) and hormone esterase in development regulation (Hanzlik and Hammock, 1987). Electrophilic TFK center reacts with the serine active-site of esterases and then forms an ionized hemiketal intermediate (Fig. 1.14) (Liang and Abeles, 1987; Takahashi et al., 1988). The complex is formed between ketone-form inhibitor with enzyme other than hydrate-form inhibitor with enzyme. Structural studies with NMR spectroscopy (Liang and Abeles, 1987) and pH dependence of inhibition of chymotrypsin (Brady et al., 1989) with TFK showed that the pKa of this hemiketal is approximately 4.9, which is 4.2-unit lower than the pKa of model hemiketals. The lowering of the pKa is most likely due to stabilization of the oxyanion by hydrogen-bond interactions with residues in the oxyanion hole, as well as electrostatic interactions between the oxyanion and imidazolium of histidine. The pKa of the active His in the enzyme-inhibitor complex is estimated to be higher than 10.0, the negative charge of the oxyanion is most probably a contributing factor to the high pKa of His (Liang and Abeles, 1987).
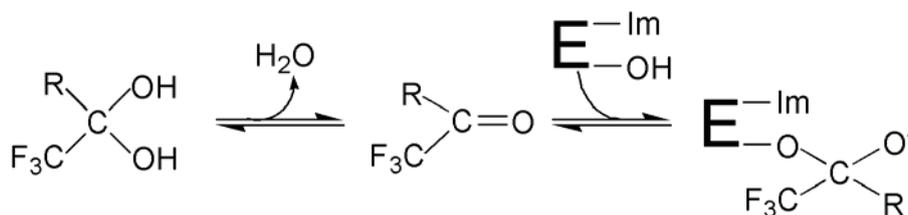
Fig. 1.14. Formation of enzyme-TFK complex. Imidazole group of histidin and hydroxyl group of serine of the enzyme catalytic center are abbreviated as Im and OH, respectively. Adapted from (Allen and Abeles, 1989).

The effect of fluorines on ketone-hydrolytic enzymes complex has also been investigated. Allen and Abeles observed that enzymes, acetylcholinesterase and pseudocholinesterase, have

a linear decrease in log Ki with decreasing pKa of the inhibitor hydrate was observed when ketones contained increasing number of fluorines. They attributed this effect to the stabilization of the hemiketal oxyanion. The reduction of the pKa of the hemiketal by the trifluoromethyl group contributes significantly to the low Ki of trifluoromethyl ketones (Allen and Abeles, 1989).

1.2.5 Affinity purification of esterase by trifluoromethyl ketones ligand

The inhibitory activity of TFK appears to be due to their ability to mimic the transition state of the ester hydrolysis by forming a hemiketal link with the putative serine at the enzyme's active site. This property allows TFK to be modified on Sepharose resin and served as a kind of affinity ligand for purification of serine-active proteins. The low abundance Juvenile Hormone esterase from *Trichoplusia ni* and Cutinases from the fungal plant pathogen *Monilinia fructicola*, can be efficiently purified by a single-step TFK ligand affinity chromatography (Hanzlik and Hammock, 1987; Wang et al., 2000). Later, affinity purification with a TFK ligand was shown to be more efficient for purification of *Bombyx mori* juvenile hormone esterase than that of DEAE ion exchange chromatography (Shiotsuki et al., 2000).

Synthesis of TFK ligand-Sepharose resin for affinity chromatography is outlined in Fig. 1.15. The affinity matrix was prepared by reacting epoxy-activated Sepharose with 3-(4-mercaptobutylthio)- 1,1,1-trifluoro-2-propanone (MBTFP), as described (bdel-Aal and Hammock, 1985).
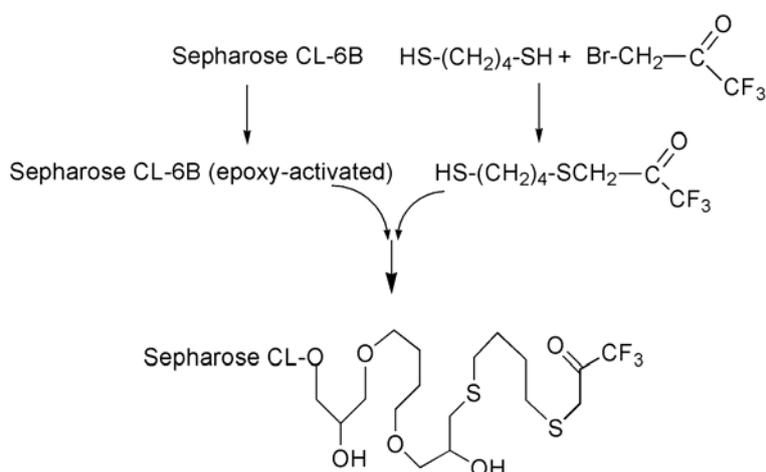
Fig. 1.15. Outline of synthesis of the MBTFP-Sepharose resin for affinity chromatography. Taken from (Wang et al., 2000).

Since TFKs are slowly reversible covalent inhibitors of serine esterases, the proteins bound to the affinity gels usually can be eluted by competition with another soluble TFK inhibitor (Hanzlik and Hammock, 1987; Shiotsuki et al., 1994; Wang et al., 2000). 3-*n*-octylthio-1,1,1-trifluoro-2-propanone is commonly used as eluant (Shiotsuki et al., 1994).

1.2.6 EST2 as a reporter enzyme

In our laboratory, EST2 from *A. acidocaldarius* has been used as a reporter protein for monitoring of newly synthesized fusion proteins in an *in vitro* transcription/translation coupled system (Agafonov et al., 2005b), suppression of amber codon (Agafonov et al., 2005a) and modification at C-terminal of enzyme (Agafonov et al., 2006). In a spectrophotometric method, EST2 as a reporter exhibits sensitivity comparable to that of radioisotope labeling (Agafonov et al., 2005b).

In summary, I pursue utilizing the EST2 as a potential reporter enzyme to substitute for traditional alkaline phosphatase in improving nucleic acids detection. Being a dimeric enzyme with 138 kDa molecular mass and having an optimal pH of 9.5, the alkaline phosphatase possess more steric hindrance effect and exhibits only suboptimal signal response when employed as a reporter enzyme in E-Chip. Moreover, the more promising characters of the reporter enzyme EST2 are its thermostability and specific conjugation via single cysteine on its native single chain polypeptide.

1.3 Hybridization behavior

Nucleic acids hybridization is a specific biological elements recognition process and thus is the most important step in the course of functionalization of DNA biosensor. This recognition is often performed by hybridizing target nucleic acids to complementary probe ODN. According to the state of the used probe ODN, the nucleic acids hybridization can be grouped into solution-phase and solid-phase hybridization.

1.3.1 Properties of solution-phase hybridization

Properties of DNA hybridization in solution is relatively simple and has been well studied by absorption spectroscopy (Morrison and Stols, 1993), calorimetry (Breslauer et al., 1986), nuclear magnetic resonance (Patel et al., 1982). The same as all natural processes, hybridization is subject to thermodynamic and kinetic constraints. Thermodynamics define limits on discrimination of different target sequences and detection of low copy targets. Kinetics determines how quickly equilibrium is approached.

Nearest-neighbors model has been widely accepted for evaluating thermodynamics of DNA duplex. The application of this model was pioneered by Zimm et al. and further developed by Breslauer (Breslauer et al., 1986) and Santalucia (SantaLucia, Jr., 1998). In this model, $\Delta G°$ was shown to be more suitable in evaluating DNA duplex stability than ΔH and ΔS due to compensating errors. The total ΔG of a given DNA duplex can be estimated by

$$\Delta G(\text{total}) = \sum_i n_i \, \Delta G(i) + \Delta G(\text{init w/term G•C}) + \Delta G(\text{init w/term A•T}) + \Delta G(\text{sym})$$

where $\Delta G(i)$ are the standard free-energy changes for the 10 individual pair of possible Watson–Crick nearest-neighbors (SantaLucia, Jr., 1998), n_i is the number of occurrences of each nearest neighbor, i. $\Delta G(\text{init w/term G•C}) + \Delta G(\text{init w/term A•T})$ represent free-energy of two type of base-pair, ''initiation with terminal G•C'' and ''initiation with terminal A•T''. $\Delta G(\text{sym})$ equals 0.43 kcal/mol if the duplex is self-complementary and zero if it is non-self-complementary.

DNA melting temperatures (Tm) considering DNA nearest-neighbor thermodynamics energy parameters use the following equation. Tm is defined as the temperature at which half of the strands are in the double-helical state and half are in the ''random-coil'' state (SantaLucia, Jr., 1998). For self-complementary oligodeoxynucleotide duplexes, the Tm is calculated from the predicted ΔH and ΔS and the total oligodeoxynucleotide strand concentration C_T, by using the equation:

$$\text{Tm} = \Delta H / (\Delta S + R \ln C_T)$$

where R is the gas constant (1.987 cal/K•mol). For non-selfcomplementary molecules, C_T in the equation is replaced by $C_T/4$ if the strands are in equal concentration or by $(C_A - C_B/2)$ if the strands are at different concentrations, where C_A and C_B are the concentrations of the more concentrated and less concentrated strands, respectively (SantaLucia, Jr., 1998).

In kinetics study, k_{on} and k_{off} is the associate and dissociate rate constant, respectively. The equilibrium constant K_E, is defined by k_{on}/k_{off}, reflect the state of the hybridization reaction (Fig. 1.16) (Morrison and Stols, 1993; Gao et al., 2006). At beginning of hybridization reaction,

k_{off} is negligible in that less duplex formed, and $K_E \gg 1$. As all solution hybridization reach 100% completion, rate constant k_{on} equal to that of k_{off}, $K_E = 1$.

$$S_1 + S_2 \underset{k_{off}}{\overset{k_{on}}{\rightleftharpoons}} S_1S_2$$
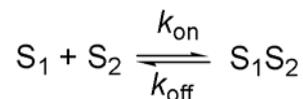
Fig. 1.16. Scheme of dynamic equilibrium of DNA hybridization. S_1 and S_2 are single-stranded target and its complementary ODN, respectively. S_1S_2 is the duplex hybridization product.

After hybridization reached equilibrium, raising the temperature above Tm, the rate constant k_{off} increases while k_{on} decreases, the equilibrium is moving to ssDNA state, $K_E < 1$ (Morrison and Stols, 1993).

Hybrid types will influence the hybridization temperature used. The thermostability of RNA:DNA hybrids are substantially greater than those of DNA:DNA duplex (Casey and Davidson, 1977). The relative strength of different hybrids is: RNA:RNA hybrids > RNA:DNA hybrids > DNA:DNA hybrids. RNA:RNA and RNA:DNA hybrids will require higher hybridization temperatures than DNA:DNA hybrids (Casey and Davidson, 1977; Wu et al., 2002).

1.3.2 Properties of solid-phase hybridization

In solid-phase or surface hybridization, association of immobilized strands, referred to as "captures", with target sequences from solution occurs at a solid–liquid interface. The interfacial environment is distinct from the bulk solution. Several important impact factors about surface hybridization are described as following.

1.3.2.1 Thermodynamics and kinetics of solid-phase hybridization

Explanation of experimental data from solid-phase hybridization is still a matter of question. A comparison study of equilibrium constants for solid-phase (K_{ES}) and bulk solution-phase (K_{EB}) hybridization indicates that bulk solution and surface thermodynamics are distinct (Levicky and Horgan, 2005). Usually K_{ES} is suppressed relative to K_{EB}, though data also indicate that hybridization on a surface can be more thermodynamically favored than in solution. Suppression of K_{ES} probably due to electrostatic and steric penalties associated with penetration of a target strand into a capture layer. On the other hand, a high local concentration

of capture ODNs has a stabilization effect of targets binding, which is not possible under solution conditions, leading to $K_{ES} > K_{EB}$ (Stevens et al., 1999; Levicky and Horgan, 2005). Modeling analysis of microarrays' hybridization shows that solid-phase hybridization is less thermodynamically favored than that of solution-phase (Held et al., 2003).

1.3.2.2 Capture surface density

Usually, capture films of the solid-surface are characterized by a density of 10^{12}-10^{13} capture ODNs/cm^2 and a layer thickness of several nanometers. These values correspond to a local ODN concentration of 0.1-1 M, much higher than that of solution-phase hybridization, implying a very different local environment for solid-phase hybridization (Levicky and Horgan, 2005).

It was demonstrated that the density of immobilized captures can influence the thermodynamics of hybridization and hence the selectivity of DNA biosensors (Watterson et al., 2000; Peterson et al., 2001). Experiments indicate that surface hybridization is suppressed when the coverage of capture molecules is too high (Steel et al., 1998; Peterson et al., 2001). However, in the coverage of sparse captures, patches of bare surface will be accessible to adsorption of target molecules, as captures are too far apart to come into contact. Under this circumstance, target ODNs might first adsorb and then diffuse along the solid support before hybridizing to a capture ODN (Chan et al., 1995).

1.3.2.3 Impact of capture layer structure

The structure of a capture layer is asymmetric in that only one terminal of the capture ODN is bound to the solid-surface. For solid-phase hybridization, nucleic acid near the grafted end of capture is least accessible (Peterson et al., 2002; Hagan and Chakraborty, 2004). This can be attributed to a strongly steric interaction between capture molecules close to the surface, a sort of steric hindrance. These observation imply the presence of an activation barrier that prevents target penetration into the probe film, which is also expected on theoretical grounds (Hagan and Chakraborty, 2004; Levicky and Horgan, 2005). This barrier probably contributes to high mismatch discrimination efficiency, as the hybridization duplex containing mismatched base-

pairs are less stable than those perfectly ones and are easy to be dissociated under this circumstance.

1.3.2.4 Impact of mismatches on solid-phase hybridization

A significant evaluation of a DNA biosensor is its ability to discriminate mismatched targets from fully complementary ones. The diversity of experimental observations regarding influence of mismatches (Okahata et al., 1998; Peterson et al., 2002; Dai et al., 2002) was partially attributed to that the formation of structures is more complicate than the simple one-to-one hybridization (Fig. 1.17a). A target molecule can even bridge and hybridize across multiple capture ODNs (Fig. 1.17b). Moreover, the presence of a mismatch within target might facilitate bridging by destabilizing duplex formation at the location of the bridge (Fig. 1.17c) (Levicky and Horgan, 2005). This potential multi-capture binding hybridization reaction will inevitable reduce mismatch discrimination efficiency.
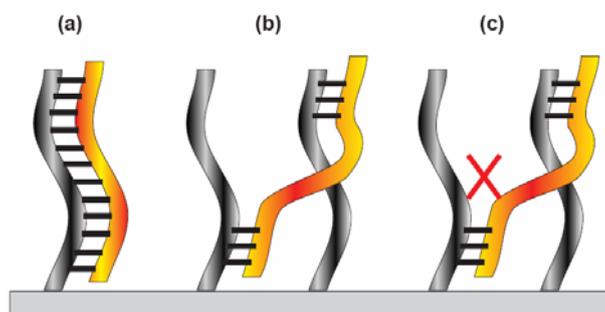
Fig. 1.17. (a) One-to-one hybridization. (b) A target bridge across two capture strands. (c) A target bridge facilitated by a mismatch (cross). Taken from (Levicky and Horgan, 2005).

In conclusion, selectivity of mismatch discrimination depends especially on the applied conditions. For a specific DNA biosensor, the first priority is to optimize the detection condition.

1.4 Bacterial species identification through detection of 16S rRNA

Traditional methods for bacterial species identification are usually based on morphological and/or physiological features of a microorganism or analysis of 16S rRNA gene sequences. Ribosomal RNA is present in high copy numbers in cells (500-70,000 copies/cell), depending

on the growth period and the respective microorganism (Cammarano et al., 1986; Woese, 1987). Using 16S rRNA as the target instead of genomic DNA is an alternative to identify bacteria and becomes more and more prevalent nowadays in that the improved method with better detection sensitivity (Small et al., 2001; Chandler et al., 2003; Wang et al., 2004). Moreover, directly rRNA detection by electrochemical chip eliminates the need of PCR amplification and enables identification and roughly quantification of bacteria (Sun et al., 2005).

The sequence information in rRNA is highly conserved throughout evolution (Woese et al., 1980) and thus microorganism can be identified through the 16S rRNA sequence. On the principle of the solid-phase hybridization detection, the region targeted by the capture sequence must present enough diversification in order to distinguish between different species, while the flanking region for binding of universal detection probe or chaperon/helper ODN should be highly conserved (Chandler et al., 2003).

Secondary structure of *E. coli* 16S rRNA was depicted in Fig. 1.18 as described (Woese et al., 1980). The intact 16S rRNA molecule consists of about 1500 nucleotides and is highly compact. To increase hybridization efficiency, whole length rRNA can be digested into short fragments (Small et al., 2001). Generally, as shown in Fig. 1.19, the fragmented rRNA is coupled to the surface through the surface-immobilized capture ODN, followed by "sandwich hybridization" with the biotinylated detection ODN. In order to make capture ODNs more accessible to some specific region, chaperone/helper ODN was designed to bind nearby the region, destabilizing rRNA structure (Elsholz et al., 2006).

In microbiology, colony-forming unit (CFU) is a measure of viable bacterial numbers, while microscopy directly counts all cells, dead and living. For CFU counting, a sample is spread or poured on a surface of an agar plate, left to incubate and the number of colonies formed is counted.

The reported detection limit of identification of bacteria through rRNA was 10^7 cells in 4 h by using pencil electrode through monitoring guanine oxidization peak (Lagier et al., 2005). About 0.5 μg of total rRNA, equivalents to approximately 7.5×10^6 *Geobacter chapellei* cells was identified from soil extraction (Small et al., 2001). 10^{11} molecules 16S rRNA can be monitored by electric chip coupled with beads-based sandwich hybridization with a 4 h assay time (Gabig-Ciminska et al., 2004). Recently, a low detection limit of RNA corresponding to 10^4 cell/ml was reported (Elsholz et al., 2006), which might be the most sensitive method by far.

A direct detection of the ribosomal RNA maybe have not matched the sensitivity of a PCR based DNA assay yet, but it allows bacterial species identification and quantification.
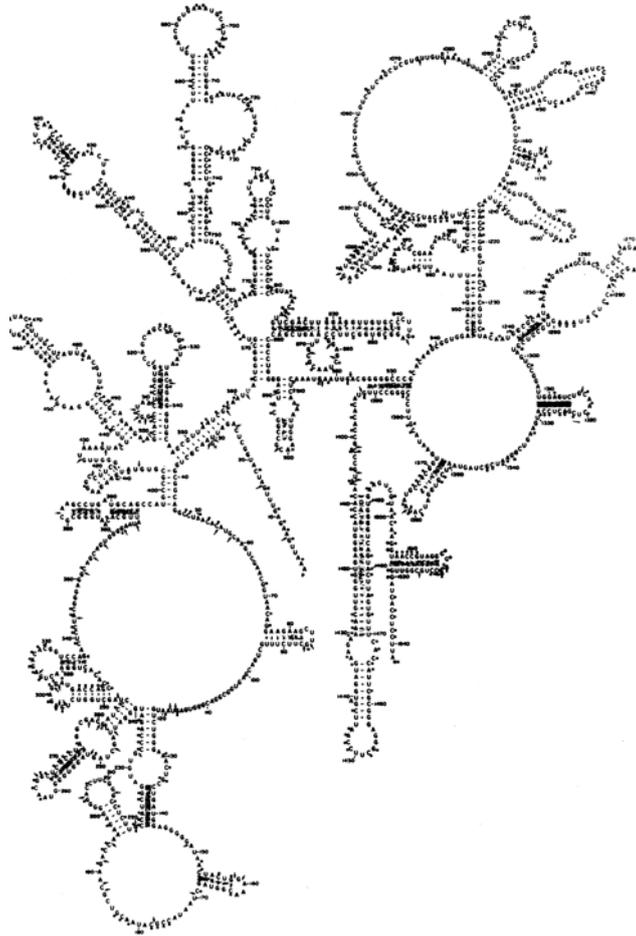
Fig. 1.18. Secondary structure model for 16S rRNA of *E.coli.* From (Woese et al., 1980).
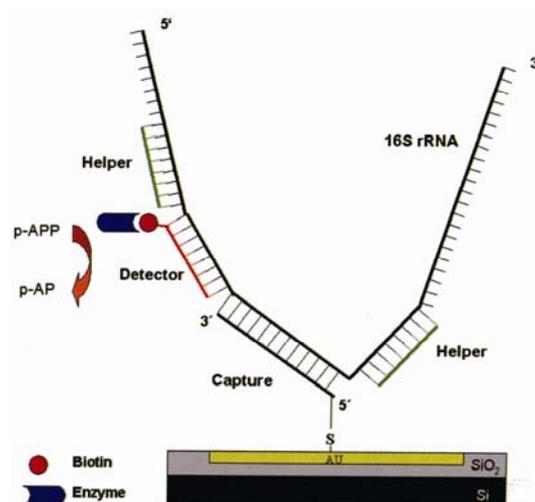
Fig. 1.19. Scheme of the 16S rRNA-based detection. Flanking the capture and detector region, helper olligodeoxynucleotide are used to increase the accessibility by breaking up secondary structures. The detector region is also chosen to be near the surface. Taken from (Hintsche et al., 2005).

1.5 Molecular beacon

Molecular beacons consist of a DNA hairpin functionalized at one end with a fluorophore and at the other with a quenching agent. In the absence of the target DNA sequence, the quencher is brought in close proximity to the fluorophore, and no signal is generated. Addition of the target sequence leads to hairpin unfolding, concomitant duplex formation, and signal generation.

For the detection of nucleic acid targets, hairpin/stem-loop structured ODN are superior to linear one. It has characters of directly detection of unlabeled nucleic acid targets and greatly improved mismatch discrimination (Bockisch et al., 2005). Molecular beacon have successfully been demonstrated for a variety of solution-phase applications such as single nucleotide polymorphism and mutation detection (Piatek et al., 2000), identification of pathogens (Vet et al., 1999), the real-time detection of PCR amplicons (Tyagi and Kramer, 1996) and mRNA detection in living cells (Perlette and Tan, 2001). Despite the advantage of DNA microarrays and biosensors, there are also several reports on surface-immobilized stem–loop structures for the detection purpose (Wang et al., 2002; Du et al., 2003).

However, immobilized beacons, show a fluorescence enhancement of only 2–5 folds (Wang et al., 2002; Yao and Tan, 2004), much less than that of 25–200 folds observed in solution (Bonnet et al., 1999; Tan et al., 2000). As a result, immobilized molecular beacons do not provide the sensitivity desirable for DNA microarrays and biosensors (Wang et al., 2002; Bockisch et al., 2005).

Recently, an electrochemical DNA sensor utilization of immobilized molecule beacon containing a terminal ferrocene as the conformational switch was investigated (Fan et al., 2003). In the absence of target, the electrochemically active ferrocene is close to the electrode surface generating redox current. Upon target hybridization, ferrocene is separated from the electrode abolishing the exponentially distance-dependent electron transfer process (Fig. 1.20A). The sensor allows sensitive detection of ODN without the use of exogenous reagents, but represents a "signal-off" model since hybridization exterminates the redox current. "Signal-off" sensors, however, have a disadvantage being highly susceptible to false-positive responses (Fan et al., 2003).

A "signal-on" sensor also based on molecular beacon mechanism was developed recently. The beacon was immobilized through one terminus to microwell surface and carrying an affinity label at the other terminus. In the absence of target, the closed conformation of the probe forces the label into close proximity to the surface of the solid support rendering it inaccessible to detector molecules (Fig. 1.20B). Upon target hybridization, the structure changes to a linear conformation and is accessible to detection reporter. This novel conformational switch system allows a detection of nucleic acids in pM range (Bockisch et al., 2005).

In this study, a kind of stem-loop structured ODN (molecular beacon) based on electrical chip was investigated. This "signal-on" biosensor combining the convenient immobilization and detection merits of electrical chip (Fan et al., 2003) and enzyme amplified detection (Bockisch et al., 2005) has a promising future.
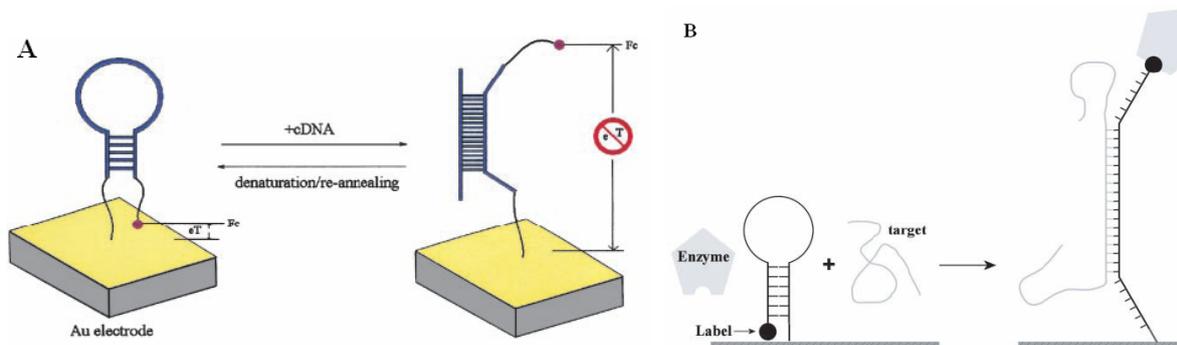
Fig. 1.20. (A) A stem–loop ODN possessing terminal thiol and a ferrocene group is immobilized at a gold electrode through self-assembly. In the absence of target, the stem–loop structure holds the ferrocene tag into close proximity with the electrode surface, thus ensuring rapid electron transfer and efficient redox of the ferrocene label. On hybridization with the target sequence, a large change in redox currents is observed, presumably because the ferrocene label is separated from the electrode surface. Taken from (Fan et al., 2003). (B) Principle of the enzymatic conformational switch system. In the closed conformation the affinity label is sterically shielded, inaccessible to the reporter enzyme. On target binding, the hairpin opens, making the label available for enzyme binding. Taken from (Bockisch et al., 2005).

1.6 Statement of objectives

The Germany's future award for technology and innovation (Deutscher Zukunftpreis) of 2004 was awarded to Fraunhofer institute, Siemens AG and Infineon AG for their development of a new conception of diagnostic platform "lab-on-chip" (Hintsche et al., 2004). The device is self-contained: the reporter enzyme streptavidin-alkaline phosphatase and substrate p-aminophenylphosphate were embedded inside channel of a thin card. In order to realize the "point-of-care" clinical diagnosis purpose optimally, the system requires further improvement and simplification.

The reporter enzyme used in this self-contained biochip and other research groups is always streptavidin-alkaline phosphatase conjugate with its specific substrate p-aminophenylphosphate. The limit of the stability of p-aminophenylphosphate impedes its application. Moreover, at pH optimal for the alkaline phosphatase activity, the instability of the resultant product p-aminophenol increased.

The enzyme-ODN conjugates have shown good selectivity and sensitivity at discrimination of mismatched DNA. It was also hoped that the thermostable esterase 2 from *A. acidocaldarius* covalently conjugated with defined ODN can substitute for streptavidin-alkaline phosphatase and function as a better reporter. Moreover, the complementary DNA sequence of the EST2-ODN can be introduced to target DNA sample through PCR amplification. In the process of E-Chip hybridization biosensing of target DNA, the separate nucleic acids hybridization and enzyme labeling steps can be simplified into one step, formation of Sandwich hybridization among EST2-ODN, target DNA/RNA and capture ODN.

With the superior detection limits on E-Chip, one of the objectives in this research is to test the possibility of bacterial species identification through 16S rRNA sequence utilization of EST2-ODN conjugate.

E-Chip based molecular beacon was also investigated to broaden the detection platform.

In summary, this study is focused on:

- EST2 substitute for alkaline phosphatase as a reporter enzyme for detection of hybridization

- E-Chip detection of target DNA by EST2-ODN conjugate reporter

- Bacterial species identification utilization of EST2-ODN reporter

- E-Chip based molecular beacon using EST2 as reporter

2. Materials and Methods

2.1 Materials

2.1.1 Instruments

Beckman Gold$^{®}$ HPLC System	Beckman, Munich
DNA Thermal Cycler	Perkin Elmer, Norwalk, USA
UV-Spectral photometer DU640	Beckman, Munich

2.1.2 Materials

Interface SCB-68	National Instruments, Munich
M-PVA SAV1 magnetic beads	Chemagen, Baesweiler
10% Palladium on activated charcoal	Sigma, Deisenhofen
Roti$^{®}$-Quant	Carl Roth, Karlsruhe
DNA extraction kit, DNA Gel recovery kit	Promega, Mannheim
SV Total RNA Isolation System	Promega, Mannheim
Brain heart infusion	BD diagnostics, Heidelberg

2.1.3 Chromatographic materials

Superdex 75 HR10/30	Pharmacia, Freiburg
Sepharose CL-6B	Pharmacia, Freiburg
MonoQ 5/50 GL	Pharmacia, Freiburg
2-Iminobiotin Immobilizationed on 4% beaded Agarose	Sigma, Deisenhofen
RP-column Bio Wide Pore C18	Sigma, Deisenhofen
Silica gel Kieselgel 60	Merck, Darmstadt

2.1.4 Chemicals, enzymes and proteins

2.1.4.1 Chemicals

dNTP	Peqlab, Erlangen
Tris, X-Gal, DEPC	Roth, Karlsruhe
acrylamide, APS, bromphenol blue,	Serva, Heidelberg
Commasie Brilliant Blue G250,	Serva, Heidelberg

N,N'-methylenbisacrylamide, TEMED	Serva, Heidelberg
p-aminophenol	Acros, Geel, Belgium
NaBH$_4$, 1,4-Butanediol diglycidyl ether,	
ethidium bromide, Triton X-100, 2-Naphthyl acetate,	
p-nitrophenylacetate, p-nitrophenylpropionate,	
p-nitrophenylbutyrate, p-nitrophenylvalerate,	
p-nitrophenylhexanoate, p-nitrophenyloctnoate,	
Biotin-Maleimide,Fast BB blue salt, Tween-20,	
N-succinimidyl 3-(2-pyridyldithio)-propionate,	Sigma, Deisenhofen
sulfosuccinimidyl 4-(*N*maleimidomethyl)cyclohexane-1-carboxylate,	
tris (2-carboxyethyl) phosphine hydrochloride,	Pierce, Rockford, USA
Other reagents were analytically pure grade.	

2.1.4.2 Enzymes and proteins

Restriction endonuclease, T4 DNA Ligase	NEB, Schwalbach
Taq DNA Polymerase	Peqlab, Erlangen
Streptavidin	Gerbu, Gaiberg

2.1.5 Bacterial strains

Listeria innocua		DSMZ, Braunschweig
Escherichia coli:		
BL21(DE3)	F⁻ omp T hsdS$_B$((r$_B$-m$_B$-) gal dcm (DE3)	Novagen, Madison, USA
XL-1 blue	F'[proAB⁺, lacI^q, lacZΔM15, Tn10], supE44, hsdR17, endA1, gyrA96, relA1, thi-1, recA1, lac⁻	Stratagene, Heidelberg

2.1.6 Plasmids

pET-30a	expression vector with T7 promoter	Novagen, Madison, USA
pGEM®-T	vector for PCR products	Promega, Mannheim

2.1.7 Oligodeoxynucleotides

2.1.7.1 Oligodeoxynucleotides for construction of mutant

Name	Oligodeoxynucleotide sequences *
Est-For	5′-<u>CATATG</u>CCGCTCGATCCCGTCATTC-3′
Est-Rev	5′-<u>GGATCC</u>TCAGGCCAGCGC-3'
Mut-For	5'-CCTGGCGCCGTGCCACAAGTTCCC-3'
Mut-Rev	5'-GGGAACTTGTGGCACGGCGCCAGGC-3'

* Underline indicates the restriction endonuclease sites

2.1.7.2 Oligodeoxynucleotides for detection of DNA

Name	Oligodeoxynucleotide sequences *
ODN-P	5'-SH-TTTTTTGACAGGCGAGGAATACAGGTATTG-3'
ODN-N	5'-SH-TTTTTTCCGCACCTTCCGGTACAGCTAC-3'
PM	5'-SH-TTTTTTTTTTTTGACAGGCGAGGAATACAGGTATTG-3'
MM-13	5'-SH-TTTTTTTTTTTTGACAGGCGAGG**T**ATACAGGTATTG-3'
MM-7	5'-SH-TTTTTTTTTTTTGACAGGCGAGGAATACA**C**GTATTG-3'
MM-4	5'-SH-TTTTTTTTTTTTGACAGGCGAGGAATACAGGT**T**TTG-3'
C-TS1	5'-GGCAGTTAACTTCCAGAATGATGCCTTTTTT-SH-3'
C-TS2	5'-GTCAGTGATTTTGCCAGCAACTTTTTT–SH-3'
C-TS3	5'-GCAACGTGCATAGCGATGTGTTTTTTT-SH-3'
C-TS4	5'-TTTTGCTTGGTTCCATAACGATTTTTT-SH-3'
C-TS2A	5'-GTCAGTGATTTAGCCAGCAACTTTTTT–SH-3'
C-TS2C	5'-GTCAGTGATTTCGCCAGCAACTTTTTT–SH-3'
C-TS2G	5'-GTCAGTGATTTGGCCAGCAACTTTTTT–SH-3'
A34	5'-NH$_2$-TTTTTTTTTTCAATACCTGTATTCCTCGCCTGTC-3'
biotin-34	5'-Biotin-TTTTTTTTTTCAATACCTGTATTCCTCGCCTGTC-3'
EFTS-F	5'-Biotin-GGCATCATTC TGGAAGTTAA CTGCC-3'
EFTS-R	5'-CAATACCTGTATTCCTCGCCTGTCTTTTGCTTGGTTCCATAACGA-3'
CM	5'-GTAGCTGTACCGGAAGGTGCGGTTTGACAGGCGAGGAATACAGGTATTG-3'
1MM	5'-GTAGCTGTACTGGAAGGTGCGGTTTGACAGGCGAGGAATACAGGTATTG-3'
2MM	5'-GTAGCTGTACTAGAAGGTGCGGTTTGACAGGCGAGGAATACAGGTATTG-3'
3MM	5'-GTAGCTGTAGTAGAAGGTGCGGTTTGACAGGCGAGGAATACAGGTATTG-3'

* Nucleotide(s) in bold is the mismatched positions in same series of captures

2.1.7.3 Oligodeoxynucleotides for bacteria species identification

Name	Oligodeoxynucleotide sequences
U1082	5- NH_2-TTTTTT GGTTGCGCTCGTTGCGGGACTTAACCCAACAT-3'
LINNOC	5'-TTTGTCCCGAAGGGAAAGCTCTG TTTTTTTTT -SH3'
ECOLI	5'-ACGGTTCCCGAAGGCACATTCTCA TTTTTTTTT-SH-3'
EU943	5'-TCGAATTAAACCACATGCTCCA TTTTTTTTT-SH-3'
Helper-1	5'- TTCACAACACGAGCTGACGACAGCCATGCAGCACCTGTCTC-3'
Helper-2	5'- CTCACGACACGAGCTGACGACAACCATGCACCACCTGTCAC-3'

2.1.7.4 Oligodeoxynucleotides for molecular beacon

Name	Oligodeoxynucleotide sequences
CMB442 *	5'-SH-TggccgtTACTCCCTTCCTCCCCGCacggccAr -biotin-3'
T442-59	5'-GCGGGGAGGAAGGGAGTA-3'
T442-Ex	5'-GGCCGTGCGGGGAGGAAGGGAGTAACGGCCTTT-3'

* Nucleotides in lowercase form a stem structure; "Ar" is ribonucleotide adenosine.

2.1.8 Bacterial media

Bacteria media was autoclaved at 121 ℃ (1 Bar) for 15 min. Solutions of antibiotics were added only before usage.

LB-Medium:	10 g	Pepton	
	5 g	Yeast extract	
	5 g	NaCl	add H_2O to 1 L

Psi Broth:	20 g	Bacto tryptone	
	5 g	Bacto yeast extract	
	5 g	$MgSO_4$	add H_2O to 1 L, pH 7.6

BHI–Medium:	37 g	brain heart infusion	add H_2O to 1 L

2.1.9 Buffers and solutions

TBE buffer:	89 mM Tris	pH 8.4
	89 mM Boric acid	
	2.5 mM EDTA	

TE buffer:	10 mM Tris-HCl	pH 8.0
	1 mM EDTA	

Ligation buffer:	20 mM Tris-HCl	pH 7.6
	5 mM $MgCl_2$	
	5 mM DTT	
	0.5 mM ATP	
	50 μg/ml BSA	
TfI buffer:	30 mM K-Acetate	pH 5.8
	100 mM RbCl	
	50 mM $MnCl_2$	
	10 mM $CaCl_2$	
	15 % (w/v) Glycerol	
TfII buffer:	10 mM Mops	pH 7.0
	10 mM RbCl	
	75 mM $CaCl_2$	
	15 % (w/v) Glycerol	
SSPE:	150 mM NaCl	
	1 mM EDTA	
	10 mM NaH_2PO_4	pH 7.4
PBS:	137 mM NaCl	
	2 mM KH_2PO_4	
	2.7 mM KCl	
	10 mM NaH_2PO_4	pH 7.4
Hybridization buffer:	0.05% Tween 20	
	1 mg/ml BSA	
	300 mM NaCl	
	2 mM EDTA	
	20 mM NaH_2PO_4	pH 7.4
Washing buffer:	0.05% Tween 20	
	75 mM NaCl	
	0.5 mM EDTA	
	5 mM NaH_2PO_4	pH 7.4

Loading buffer of Agarose-Gel:

     30 % (v/v) Glycerol
     0.25 % (w/v) Xylencyanol
     0.25 % (w/v) Bromphenolblue

Loading buffer of SDS-PAGE:

     100 mM Tris-HCl   pH 8.3
     30 % (v/v) Glycerol
     0.06 % (w/v) Bromphenolblue
     5 % (w/v) SDS
     0.7 M β-Mercaptoethanol

Coomassie-staining solution:

30 % (v/v) Ethanol
10 % (v/v) Acetic acid
0.4 % (w/v) Coomassie Brilliant Blue G250 in H_2O

Destaining solution:

30 % (v/v) Ethanol
10 % (v/v) Acetic acid in H_2O

2.2 Methods

2.2.1 Standard methods

2.2.1.1 Spectrophotometer determination of protein and nucleic acids

Absorbance measurements in UV-region were carried out in 1-cm quartz cuvettes. Protein concentration especially in the presence of nucleic acids was determined as described (Ehresmann et al., 1973):

$$(A_{228.5}-A_{234.5}) / 3.14 = mg/ml \text{ (protein)}$$

The concentration of DNA and RNA was determined by measurement of the absorbance at 260 nm. One A_{260} unit corresponds to approximately 50 µg dsDNA, 30 µg ssDNA or 40 µg RNA.

2.2.1.2 Bradford protein assay

Proteins detected by the Bradford reagent are based on the blue stain of Coomassie blue in acidic solution upon reaction with proteins (Bradford, 1976). In a range of 0.1 to 20 µg/ml the protein concentration can be determined spectrophotometrically according to the Lambert-Beer law. To this means, a calibration curve is calculated from the absorbance obtained from the standard solutions ranging from 0.1 to 2.0 µg/ml. 20 µl of standard or protein sample at varying dilutions are added to 200 µl of Roti®-Quant Bradford reagent diluted 1:4 in PBS. Sample concentrations are carried out spectrophotometrically by absorbance measurement at 590 nm/450 nm (Zor and Selinger, 1996).

2.2.1.3 Culture of bacteria

For the small-scale preparation of plasmid DNA, *E. coli* strains were grown in 5 ml LB-medium supplemented with the appropriate antibiotic. Single colony was picked with a pipette

tip from LB-agar plates in petri dishes. Cultures were incubated overnight at 37 ℃ with agitation of 170 rpm in the shaker.

For expression of *A. acidocaldarius* EST2 proteins in *E.coli*, single colony of *E. coli* strain BL21(DE3) harboring the appropriate genes were inoculated to 5 ml LB medium, supplemented with 30 μg/ml kanamycin or 50 μg/ml ampicillin and grown overnight at 37 ℃ with agitation. A 3 ml aliquot of this culture was inoculated to 250 ml LB medium supplemented appropriate antibiotics, and grown overnight at 37 ℃ with agitation. The 250 ml culture was used to inoculate 10 L LB medium supplemented with appropriate antibiotics. This culture was grown at 37 ℃ until A_{600} reached 0.8, at which point IPTG was added to a final concentration of 0.1-1 mM to start the overexpression of proteins. The culture was grown further for 4 h. Cells were harvested by centrifugation at 5 000 g for 10 min at 4 ℃.

2.2.1.4 Gel electrophoresis

2.2.1.4.1 Agarose gel electrophoresis

Agarose gels (0.5-2.0 % (w/v) agarose, 0.5 μg/ml ethidium bromide, 0.5xTBE) were used for analysis and preparation of nucleic acids. The samples were mixed with 1/3 volume of loading buffer and loaded on the gel. Electrophoresis was run at 5-7 V/cm. The bands of DNA were visualized using a long wavelength UV lamp.

2.2.1.4.2 SDS-polyacrylamide gel electrophoresis

The discontinuous-pH SDS-polyacrylamide gel electrophoresis was performed as described (Laemmli, 1970) in the Mighty Small Vertical Slab Unit (Hoefer Scientific Instruments) with 25 mM Tris-HCl pH 8.3, 250 mM glycine, 0.1% (w/v) SDS, as the running buffer. The separating gel (10-15%, acrylamide/N,N'-methylenbisacrylamide 29:1) contained 375 mM Tris-HCl pH 8.8, 0.1% (w/v) SDS. The 4 % stacking gel (acrylamide/N,N'-methylenbisacrylamide 29:1) contained 125 mM Tris-HCl pH 6.8, 0.1% (w/v) SDS. Polymerization was started by addition of 0.05% (v/v) TEMED and 0.1% (w/v) APS. Protein samples were mixed with 1/5 volume of SDS-PAGE loading buffer and heated at 95 ℃ for 3 min. Electrophoresis was carried out at 15 V/cm, 50 mA. The bands of proteins were visualized by staining with Commasie Brilliant Blue G250.

2.2.2 Isolation and purification of nucleic acids

2.2.2.1 DEPC treatment

When working with RNA samples, all equipment was treated with DEPC to inactivate RNase and solutions were made in DEPC-treated water. For treatment, 0.1% (v/v) DEPC was added and incubated at 37 ℃ for 1 h followed by autoclaving at 121 ℃ for 15 min.

2.2.2.2 Isolation of plasmid DNA

E. coli cells were opened by the alkali treatment and plasmid DNA was purified by binding to a glass matrix in the presence of chaotropic ions using the "DNA extraction Kit" (Promega, Mannheim) according to the manufacturer's instructions.

2.2.2.3 Purification of DNA fragments from agarose gels

DNA fragments obtained after restriction digestion were resolved by agarose gel electrophoresis and purified using "DNA Gel recovery Kit" (Promega, Mannheim) according to the manufacturer's instructions.

2.2.2.4 Acidified phenol method extraction of ribosomal RNA

Thirty ml culture with OD_{600} 0.6 were collected by centrifugation at 5 000 g for 10 min at 4 ℃. The pellet was suspended in 2 ml of acidified phenol saturated by sodium acetate, pH 4.5 at the ratio of 1:1, quickly frozen in liquid nitrogen. Lysis of bacterial cells for rRNA isolation was performed as described with minor modification (Gabig-Ciminska et al., 2004). Lysed cells were thawed at 20 ℃ and frozen at liquid nitrogen for three cycles, then were centrifuged for 15 min at 12,000 g at 4 ℃, supernatant were extracted with 0.7 volume of phenol-chloroform-isoamyl alcohol (25:24:1) and then with same volume of chloroform-isoamylalcohol (95:5) at the amber temperature.

Total ribosomal RNA was precipitated with two volumes of ethanol in 0.3 M sodium acetate, pH 5.2. The precipitates were washed with chilled ethanol (70%), dissolved in water, and stored at -70 ℃. The RNA concentration was determined by absorbance at 260 nm.

2.2.2.5 Mini-preparation of ribosomal RNA

For mini-scale preparation of rRNA, bacteria cells were lysed by lysozyme and total rRNA was isolated by binding to silicon surface of the glass fibers fixed in the spin column using the kit "SV Total RNA Isolation System" (Promega, Mannheim) according to the manufacturer's instructions.

2.2.3 Recombinant DNA techniques

2.2.3.1 Digestion of DNA with restriction endonucleases

Type II restriction endonucleases were utilized to clone DNA-fragments or to analyze recombinant vectors. Thus, the DNA was cleaved within the recognition sequence leading to single-stranded overhangs on both sides (sticky ends). Reaction conditions are adjusted according to the manufacturer's protocol for every given enzyme or set of enzymes. For digestion, 0.1 -0.5 μg of plasmid DNA was digested for 1 h in a volume of 10 μl, with 0.5-1 U of appropriate restriction endonuclease.

2.2.3.3 Cloning of PCR products

PCR products were directly ligated with the pGEM®-T Vector (Promega, Madison, USA) according to the manufacturer's instructions. The ligation reaction was used to transform *E. coli* XL-1 blue competent cells.

2.2.3.4 Ligation of DNA fragments

The formation of phosphodiester bonds between matching sticky ends produced by a type II endonuclease is catalyzed by T4-ligase. The vector of interest was cleaved with corresponding

restriction endonucleases, purified by gel electrophoresis and recovered from the gel as described above. A 50 to 200 ng of the purified vector and a 2 to 100 fold molar excess of insert-DNA with sticky ends were added together with 1 µl of 10 x ligation buffer yielding a typical volume of 9 µl. 1 µl (5 U) of T4-ligase was added and the reaction mixture was incubated at 16 ℃ for 2 h or 4 ℃ overnight.

2.2.3.5 Site-directed mutagenesis of EST2 by overlap extension

pT7-SCⅡ-EST2 plasmid DNA (Manco et al., 1998) was used as template for this PCR amplification. Primer Est-For and Est-Rev contain *Nde* I and *BamH* I restriction sites, respectively. EST2E118C mutant was constructed as following: Est-For and Mut-Rev were used to amplify 5'-fragment of mutant EST2E118C, Est-Rev and Mut-For were used to amplify 3'-fragment of EST2E118C. After recovery of PCR product from Agarose gel, 5'-fragment and 3'-fragment were mixed to approximately equivalent molar concentration as template and Est-For and Est-Rev were used to PCR overlap amplification to obtain EST2E118C whole gene. Final PCR product was cloned into pGEM$^{®}$-T vector and sequenced.

DNA sequencing was done by MWG (Ebersberg, Germany).

2.2.4 Preparation and transformation of competent cells

Rubidium Chloride method for Transformation Competent *E. coli* was used (Inoue et al., 1990). Inoculated 1 ml from overnight culture into 100 ml Psi broth and incubated at 37 ℃ with agitation to A_{550} of 0.48. The culture was immediately placed on ice for 15 min and centrifuged at 3500 g at 4 ℃ for 5 min. The pellet of cells was suspended in 40 ml of ice-cold TfB I buffer and incubated on ice for 15 min before centrifugation again. The supernatant was removed and the pellet of cells was resuspended in 4 ml of ice-cold TfBII buffer. Subsequently, the cell suspension was incubated on ice for 15 min. The aliquots of 100 µl were quickly frozen in liquid nitrogen prior to storage in -70 ℃ freezer.

A 100 µl aliquot of the suspension of competent cells was thawed on ice and 0.1 µg of plasmid DNA or 2-10 µl of ligation reaction mixture was added. The suspension was kept on ice for 30 min, and subsequently heated for 90 sec at 42 ℃ before kept on ice for another 5 min. After

addition of 1 ml LB medium which was preheated to 42 ℃, transformed cells were incubated for 45 min at 37 ℃ with agitation. A 50-200 μl aliquot of the cell suspension was spread on LB agar plates containing appropriate antibiotic and incubated at 37 ℃ incubator for 14-18 h.

For pGEM-T with PCR product ligation, cell suspension mixed with 8 μl of 1M IPTG and 40 μl of 20 mg/ml X-gal in dimethylformamide before spread on LB agar.

2.2.5 Normal PCR and asymmetry PCR

The polymerase chain reaction was performed in a final volume of 50 μl in the DNA Thermal cycler. The reaction mixture contained approximately 5 ng of plasmid DNA (template), 0.2-1 μM primers, 200 μM each dNTP and 2.5 U *Taq* DNA polymerase in 10 mM Tris-HCl pH 9.0, 50 mM KCl, 1.5 mM MgCl$_2$, 0.1 % (v/v) Triton X-100.

Asymmetry PCR was performed at the same condition as standard PCR, except the primer that has the same sequence to protein-ODN reporter, was reduced to only 2% of the other one.

2.2.6 Protein purification

2.2.6.1 Purification of *A. acidocaldarius* EST2 from *E. coli* Bl21(DE3)

Cell extracts were prepared according to (Leberman et al., 1980) with some modifications. The whole procedure was carried out at 4 ℃. Frozen cells of 15 g were suspended in 30 ml of 50 mM Tris/HCl, pH 7.5, 5 mM EDTA, 1mM β-Mercaptoethanol, 5% Glycerin, 5 U DNase I, 1 mM MgCl$_2$ and stirred for 15 min at 0 ℃. The lysis of cells was achieved by ultrasonic cell disruptor B15 (Heinemann, Schwaebish Gmuend) for 2 min on ice. The cell homogenate was centrifuged at 30,000 g for 30 min to remove cell debris. The supernatant was centrifuged at 100,000 g for 3 h to obtain a ribosome-free extract. The supernatant was treated at 60 ℃ for 5 min and centrifuged at 10,000 g for 10 min at 4 ℃; again the supernatant was heat denatured at 65 ℃ for 5 min and 10,000 g for 10 min at 4 ℃ to denature heat sensitive protein and collect the supernatant as the S 100 lysate.

The S 100 lysate was loaded to 1.0 ml of TFK modified Sepharose CL-6B in 1 cm diameter glass column at 0.2 ml/min and washed with 5 ml of 8 M Urea, 50 mM sodium phosphate, 150 mM NaCl, 1 mM DTT, pH 7.5. After that, EST2E118C was eluted with 10 ml elution buffer

(20 mM sodium acetate, 150 mM NaCl, 8 M urea, 1 mM DTT, pH 4.0) and the combined eluate was first dialyzed against 500 ml of 50 mM sodium phosphate, 150 mM NaCl, 4 M urea, 1 mM DTT, pH 7.5 for 2 hour, then transferred to 25 mM Tris-HCl, 100 mM NaCl, 1 mM TCEP, pH 7.5 with two buffer changes. Protein concentration was determined according to the Bradford assay.

2.2.6.2 Preparation and purification of EST2-ODN conjugate

Preparation of EST2-A34 conjugates were performed as follows: 300 μl of 200 μM ODN A34 were dissolved in 100 mM sodium phosphate, 100 mM NaCl, pH 7.3 and incubated 1h with 60 μl of 120 mM sulfo-SMCC dissolved in *N,N*-dimethylformamide. Ethanol precipitation was used to remove the excess of sulfo-SMCC and the precipitates were dissolved in 100 μl of 100 mM sodium phosphate, 100 mM NaCl, pH 7.3. 1 ml of 100 μM EST2E118C was incubated with 5 mM TCEP for 15 min at 37 ℃ to reduce any disulfide bonds formed upon storage. The 100 μl maleimide group activated A34 together with EST2E118C were combined and shook at 20 ℃ for 1h.

The conjugates were purified by anion-exchange chromatography on a MonoQ 5/50 GL column by gradually increasing the NaCl from 0 to 0.7 M. Peak fractions were pooled, concentrated and the buffer was exchanged to storage buffer (50mM Tris-HCl, 100 mM NaCl, 5 mM EDTA, pH 7.5). The concentration of conjugate was determined by Bradford assay.

2.2.6.3 Preparation of EST2-streptavidin conjugate

One ml of 60 μM EST2E118C in 100 mM sodium phosphate, 100 mM NaCl, pH 7.3 was incubated with 5 mM TCEP for 15 min at 37 ℃. Then 150 μl of 20 mM biotin-maleimide in dimethyl sulfoxide was added into and incubated at 37 ℃ for 2 h. Dialysis against PBS was used to remove excess biotin-maleimide. Two ml of 50 % suspension iminobiotin-agarose were washed by 10 ml of 50 mM Na_2CO_3, 500 mM NaCl, pH 11.0, and incubated with 1 ml of 28 μM streptavidin for 30 min with periodic mixing. The resulting agarose•streptavidin conjugates were washed with 5 ml PBS and incubated with EST2-biotin at 20 ℃ for another 30 min. Agarose•streptavidin•biotin-EST2 was washed with 0.1 M NaOAc, pH 4.0 and eluted fractions were collected and dialyzed against PBS. The resultant EST2-biotin•SA conjugate

was characterized by 10% SDS-PAGE. In this report, "-" in EST2-biotin•SA conjugate represents covalent coupling and "•" means streptavidin/biotin high affinity binding.

2.2.7 Chemical synthesis

2.2.7.1 Preparation of trifluoromethyl ketone modified Sepharose

Scheme of preparation of TFK modified Sepharose is shown in Fig. 1.15. Sepharose CL-6B (40 ml) was washed first with 10 volume of ddH₂O and then added to 28 ml of 1 M NaOH containing 57 mg NaBH₄ (1.5 mmol). 1,4-Butanediol diglycidyl ether (5.7 ml, 5.9 g, 29,6 mmmol) was added slowly into stirring mixture. The slurry was swirled at 20 ℃ for about 10 h using an orbital shaker. Then the epoxy-activated resin was washed successively with water, water:methanol (l :l), and water, and then dried under suction. An aliquot of the resin was assayed for free epoxides by adding 1.5 ml of 1.3 M Na₂S₂O₃, pH 7.0 to 0.3 g of the resin followed by back-titration of the resultant base using 0.01 M HCl.

MBTFP was synthesized by reaction of 1,4-dimercaptobutane with equimolar 3-bromo-l,l,l-trifluoroacetone (Prestwich and Hammock, 1985) and used for TFK-modification of epoxy-activated Sepharose as follows:

For 10 g of moist epoxy-activated resin, 10 ml of methano1:0.1 mM NaHCO₃ in H₂O (1:l) was added to obtain pH 8.7-8.9, followed by 10 ml of 40 mM MBTFP in methanol. The slurry was swirled for 24 h at 20 ℃ and then excess of 2-mercaptoethanol was added to inactivate unreacted epoxy groups. The slurry was first washed in a sintered-glass funnel with 20 volumes methanol:water (1:1) and methanol, then followed by 0.5 M NaCl, 1% Lubrol-PX (ethylene glycol monododecyl ether), ethanol:water (1:1) and ethanol successively. Resin was stored at 4 ℃ in absolute ethanol containing a crystal of butylated hydroxyanisole as an antioxidant (Bdel-Aal and Hammock, 1985).

2.2.7.2 Synthesis of p-aminophenyl esters

2.2.7.2.1 Preparation of p-aminophenyl esters

General procedure for acylation of p-nitrophenol was described (Ghosh et al., 2003). Solution of p-nitrophenol (0.2 g, 1.44 mmol) in dry CH₂Cl₂ (7 ml) was treated with pyridine (0.17 g, 0. 17 ml, 2.15 mol) and followed by adding acylchloride (1.44 mmol) dropwisely into the

solution at 0 ℃. Resulting reaction mixture was stirred at 0 ℃ for 1 h before diluted with CH_2Cl_2 (15 ml) and washed with 1 M aqueous HCl (25 ml) and water (25 ml). The organic layer was dried over anhydrous Na_2SO_4, filtered and evaporated under reduced pressure. Crude product was used without further purification in followed reduction step.

General procedure for reduction of p-nitrophenyl esters with modification was described (Ram and Ehrenkaufer, 1984). Crude p-nitrophenyl ester prepared above was dissolved in dry methanol (12 ml) under N_2 atmosphere and the solution was cooled to 0 ℃. 10% palladium on activated charcoal (0.34 g, 0.32 mmol) was added to the solution of p-nitrophenyl ester followed by ammonium formate (1.65 g, 26.2 mmol). The resulting reaction mixture was stirred at 0 ℃ under N_2 for 5 min, and then kept at 20 ℃ for 15 min before diluted with ethyl acetate (20 ml) and filtered through short pad of silica. The filtrate was evaporated under reduced pressure; the resulting residue was redissolved in toluene (40 ml) the insoluble part was removed by filtration. Toluene was evaporated under reduced pressure and crude products were purified by column chromatography on silica gel (n-hexane/ethyl acetate =2.5:1, column 4×15 cm).

2.2.7.2.2 EI-MS and NMR analysis of p-aminophenyl esters

The synthesized p-aminophenyl esters were identified by electroionization mass spectroscopy (Table 2.1). The analysis results are coincident with the expected molecular mass.

Table 2.1 EI-MS of synthesized p-aminophenyl esters

p-aminophenylacetate, $C_8H_9NO_2$, Mol. Wt.: 151.16, EI MS, *m/z* (%): 151 [M]$^+$ (14), 109 (100)

p-aminophenylpropionate, $C_9H_{11}NO_2$, Mol. Wt.: 165.19, EI MS, *m/z* (%): 165 [M]$^+$ (11), 109 (100)

p-aminophenylbutyrate, $C_{10}H_{13}NO_2$, Mol. Wt.: 179.22, EI MS, *m/z* (%): 179 [M]$^+$ (8), 109 (100)

p-aminophenylvalerate, $C_{11}H_{15}NO_2$, Mol. Wt.: 193.24, EI MS, *m/z* (%): 193 [M]$^+$ (20), 109 (100)

p-aminophenylhexanoate, $C_{12}H_{17}NO_2$, Mol. Wt.: 207.27, EI MS, *m/z* (%): 207 [M]$^+$ (21), 109 (100)

p-aminophenyloctanoate, $C_{14}H_{21}NO_2$, Mol. Wt.: 235.32, EI MS, *m/z* (%): 235 [M]$^+$ (21), 109 (100)

NMR analysis of p-aminophenylbutyrate was performed to confirm the substrate structure. ^{1}H and ^{13}C NMR spectra were recorded on Jeol JNM-EX-270-FT-Spektrometer, using tetramethylsilane as internal standard. ^{1}H-NMR (270 MHz, CDCl$_3$): δ = 1.01 (t, 3H, *J* = 7.4 Hz), 1.75 (m, 2H, *J* = 7.4 Hz), 2.48 (t, 2H, *J* = 7.4 Hz), 3.35 (bs, 2H), 6.63 (d, 2H, *J* = 8.6 Hz), 6.84 (d, 2H, *J* = 8.6 Hz); ^{13}C-NMR (90 MHz, CDCl$_3$): δ 13.72, 18.59, 36.28, 115.68, 122.21, 142.97, 144.17, 172.79.

2.2.7.2.3 Analysis of purity and stability of p-aminophenyl esters

Purity and stability of prepared p-aminophenyl esters were carried out on HPLC furnished with RP-column Bio Wide Pore C18 (150 x 4.6 mm) and variable-wavelength detector. Isocratic elution was performed with methanol/ddH$_2$O in different ratio dependent on substrate over 30 min at 1ml/min flow rate and detected at 260 nm. Volume of each injected samples was 20 μl. For p- aminophenyloctanoate MeOH/H$_2$O=80/20 was used, for p-aminophenyl -butyrate, -valerate and -hexanoate MeOH/H$_2$O was 60/40, p-aminophenylpropionate was analyzed with MeOH/H$_2$O=40/60 and for p-aminophenylacetate was used MeOH/H$_2$O=30/70.

2.2.8 SDS-PAGE gel esterase activity staining

SDS gels after protein renaturation were stained for esterase activity as described (Higerd and Spizizen, 1973). In brief, gels of 0.75 mm x 8 cm x 12 cm were incubated in 100 ml of 100 mM Tris-HCl, pH 7.5, containing 5 mg of β-naphthylacetate (dissolved in 0.5 ml of acetone) and 25 mg of Fast Blue BB salt at 20 ℃. Reactions were stopped after 5-10 min by rinsing with tap water.

2.2.9 Chip construction and instrumentation

Electrical chip and instrumentation used are as described (Nebling et al., 2004) with minor modification. Each chip (11x13 mm) consisted of 8 individual 0.85 mm diameter (0.6 mm^2) electrodes with spaces of 2.0 mm to the next positions. For measurement, as shown in Fig. 2.1, the printed circuit board of the chip was connected to multipotentiostat device through physical contact. The potentiostat was connected to a PC through a serial interface SCB-68. The four reference electrodes were short-circuited and a ±200 mV potential was applied to working electrode via reversible potentialstat. Software Labview 6.0 (National Instrumentations, Munich) was applied to control the potentiostat, collect the data and plot figures. In each second, a +200 mV potential was applied during the 250 ms oxidization step and a -200 mV potential was applied for the rest 750 ms reduction stage. The data were collected with 1 data point/sec at the beginning of reduction step.
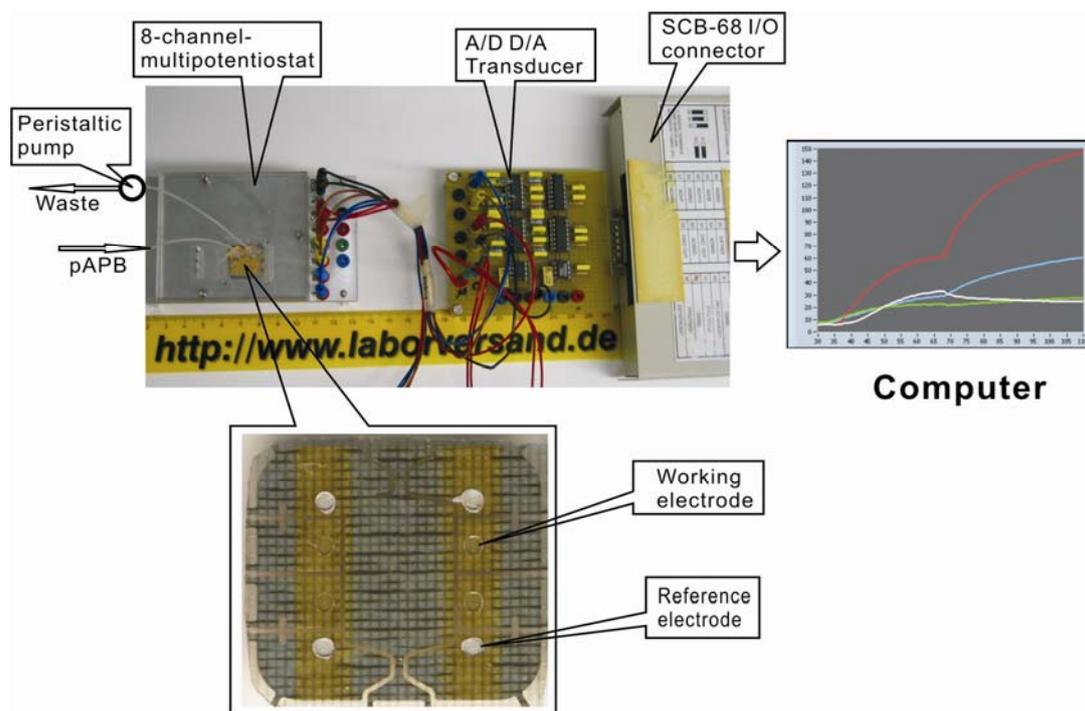
Fig. 2.1 Photograph and scheme of the electrical chip and its measuring system. A/D D/A transducer is analogue/digital, digital/analogue transducer, I/O represents input/output, and pAPB is p-aminophenylbutyrate flow. The SCB-68 is a shielded I/O connector block for interfacing I/O signals to plug-in A/D D/A transducer.

2.2.10 Esterase activity and kinetics spectrophotometer measurements

2.2.10.1 Esterase activity assay by spectrophotometer

Activity determination was performed as described (Manco et al., 1998) with minor modifications. The time course of the esterase catalytic hydrolysis of p-nitrophenyl esters was followed by monitoring the product p-nitrophenol at 405 nm in 1 cm pathlength cells with a double beam in spectrophotometer. The rate of spontaneous hydrolysis of the substrates was deducted by using a reference sample of identical composition to the incubation mixture except that esterase was omitted.

For standard EST2 assay, solutions containing EST2 and substrate were prepared by mixing 980 µl certain concentration of EST2 in 100 mM sodium phosphate, pH 7.1 with 20 µl of 10 mM p-nitrophenylbutyrate dissolved in acetonitrile. Esterase activity assays were determined at 20 ℃ after 1 min.

For assay of substrate specificity of EST2, solutions containing EST2 and substrate were prepared by mixing 980 µl of 5 nM EST2 in 100 mM sodium phosphate, pH 7.1 with 20 µl of

10 mM different p-nitrophenyl esters dissolved in acetonitrile. Esterase activities were registered at 20 ℃ after 1 min.

2.2.10.2 Kinetic parameters measurement by spectrophotometer

For determination of kinetic properties, absorbance at 405 nm (A_{405}) of 5 nM EST2 in 100 mM sodium phosphate, pH 7.1 according to different concentration of p-nitrophenylacetate was measured. Initial rates were calculated by linear least squares analysis of time courses comprising less than 10% of the total substrate turnover. Initial velocity versus substrate concentration data were fitted to the Lineweaver-Burk transformation of the Michaelis-Menten equation, by weighted linear least-squares analysis with a personal computer and the origin program.

2.2.11 Amperometric detection of EST2

2.2.11.1 p-Aminophenol measurement

For current calibration curve of p-aminophenol, solution of p-aminophenol from 5 to 500 μM in 100 mM sodium phosphate, pH 7.1 were prepared and pumped through E-Chip at a flow rate of 0.2 ml/min. The resultant current value versus concentration of p-aminophenol was plotted as a standard curve.

2.2.11.2 Determination of soluble esterase activity

Time course of the soluble esterase catalytic hydrolysis of p-aminophenyl ester was followed by monitoring current signal of p-aminophenol in E-Chip. In standard EST2 amperometric assay, 980 μl of 5 nM EST2 in 100 mM sodium phosphate, pH 7.1 mixed with 20 μl of 10 mM p-aminophenylbutyrate dissolved in acetonitrile was flowed through E-Chip at 0.2 ml/min at 20 ℃. The current signal after 1 min was determined. The background hydrolysis of the substrate was deducted by using a reference sample of identical composition to the incubation mixture except EST2 was omitted.

For substrate specificity of soluble EST2, 980 µl of 5 nM EST2 in 100 mM sodium phosphate, pH 7.1 mixed with 20 µl of 10 mM different p-aminophenyl esters dissolved in acetonitrile. Other procedures are the same as the standard EST2 amperometric assay protocol.

2.2.11.3 Measurement of substrate specificity of immobilized esterase

EST2 was immobilized on surface of gold electrode by hybridization of EST2-A34 (esterase 2–ODN conjugate) to its complementary capture ODN-P, which had been assembled on gold electrode surface (M&M 2.2.12). Upon conjugate hybridization and after cleaning the chip for 3 times with 100 µl washing buffer, the printed circuit board of the chip was connected to multipotentiostat device as shown in Fig. 2.1. Subsequently, solutions of 1 mM p-aminophenyl esters in 100 mM sodium phosphate, pH 7.1 were delivered to chamber of E-Chip at 0.2 ml/min at 20 ℃. Different p-aminophenyl esters solutions were applied to the same chip successively. The increased current of "Steady State current" and value of "Slope" from the first 5 sec under stopped-flow mode were determined separately.

2.2.12 Pretreatment of electrodes and immobilization of capture ODN

Gold electrodes were immersed in ethanol for 5 min, rinsed by deionized water and dried by 0.2 µm filtered air stream. For immobilization of thiolated capture ODNs, a thiol-gold interaction at gold surfaces was used. One µl of 0.2 µM capture ODN in immobilization buffer were spotted onto electrodes and then incubated at 20 ℃ for 30 min before rinsed by ddH$_2$O. DNA immobilization and following hybridization procedures were always performed in humidity chamber.

2.2.13 E-Chip detection of nucleic acids

2.2.13.1 Low limit of detection

For binding of EST2-A34 conjugates to immobilized captures, 1 µl of 20 nM EST2-A34 in hybridization buffer was applied onto each electrode and incubated for 30 min at 50 ℃. Afterwards, the chip was washed three times with washing buffer.

For estimation of detection limit, after stepwise dilution of EST2-A34 with hybridization buffer, 0.5 µl of diluents were applied onto each electrode that had been immobilized with the capture ODN-P, and incubated for 30 min at 20 ℃, and then chip was washed thrice with 100 µl washing buffer.

2.2.13.2 Directly detection of mismatched capture ODN

For determination of mismatch selectivity among immobilized captures, 1 µl of 100 nM EST2-A34 in hybridization buffer was incubated with electrodes, which had been immobilized with Capture PM, MM-13, MM-7 and MM-4 respectively, for 30 min and washed three times with 100 µl of washing buffer before measurement. To detect mismatches by ODN biotin-34, 1 µl of 100 nM biotin-34 in hybridization buffer was dropped onto electrodes and incubated for 30 min, followed by three times 100 µl washing buffer. Afterward, they were exposed to a 400 nM EST2-biotin•SA in hybridization buffer for 30 min and washed thrice with 100 µl washing buffer.

In order to investigate the effect of salt to duplex stability, an additional 20 min, three times washing steps with 30 mM NaCl, 10 mM Tris-HCl, pH 8.0 was performed.

2.2.13.3 Detection of 49-mer ODN analyte

Capture CM was immobilized on gold surface of electrode as described. Then 1 µl of 100 nM EST2-A34 conjugate in hybridization buffer mixed with 20 nM target ODN 1MM, 2MM, 3MM (sequence in M&M 2.1.7.2) and dropped onto electrode. After 20 min hybridization and washing procedure, the chip was ready for measurement.

2.2.13.4 Detection of a mismatch in a 510-nucleotide partial gene

To detect PCR product, 1 µl of 13 nM ssDNA of 510-nucleotide EF-Ts (elongation factor Ts, RiNA GmbH, Berlin) together with 100 nM EST2-A34 in hybridization buffer were applied onto electrode immobilized capture and incubated at 20 ℃ for 30 min. Subsequently three washing steps were applied to remove abundant ssDNA and reporter.

2.2.13.5 Identification of bacterial species through 16S rRNA sequence

Total rRNA including 23S, 16S and 5S were extracted from bacteria and quantified spectrophotometrically. A 4.9 μl of total RNA mixed with 0.7 μl of 50 μM Helper-1 and Helper-2 mixture and 1.4 μl of 150 mM Mg(OAc)$_2$, 500 mM KOAc, 200 mM Tris-acetate, pH 8.1 was incubated at 95 ℃ for 10 min, then cooled down at 20 ℃ for 5 min. After fragmentation, 3 μl fragmented rRNA sample, 4 μl of 900 mM NaCl, 0.1% Tween-20, 50 mM EDTA, 4 mg/ml BSA and 60 mM NaH$_2$PO$_4$, pH 7.4, and 1 μl of 2 μM EST2-U1082 conjugates were mixed and 1 μl of the mixture were applied onto each electrode. Hybridization was performed at 65 ℃ for 20 min in humid chamber before chip was transferred to 20 ℃ for 5 min for annealing. Finally the chip was washed with 100 μl washing buffer for three times.

2.2.13.6 E-Chip EST2 activity assay

After hybridization and washing steps, the chip was fixed onto the multipotentiostat device as shown in Fig. 2.1, and 1 mM pAPB in 100 mM sodium phosphate, pH 7.1 was delivered to chamber at 0.2 ml/min for 1 min. Current slope after pump stopped was used to assay the EST2 enzymatic activity. It was assumed slope value is proportional to the amount of analyte on the measured positions.

2.2.14 Magnetic beads assisted preparation of ssDNA

Biotinylation of DNA was done during the PCR by the biotinylated primer EFTS-F and the whole length of dsDNA was 534 bp including 24 nucleotides complement to A34. The biotinylated dsDNA was directly incubated with pretreated 20 μl magnetic beads in binding and washing buffer (20 mM Tris-HCl, 1 mM EDTA, 2 M NaCl, pH 7.5) at 20 ℃ for 30 min, then washed thrice with binding and washing buffer and the beads were collected with external magnets. A 50 μl 0.3 M NaOH was applied to beads and incubated for 5 min before the supernatant was removed. The final beads were washed twice by binding and washing buffer and 25 μl of water was incubated with beads at 95 ℃ for 5 min to dissociate biotinylated ssDNA from the beads. The final ssDNA was analyzed by agarose gel electrophoresis, and the

concentration was assumed to be 0.2 μM (derived from the original primer EFTS-F concentration 0.2 μM).

2.2.15 Modification of stem-loop structured ODN with 5' thiol and 3' biotin

Stem-loop structured ODN (Molecular beacon) CMB442 (all ODNs sequence related with molecular beacon assay are listing in M&M 2.1.7.4) was synthesized with double modification, 5'-amino-T and 3' ribo-A (Fig. 2.2). 20 μL of 100 μM CMB442 was mixed with 30 μL of 100 mM sodium phosphate, pH 8.6 and the resultant solution was added with 10 μL of 10 mM N-succinimidyl 3-(2-pyridyldithio)-propionate in *N,N*-dimethylformamide. Reaction mixture was incubated at 20 ℃ for 30 min. Product was isolated by ethanol precipitation, dissolved in 20 μL ddH$_2$O and added with 20 μL of 20 mM NaIO$_4$. Then the reaction mixture was incubated in the dark at 4 ℃ for 40 min. 10 μL of 100 mM Na$_2$S$_2$O$_3$ was added to remove excess of periodate and the reaction mixture was incubated for 30 min at 37 ℃. After addition of 10 μL of 30 mM biotin hydrazide (Liang et al., 2005), incubation was continued for 1 h at 37 ℃ before product purified by ethanol precipitation. The final product was analyzed by HPLC analysis on C18 column to confirm the double modification.

2.2.16 Construction and hybridization assay of stem-loop structured ODN

Construction of stem-loop structured ODN on electrode of electrical chip is illustrated in Fig. 2.3. One μl of 10 μM CMB442 ODN in 20 mM sodium phosphate, 300 mM NaCl, 2 mM TCEP, pH 7.4 was applied to each electrode for 1 h before rinsed by ddH$_2$O. 1 μl of 1 mM of *tert*-dodecylmercaptan solution was used to construct monolayer for shielding biotin label. Afterwards, chip was washed by hot water for five times and incubated with 4xSSPE at 20 ℃ for 5 min. A 0.5 μl of 500 nM of ODN T442-59 or T442-Ex solution in 4xSSPE was incubated with electrodes 30 min at 20 ℃. Then chip was washed by 100 μl of chilled 0.5xSSPE with 0.05% Tween 20 for three times. One μl of 100 nM EST2-biotin•SA in 2xPBS with 0.1% BSA was applied for 10 min at 4 ℃, then washed by chilled 0.5xSSPE with 0.05% Tween 20 for three time. The chip was ready for measurement.
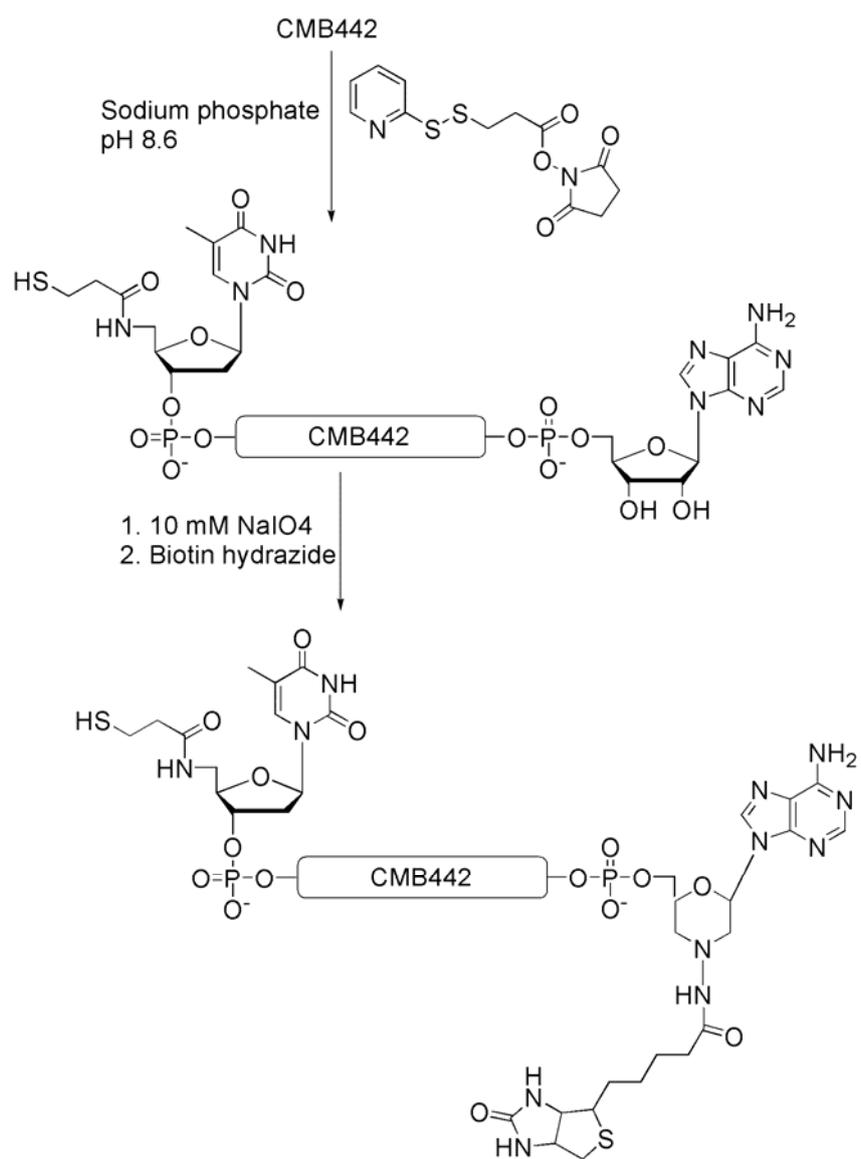
Fig. 2.2. Scheme of preparation of 5'-thiol and 3'-biotin double modified, stem-loop structured ODN.
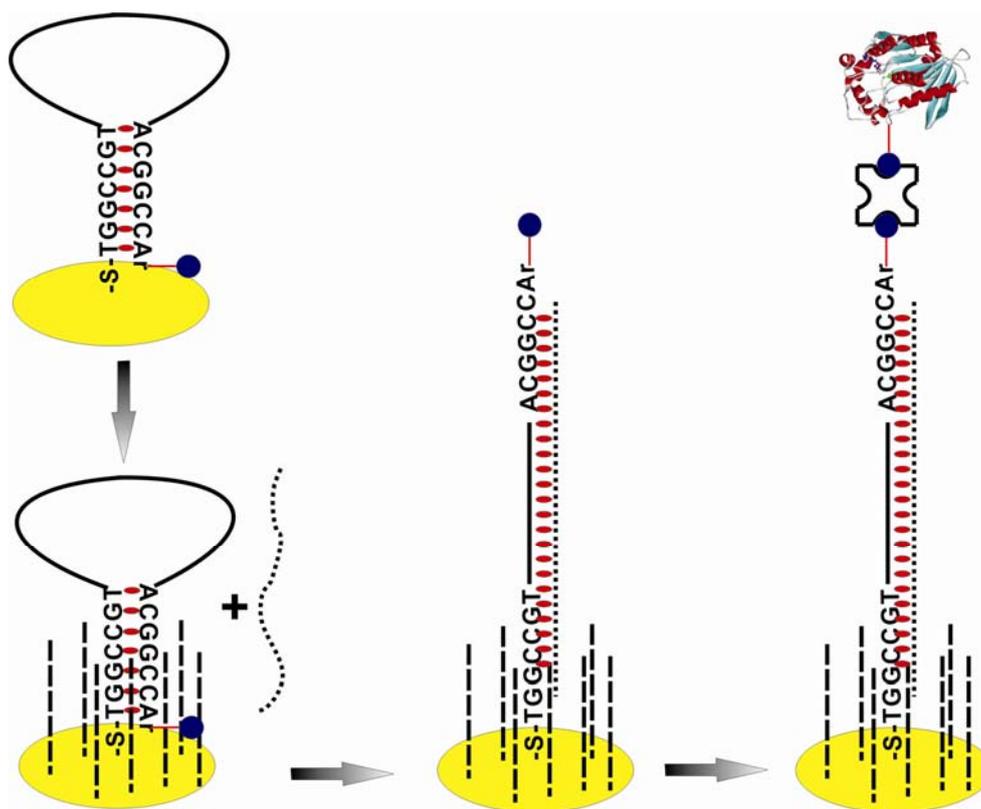
Fig. 2.3. Principle and construction of chip based molecular beacon. A stem-loop structured ODN CMB442 possessing 5'-thiol and 3'-biotin group is immobilized at a gold electrode through gold-thiol self-assembling. In the absence of target, the stem–loop structure holds the biotin label into close proximity with the electrode surface and shielded by *tert*-dodecylmercaptan monolayer, thus biotin is not accessible to EST2-biotin•SA reporter. In the case of target binding, the stem-loop structure opens and biotin label releases from the shield of *tert*-dodecylmercaptan monolayer, making the label available for enzyme binding.

3. Results

3.1 Purification and biochemical properties of EST2, and synthesis and amperometric characterization of its electrochemical substrate

3.1.1 Construction of EST2 mutant plasmid and its expression

Wild-type EST2 contains only one cysteine at the 97th codon (Table 1.1) buried inside of the structure which is therefore inaccessible for chemical modification (data not shown). Site-directed mutagenesis was used to substitute Cys for Glu at 118th codon, which is supposed to be present on the surface according to X-ray analysis of crystal structure (De Simone et al., 2000).

This mutant esterase 2 referred to as EST2E118C, was ligated in pET-30a (M&M 2.2.3.5) to obtain the expression vector pET-30a-EST2E118C (Fig. 3.1). The proper plasmid construct was verified by DNA sequencing using universal primer T7 terminator, which shows that GAG (Glu118) was successfully mutated to TGC (Cys118) (Fig. 3.2).
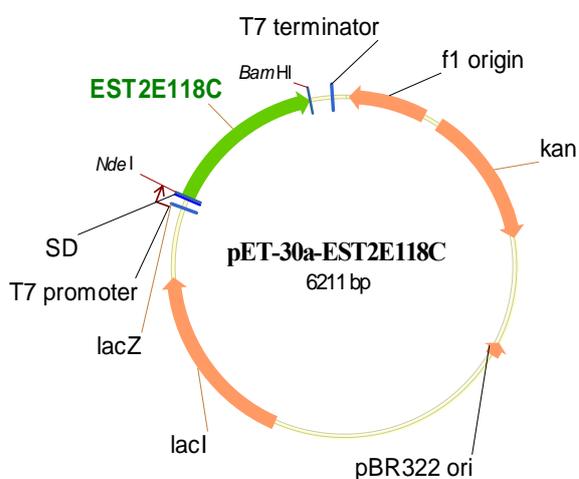
Fig. 3.1. Map of the constructed expression vector for expression of *A. acidocaldarius* EST2E118C.
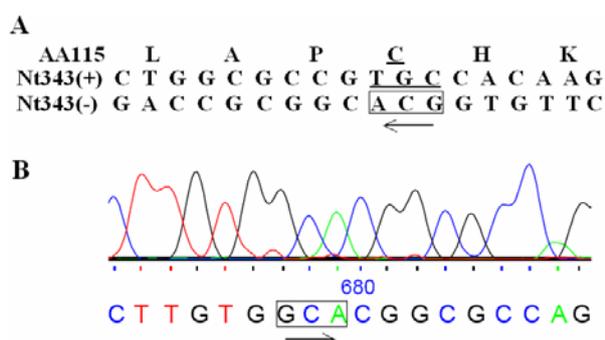
Fig.3.2. Partial DNA sequence of EST2E118C gene. (A) The expected partial nucleotide and amino acid sequence. (B) The DNA sequencing result using universal T7 terminator primer. The underlined and boxed nucleotides are corresponding to codon triplet of 118th amino acid. AA115 means the partial amino acid sequence starting from the 115th amino acid of EST2; Nt343 is the partial nucleotide sequence starting from the 343th of 930 nucleotides of EST2. (+) and (-) represent plus strand and negative strand of dsDNA, respectively. Arrows show the sequence reading direction (from 5' to 3').

3.1.2 TFK-Sepharose purification of EST2E118C from *E. coli* Bl21(DE3)

Expression and purification of EST2 from *A. acidocaldarius* were performed as described in M&M 2.2.1.3 and M&M 2.2.6.1. Fractions from different chromatography steps were resolved by SDS-PAGE and only the elution fractions containing the highest concentration of EST2 (Fig. 3.3) were pooled and dialyzed to refold the denatured protein.
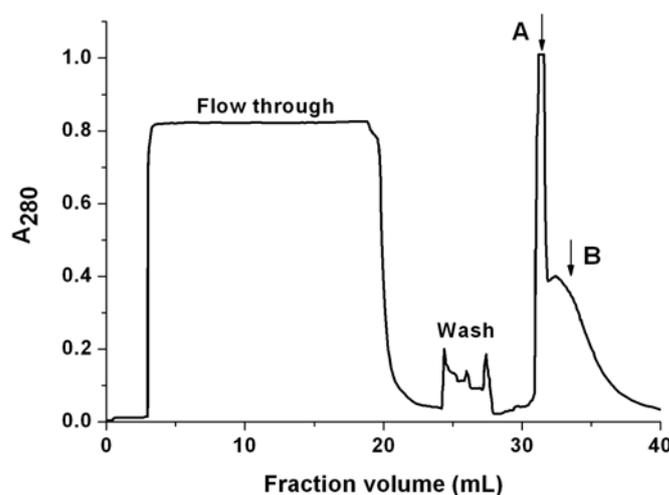
Fig. 3.3. Profiles of affinity chromatography of *A. acidocaldarius* EST2E118C from *E. coli* Bl21 (DE3) on TFK-Sepharose column. A_{280} is the spectrophotometer absorbance at 280 nm. Peaks labeled with arrows A and B are the elution peak containing most EST2. The peak labeled with "Flow through" contains proteins which did not bind to the column. Peaks labeled with "Wash" is the washed step with 8 M urea, 150 mM NaCl, 1 mM DTT and 50 mM sodium phosphate, pH 7.5. Peaks with arrow A and B are esterase eluted by 8 M urea, 150 mM NaCl, 1 mM DTT and 20 mM NaOAc, pH 4.0.

As depicted in Fig. 3.3, a small peak was observed under washing condition of 8 M urea, 150 mM NaCl, 1 mM DTT and 50 mM sodium phosphate, pH 7.5. However, most protein was eluted by 8 M urea, 150 mM NaCl, 1 mM DTT and 20 mM NaOAc, pH 4.0. This implies the specific binding of EST2 to TFK-Sepharose.

After refolding of esterase by dialysis, the dialysate appeared cloudy and a centrifugation step was used to separate native enzyme from insoluble probably partially-folded molecules. The SDS-PAGE analysis of representative sample of each purification step is shown in Fig. 3.4 and the purification procedure is summarized in Table 3.1. The enzyme was purified with a 5.8% final yield using 1 ml of TFK-Sepharose resin and purification factor (ratio of purified EST2 specific activity to EST2 specific activity in S 100 lysate) of 7.6 and 7.7 in peak A and peak B after a single-step chromatography, respectively.

As shown in lane 1 of Fig. 3.4, a high level of expression of EST2E118C was achieved with pET-30a/Bl21(DE3) expression system and it can be easily visualized on SDS gel with Coomassie Brilliant blue staining. This was an improvement compared to the original EST2WT expression in pT7-SCⅡ-EST2 vector (Manco et al., 1998), which was barely detectable using a western-blot.
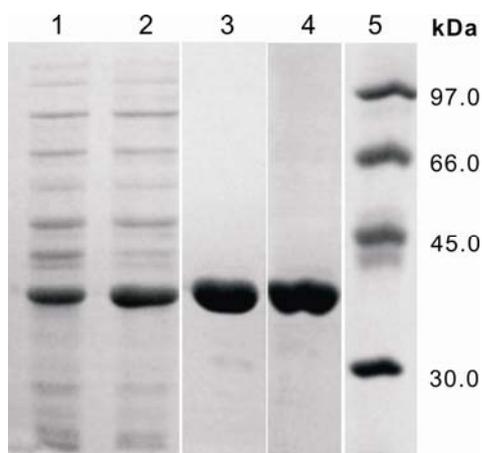
Fig. 3.4. 10% SDS-PAGE gel of EST2E118C purification by TFK ligand affinity chromatography. Lane 1, S 100 lysate sample; lane 2, flow through sample; lane 3, sample of elution peak A; lane 4, sample of elution peak B; lane 5, protein molecular mass marker. Gel was visualized by Coomassie Brilliant Blue G250 staining.

Table 3.1 Purification scheme for recombinant *A. acidocaldarius* EST2

Sample	Total protein	Total activity	Specific activity*	Purification
	(mg)	(units)	(units/mg)	(fold)
S 100	1604.5	237706	148.1	1.0
Elution peak A	0.9	1068	1124.4	7.6
Elution peak B	11.1	12674	1146.3	7.7

* One unit is defined as the amount of EST2 that produces 1 μmol of p-nitrophenol in 1 min at 20 ℃ in 100 mM sodium phosphate, pH 7.1 containing 0.2 mM p-nitrophenylbutyrate.

3.1.3 Kinetic characterization of EST2E118C

To investigate the effect of substitution Cys for Glu at 118th codon on the esterase 2 activity, enzymatic kinetic parameters of EST2E118C and EST2WT (purified by the same scheme as EST2E118C) were determined spectrophotometrically in solution by published procedure (Manco et al., 1998). Michaelis constant K_m and catalytic efficiency k_{cat}/K_m at the applied condition are summarized in Table 3.2. K_m and k_{cat} were in the same order of magnitude

compared with the wild type enzyme, differing at most by a factor of 1.5 in the relative k_{cat}/K_m. The introduction of cysteine at 118th codon position did not therefore significantly change the activity of the enzyme.

Table 3.2 Kinetic parameters of EST2WT and EST2E118C on p-nitrophenylacetate

Enzyme	V_{max} (M*min^{-1})	K_m (M)	k_{cat} (min^{-1})	k_{cat} /K_m (M^{-1}*min^{-1})
EST2WT	1.51×10^{-5}	3.52×10^{-4}	1.83×10^{3}	8.81×10^{6}
EST2E118C	9.48×10^{-5}	1.59×10^{-3}	8.94×10^{3}	5.60×10^{6}

3.1.4 Detergent effect and substrate specificity of EST2

3.1.4.1 Effects of detergents to the activity of EST2

The effects of detergents on the activity of EST2 were investigated. EST2 at 5 nM concentration solution was incubated for 5 min in the presence of different detergents and the remaining EST2 activities were spectrophotometrically determined (M&M 2.2.10.1). As shown in Table 3.3, 0.01% SDS and 0.1% CTAB led to almost complete loss of the enzymatic activity, while 0.1% Triton X-100 and Tween-20 did not exhibit inhibitory effect.

Table 3.3 Effects of various detergents on the activity of *A. acidocaldarius* EST2

Agent	Agent final concentration	Residual EST2 activity
No agent	0	100%
SDS	0.01%	1%
Triton X-100	0.1%	141%
Tween 20	0.1%	121%
Ficoll 400	0.1%	80%
CTAB	0.1%	3%

* Standard errors were less than 5%; ** All reaction conditions except agent concentration were constant; ***Esterase activity measured in the absence of any agent was taken as 100%.

3.1.4.2 Substrate specificity of EST2

EST2 can hydrolyze a variety of esters albeit with different specificity. To achieve highest sensitivity and best reproducibility from EST2 as a reporter enzyme, the suitable substrate that fit the demand of detecting trace amount of EST2 was expected. Outcome of p-nitrophenyl esters' specificity to EST2 in solution is shown in Fig. 3.5 following a procedure in M&M 2.2.10.1. Among six tested p-nitrophenyl esters, p-nitrophenyl -butyrate, -valerate and -octanoate were the optimal substrates to EST2, showing approximately 9 to 11 folds higher activity than that of p-nitrophenylacetate. Moreover, considering the background signal, caused by the spontaneous hydrolysis of the substrate, p-nitrophenylbutyrate was chosen as optimal EST2 substrate in this study. The strongly differing specificity of substrates on EST2 activity gives a good hint for further development of optimal electrochemical active substrates and indicates one further avenue to optimize the signal-to-noise ratios in the detection process.
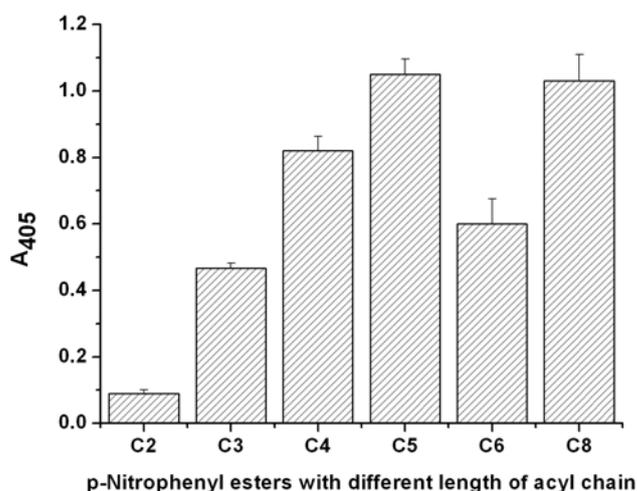
Fig. 3.5. Results of the spectrophotometeric analysis of substrate specificities for *A. acidocaldarius* EST2. A_{405} is the spectrophotometer absorbance at 405 nm. p-Nitrophenyl -acetate (C2), -propionate (C3), -butyrate (C4), -valerate (C5), -hexanoate (C6), and -octanoate (C8) correspond to p-nitrophenyl ester with acyl chain length of 2, 3, 4, 5, 6 and 8 carbons, respectively. In this assay, all reaction conditions except substrate were constant. Shown are increases in signal in 1 min.

3.1.5 Synthesis and stability of p-aminophenyl esters

3.1.5.1 Synthesis of p-aminophenyl esters

p-Nitrophenyl esters for spectrophotometrical determination of esterase activities are commercial available. However, the development of electrochemical substrates based on p-aminophenyl esters, was required for E-Chip system. Details of synthesis of p-aminophenyl

esters are described in M&M 2.2.7.2 and the simplified scheme is shown in Fig. 3.6. p-Aminophenyl esters (3a-3f) were finally purified by chromatography on Silica gel with 68-79% overall yields from starting material, p-nitrophenol. Compounds 3a-3f correspond to p-aminophenyl -acetate, -propionate, -butyrate, -valerate, -hexanoate and -octanoate, respectively. (All the p-aminophenyl esters used in this study were synthesized by Dr. Humenik)
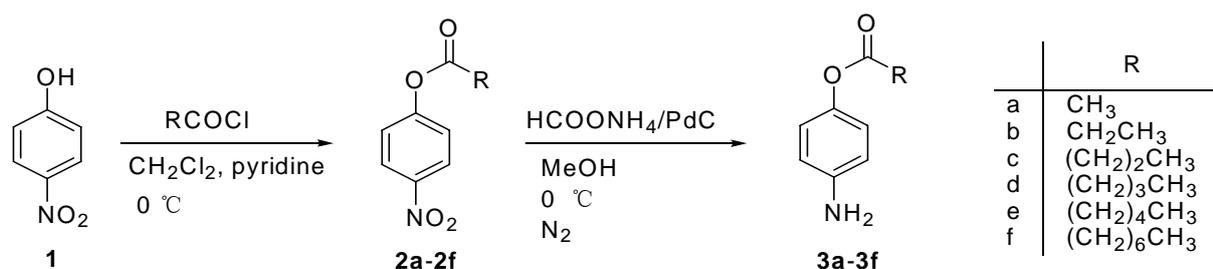
Fig. 3.6. Scheme of synthesis of p-aminophenyl esters. PdC is 10% Palladium on activated charcoal.

3.1.5.2 Analysis of the stability of p-aminophenyl esters

Sample purity was determined by HPLC analysis of 10 mM of p-aminophenyl esters in methanol (M&M 2.2.7.2.3) and summarized in Table 3.4. The main impurity of the product was p-aminophenol (Table 3.4). However, the purity of p-aminophenyl esters was around 97-99%.

Table 3.4 Purity of p-aminophenyl esters determined by HPLC

Substrate	Content of p-aminophenyl ester (%)	Content of p-aminophenol (%)
p-aminophenylacetate	98.7	0.72
p-aminophenylpropionate	99.4	0.29
p-aminophenylbutyrate	99.7	0.25
p-aminophenylvalerate	99.2	0.67
p-aminophenylhexanoate	98.2	1.45
p-aminophenyloctanoate	97.5	1.11

Sample stability was tested by incubation of 10 mM p-aminophenyl ester dissolved in 100 mM sodium phosphate, pH 7.1 for different time at 20 ℃ as shown in Fig. 3.7 and immediately

analyzed by HPLC (M&M 2.2.7.2.3). This pH was chosen based on the optimal esterase activity (Manco et al., 1998) and satisfying stability against hydrolysis of p-aminophenyl esters (Pariente et al., 1993).

The result is summarized in Fig. 3.7. It revealed that the stability of esters was influenced by carbon chain length. The shorter the ester chain, the lower stability was observed, i.e. p-aminophenyl -acetate, -propionate and -butyrate (Fig. 3.7). The most stable p-aminophenyl ester was p-aminophenylvalerate. p-Aminophenyloctanoate was observed to have obviously increased spontaneous hydrolysis rate of ester bond accompanied by decreased solubility, as revealed by the appearance of turbidity. In fact, substrates p-aminophenyl -propionate, -butyrate and -valerate under testing condition appeared no substantial change of their contents in 60 min (Fig. 3.7), underlying the expected stability against spontaneous hydrolysis.
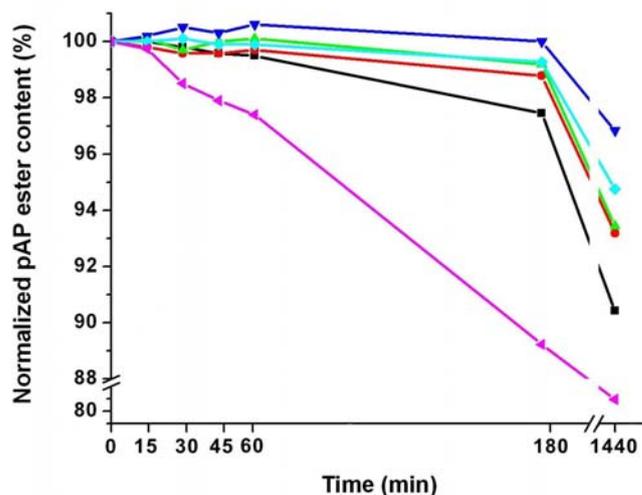
Fig. 3.7. Stability of p-aminophenyl esters in 100 mM sodium phosphate, pH 7.1. The content of p-aminophenyl esters at 0 min were set as 100 %. The incubation time is indicated in x-axis. The different curves represent stability results of p-aminophenyl -acetate (—■—), -propionate (—•—), -butyrate (—▲—), -valerate (—▼—), -hexanoate (—•—) and -octanoate (—◄—), respectively.

3.1.6 Amperometric detection of EST2

3.1.6.1 Effect of various solvents to the activity of EST2

For the most enzymatic assays, substrates are prepared and stored as concentrated stock solution, and diluted to a proper varying concentration just prior to use. For p-aminophenyl esters, organic solvents are used to increase the solubility and storage stability. However, even

so the final concentration of organic solvent is relatively low (2% v/v), which could affect the enzymatic activity.

Five commonly used solvents were investigated to a final 2% (v/v) in EST2 solution. Solutions containing EST2 and substrate were prepared by mixing 980 μl of EST2 at 1 nM concentration in 100 mM sodium phosphate, pH 7.1 with 20 μl of 10 mM p-aminophenylbutyrate dissolved in different solvents. The solutions were immediately pumped into measurement chamber at a flow rate of 0.2 ml/min and the resulting electrochemical signals were registered. All reaction parameters except the nature of the initial solvent remained unchanged (Fig. 3.8). The highest signal was obtained in the presence of acetonitrile. In one min, the presence of acetonitrile in enzymatic reaction mixture gave 5 times more current than that of ethanol did.
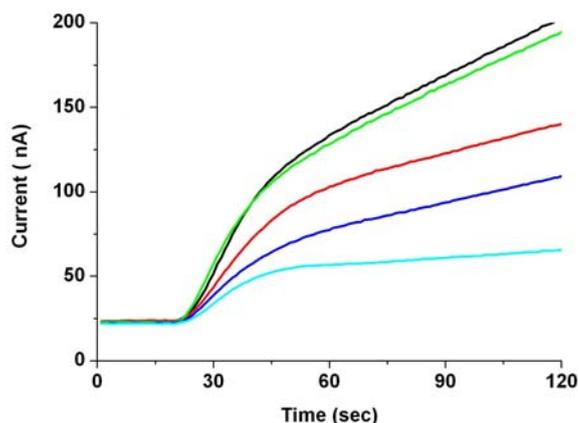
Fig. 3.8. Effect of various solvent to the activity of EST2. Different curves represent the influencing of acetonitrile (——), dioxan (——), dimethyl formamide (——), dimethyl sulfoxide (——) and ethanol (——) used to prepare the p-aminophenylbutyrate respectively.

In a preliminary experiment, however, 1 mM p-aminophenol in 100 mM sodium phosphate, pH 7.1 in presence of 2% of different solvents presented approximately the same current signal (data not presented). This indicates that solvents themselves did not contribute to the signal variance. The highest signal achieved (Fig. 3.8) in the presence of acetonitrile is due to the improved catalytic efficiency of EST2.

Therefore, acetonitrile was utilized as solvent to prepare its substrates in all EST2 activity assays carried out in this study.

3.1.6.2 Substrate specificity of soluble EST2

The enzymatic activity of EST2 exploiting p-aminophenyl ester substrates can be followed by amperometric detection (M&M 2.2.11.2). The current resulting from the EST2 catalytic hydrolysis of different p-aminophenyl esters were determined as shown in Fig. 3.9. Obviously, the commonly used p-aminophenylacetate is not the best substrate for *A. acidocaldarius* EST2.

As shown in Fig. 3.5, p-nitrophenylhexanoate did not exhibit highest activity to EST2, the reason is not clear. It was observed that the rate of spontaneous hydrolysis of p-nitrophenylhexanoate was obviously higher than that of other p-nitrophenyl esters. However, this is not the case for p-aminophenylhexanoate, it appeared highest activity to soluble EST2 while has almost the same rate of spontaneous hydrolysis (Fig. 3.7). Probably the more stable ester bond of p-aminophenylhexanoate than that of p-nitrophenylhexanoate is responsible for the change.
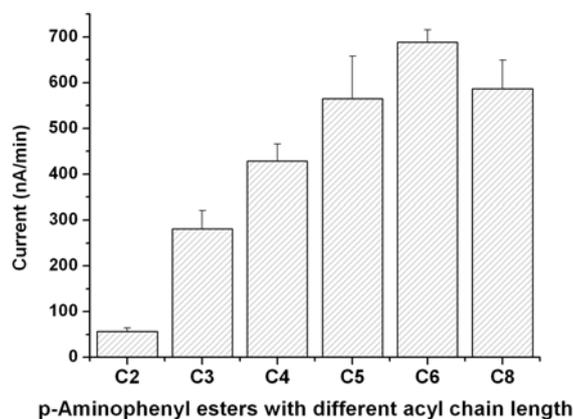
Fig. 3.9. Electrochemical active substrate specificity of soluble EST2. p-Aminophenyl -acetate (C2), -propionate (C3), -butyrate (C4), -valerate (C5), -hexanoate (C6), -octanoate (C8) are corresponding to p-aminophenyl ester with acyl chain length of 2, 3, 4, 5, 6 and 8 carbons, respectively. In this assay, all reaction conditions except substrate were constant. Shown are current signals in 1 min from three measurements with standard deviation.

3.1.6.3 Substrate specificity of immobilized EST2

The main purpose of this work is to detect target nucleic acids through solid-phase hybridization. EST2 was brought to vicinity of the solid-surface upon hybridization in the initial experimental design, and the immobilized EST2 began to catalyze hydrolysis of p-aminophenyl esters. However, there were variant responses from soluble EST2 with different

acyl chain length of p-nitrophenyl/aminophenyl esters. Moreover, being immobilized by hybridization on a gold-coated surface of electrode, the complexity of enzymatic catalysis procedure increased. To select an optimal substrate under this confined condition, the responses of immobilized EST2 to different p-aminophenyl esters were investigated according to M&M 2.2.11.3. This method was based entirely on the fact that, double-stranded DNA hybrid on surface were stable during the whole measurement and EST2 itself was reusable without obvious loss of enzymatic activity under applied conditions.

The results are shown in Fig. 3.10. The "steady-state current" and value of "slope" are decided by p-aminophenyl esters affinity to EST2 and the diffusion rate to the immobilized EST2. The latter is more accurate to quantify nucleic acids in the case of solid-phase hybridization, due to the better signal-to-noise ratio (Nebling et al., 2004).

Substrate	Steady State current (nA)	Slope (nA/sec)
pAPA	18.5	0.10
pAPP	37.4	0.17
pAPB	38.2	0.65
pAPV	49.2	0.63
pAPH	92.7	0.73
pAPO	55.6	0.37
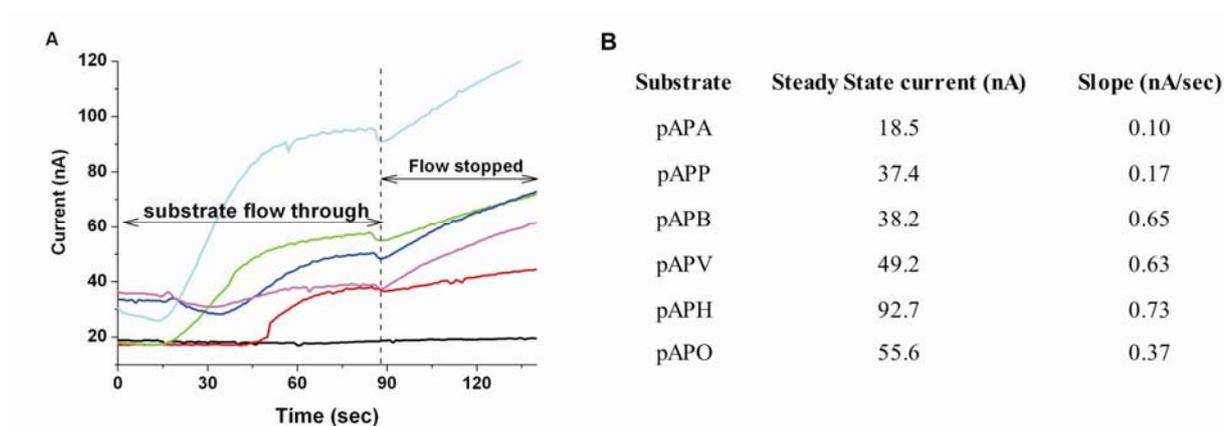
Fig. 3.10. Substrate specificity of immobilized EST2 on electrical biochip. (A) Signals registered and (B) Comparative analysis results from the immobilized EST2's response to different p-aminophenyl esters. The substrate flow were applied successively according to the following sequence: p-Aminophenyl - acetate (pAPA ——), -propionate (pAPP ——), -octanoate (pAPO ——), -valerate (pAPV ——), -hexanoate (pAPH ——) and -butyrate (pAPB ——). "steady-state current" was defined as the increased current between the mean of 10 sec signals at the end stage of the steady state and the mean of background current at the first 5 second of the substrate flow through; "slope" is the change in y-axis at first 5 sec of stopped-flow step. This experiment was repeated and showed similar results.

As shown in Fig. 3.10B, the relatively low "steady-state current" and high "slope" value makes p-aminophenylbutyrate an optimal substrate for enzymatic amplified detection of nucleic acids on E-Chip. The preference of p-aminophenylbutyrate over p-aminophenylhexanoate was a consideration of the lower "steady-state current", the less inevitable enzyme deactivate effect caused by catalytic hydrolysis of substrate. This is very important for the E-Chip application

because the substrate flow requires a certain time to reach the different electrode positions distributed over the whole chip.

In addition, p-aminophenylhexanoate, having the highest "steady-state current" to immobilized EST2 (as shown in Fig. 3.10) and the highest activity to soluble EST2 (Fig. 3.9), is the best substrate for measurement of trace amount of soluble esterase 2 from *A. acidocaldarius*. However, this work focuses only on p-aminophenylbutyrate as electrochemical active substrate of EST2.

3.1.7 Comparison of spectrophotometric and amperometric detection of EST2

Spectrophotometry is the most widely used method in detecting EST2 activity as well as alkaline phosphatase activity. Besides the spectrophotometric determination, the catalytic activity of EST2 to different p-aminophenyl esters was monitored by method of amperometry. Detailed studies were carried out in order to investigate the efficiency of these two methods.

3.1.7.1 Calibration curve of p-nitrophenol and p-aminophenol

Calibration curves for p-nitrophenol (5-100 μM) and p-aminophenol (5-500 μM) were measured in order to determine the detection limits and to establish the relationship between the substrate concentration and amperometric signals. The data plots are depicted in Fig. 3.11, and linear regression analyses are summarized in Table 3.5. The Linear regression method determined how the responded signals depend on the varied concentration of p-nitrophenol and p-aminophenol, respectively.

Under the conditions specified in this particular protocol, the molar extinction coefficient of p-nitrophenol was determined to be 1.4×10^4 $M^{-1} \cdot cm^{-1}$, which had been derived from the slope value of Fig. 3.11A.

Noises presented in Table 3.5 were estimated from the standard deviation of repetitive measurements of the least concentrated standard (Fig. 3.11). Defined by signal/noise > 3, the detection limit for the amperometric method (0.5 μM) was approximately 4 times lower than the spectrophotometric method (2 μM).
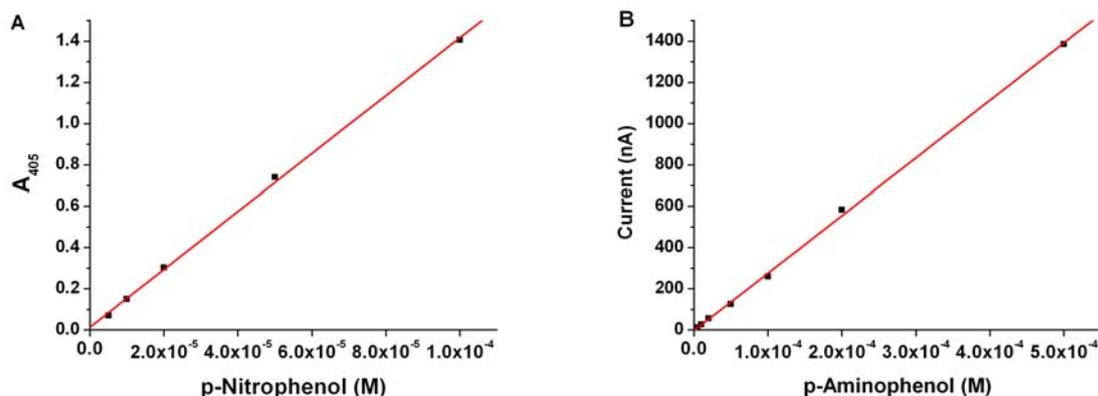
Fig. 3.11. Concentration to resulting spectrophotometric or amperometric signals. (A) p-nitrophenol and (B) p-aminophenol. AU is the arbitrary unit of the absorbance at 405 nm (A_{405}). Each point is the mean value of three repeats. Shown are results from three repeats with standard deviation. The curve fitted to the linear regression equation (y=ax+b) and resulted in correlation coefficient $R^2 > 0.9996$.

Table 3.5 Figures-of-Merit for the determination of p-nitrophenol and p-aminophenol

Method	Compound	Linear regression (y=ax+b)	Noise	Detection Limit
Spectrophotometry	pNP	A_{405} (AU) =1.40×10^4 x (pNP, M) + 0.0145	0.0145	2 μM
Amperometry	pAP	Current (nA) =2.79×10^6 x (pAP, M) - 0.41	0.31	0.5 μM

3.1.7.2 Detection of EST2 by spectrophotometric and amperometric methods

Calibration curves for the enzyme were generated by incubating 0.2 mM p-nitrophenylbutyrate with varying concentrations (0.02-1 nM) of EST2 (Fig. 3.12A) or delivering 0.2 mM p-aminophenylbutyrate with varying concentrations (0.005 - 2 nM) of EST2 to chamber of E-Chip (Fig. 3.12B). The variant concentrations of EST2 were prepared by serial dilution in 100 mM sodium phosphate, 1.0 mg/ml BSA, pH 7.1 to reduce the possible non-specific adsorption effect. The comparative analysis results are summarized in Table 3.6. The noise shown in Table 3.6 for the spectrophotometric method was taken from the spontaneous hydrolysis rate of p-nitrophenylbutyrate, while the noise for the amperometric method was determined by the mean of background current of p-aminophenylbutyrate.

When signal/noise > 3 was taken as evaluation standard, as shown in table 3.6, the amperometric detection limit is almost 5 times more sensitive than that of spectrophotometric one. The electrochemical method allows a detection of 15 fmol of enzyme in 1 ml volume, which corresponds to the reliable determined picomolar concentrations. This limit could be

still reduced if reaction conditions are optimized, particularly longer reaction time, smaller reaction volume, higher substrate concentration and optimal temperature are used.
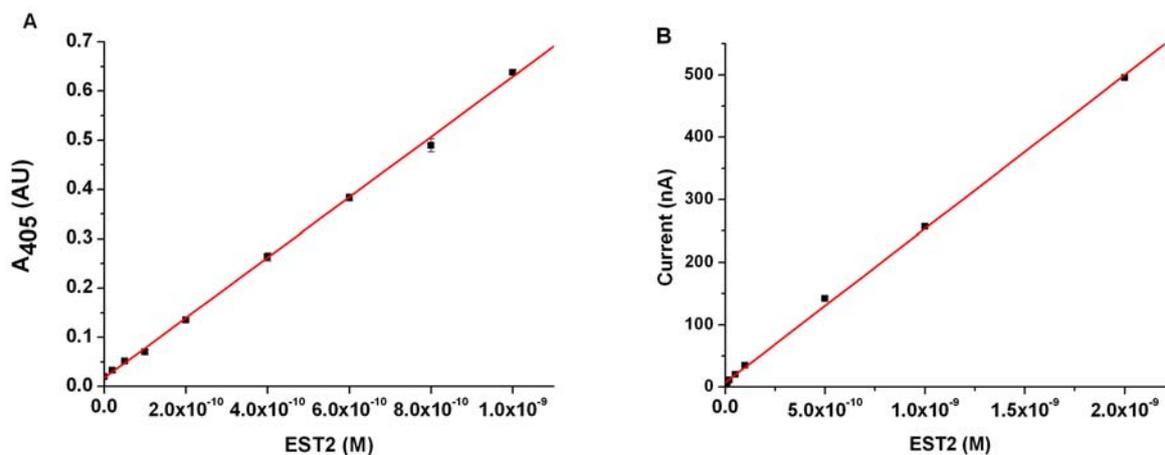
Fig. 3.12. Concentration of EST2 and its resulting spectrophotometric or amperometric signals. EST2 catalytic hydrolysis of substrates (A) p-nitrophenylbutyrate and (B) p-aminophenyl butyrate. The absorbance at 405 nm and current were measured after 1 min of reaction. Each point is the mean of three repeats. AU is arbitrary unit. Shown are results from three repeats with standard deviation. The curve fitted to the linear regression equation (y=ax+b) and resulted in correlation coefficient $R^2 > 0.9995$.

Table 3.6 Figures-of-Merit for the determination of EST2

Method	Substrate	Linear regression (y=ax+b)	Noise	Detect limit
Spectrophotometry	pNPB	A_{405} (AU) = 6.10×10^8 x (EST2, M) + 0.016	0.020	72 pM
Amperometry	pAPB	Current (nA) = 3.18×10^{11} x (EST2, M) + 3.42	2.7	15 pM

3.2 E-Chip based EST2-ODN conjugates detection of DNA

3.2.1 Preparation and purification of EST2-A34 conjugates

The EST2-A34 conjugates were prepared (M&M 2.2.6.2) by covalent coupling following a described procedure (Kukolka and Niemeyer, 2004) of a 5'-amino modified 34-mer ODN (A34) with EST2 mutant (EST2E118C) in which the 118th residue, a glutamate, was replaced by a cysteine. The introduction of another cysteine, on the surface of the molecule, allowed a specific reaction of the EST2 with maleimide activated ODN (Fig. 3.13A). The EST2-A34 conjugates were purified by anion-exchange chromatography on a MonoQ column. The peak indicated by an arrow contained the expected conjugates and was eluted at about 0.5 M NaCl (Fig. 3.13B). SDS-PAGE was used to resolve EST2-A34 conjugate, which can be localized by both ethidium bromide and esterase activity staining (Higerd and Spizizen, 1973) (Fig. 3.14A). SDS-PAGE analysis of the purified conjugate revealed a main band with an apparent mass of about 58 kDa (Fig. 3.14A lane 3), which is larger than theoretically expected value of 44 kDa. MALDI-TOF MS, however, showed that the conjugate has a molecular mass of about 44.2 kDa (Fig. 3.14B), which correlates to the anticipated value. As expected, one A34 coupled to one EST2, i.e. the buried sulfhydryl group of the Cys97 remained unmodified under applied conditions.
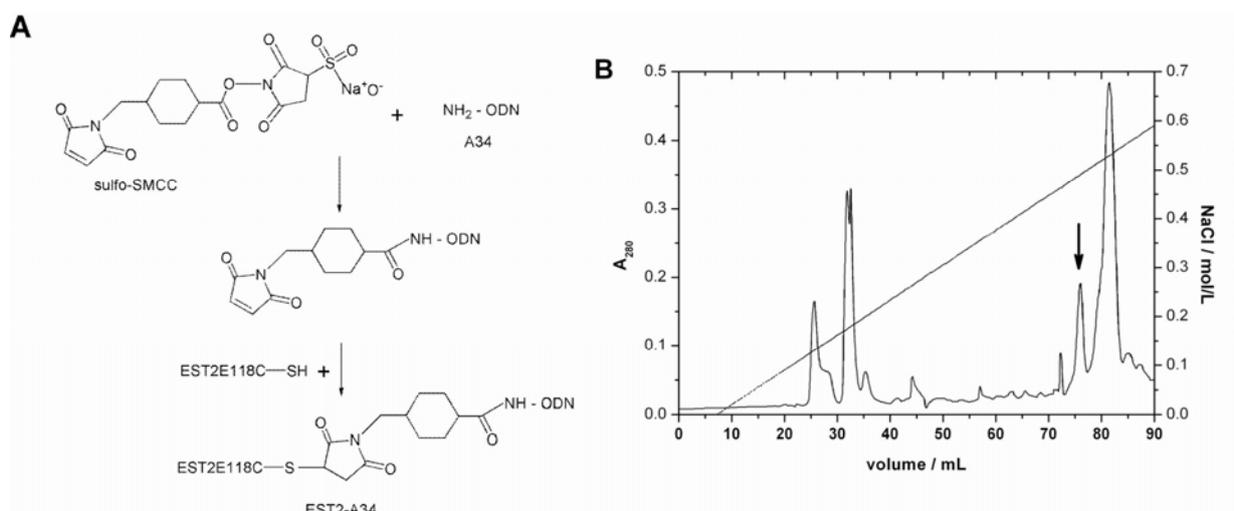
Fig. 3.13. Preparation and purification of the EST2-A34 conjugate. (A) Scheme of covalent coupling of 5'-NH2 modified A34 to EST2E118C; (B) purification of conjugate by ion-exchange chromatography. Peak of EST2-A34 conjugate is indicated by an arrow.
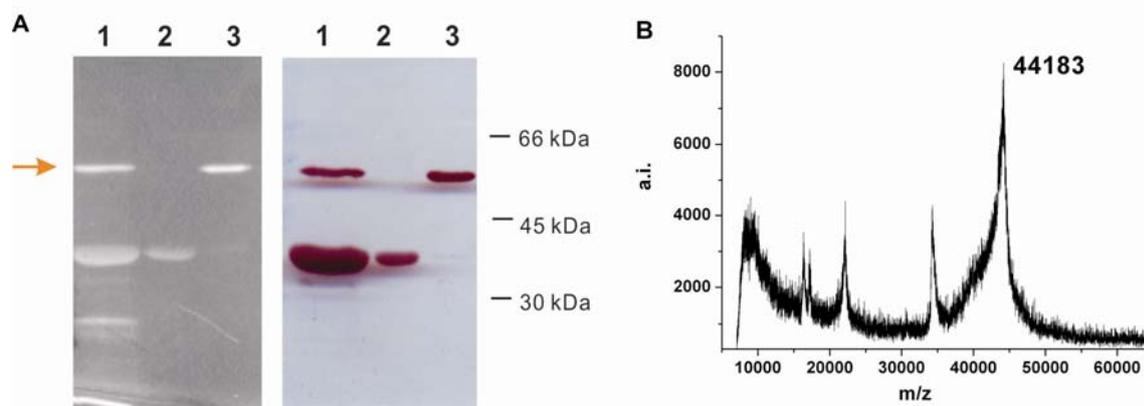
Fig. 3.14. Characterization of EST2-A34 conjugates by 10% SDS-PAGE and MALDI-TOF MS. (A) SDS-PAGE gel was stained with ethidium bromide (left) and by EST2 activity staining (right). Lane 1, crude product; lane 2, EST2E118C; lane 3, purified EST2-A34 from the arrowed peak in Fig. 3.12B. Arrow indicates the position of EST2-A34 conjugates. (B) The molecular masses of the conjugate determined by MALDI-TOF MS. a.i. is arbitrary intensity.

3.2.2 Preparation of EST2-streptavidin conjugates

An EST2-streptavidin conjugate was prepared to compare the efficacy of two kinds of EST2 reporter enzymes, EST2-streptavidin and EST2-ODN conjugates. The EST2-streptavidin conjugate works through the high-affinity streptavidin and biotin interaction, while the EST2-ODN functions via specific nucleic acid hybridization. The scheme of preparation is shown in Fig. 3.15A and details were described in M&M 2.2.6.3. Biotin labeled EST2 bound to Agarose attached streptavidin and subsequently EST2-biotin•SA was eluted by sodium acetate. The final product after dialysis renaturation was analyzed by SDS-PAGE without the 95 ℃ heat treatment prior to gel loading. Arrows in Fig. 3.15B indicate two kinds of EST2-biotin•SA conjugates. This is probably due to that tetramer streptavidin, was dissociated into two dimmers, as judged by the two streptavidin bands in lane 3 of Fig. 3.15B (left). Both these two forms of streptavidin were able to be bound with one EST2-biotin molecule and presented two EST2-streptavidin conjugate bands in lane 2 of Fig. 3.15 (right). In this report, "-" in EST2-biotin•SA conjugate represents covalent coupling and "•" means streptavidin/biotin high affinity binding.
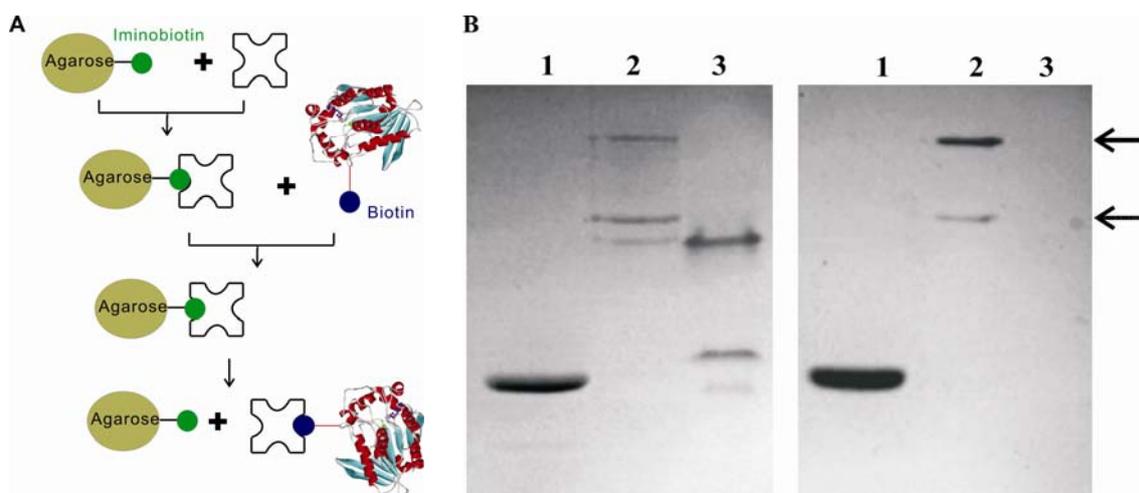
Fig. 3.15. Preparation and SDS-PAGE characterization of EST2-biotin•SA conjugates. (A) Scheme of preparation of conjugates; (B) 10% SDS-PAGE characterization of EST2-biotin•SA. Gels were visualized by Coomassie Brilliant Blue G250 (left) and esterase activity staining (right). Lane 1, EST2-Biotin; lane 2, EST2-biotin•SA; lane 3, streptavidin. Arrows (in B) show the position of conjugates visualized by esterase activity.

3.2.3 Sensitivity of the detection

To demonstrate the application of EST2-A34 as a reporter for binding to complementary ODNs, two components DNA hybridization experiment was performed (M&M 2.2.13.1) as outlined in Fig. 3.16A. A capture ODN with a sequence complementary to EST2-A34 was covalently immobilized via 5'-SH group to the gold surface of the electrode and the EST2 was brought to its vicinity by means of hybridization with the EST2-A34 conjugate. Afterwards, the chip was connected to multipotential (Fig. 2.1) and p-aminophenylbutyrate was delivered into chamber and started to be hydrolyzed by the position-specific EST2. A redox recycling mode (Niwa et al., 1990) was applied to measure the amount of produced p-aminophenol (Fig. 3.16B). A representative time versus amperometric signal plot generated in presence pAPB at 20 ℃ is shown in Fig. 3.16C. During the first 75 sec, 1 mM pAPB was continuously delivered to the chip. After 30 sec of pAPB supply, a steady state situation was reached for the current, indicating the supply of p-aminophenylbutyrate and release of p-aminophenol at the electrode position was in equilibrium. The slow decrease from the plateau over the time is probably due to EST2's inevitable deactivation after hydrolysis of substrate. Increase of the signal was registered under stop-flow conditions (76-120 sec). Theoretically, a linear increase of the signal is expected when the redox recycling is fully efficient and p-aminophenol is permanently regenerated. Probably, as a result of EST2 deactivation, quinonimine hydrolysis,

substrate consumption and redox recycling's damage, the current becomes constant after about 45 sec of the stop-flow mode. Therefore, the slope derived from the signal at the beginning of the stopped-flow modus was used as an indicator for EST2 activity.
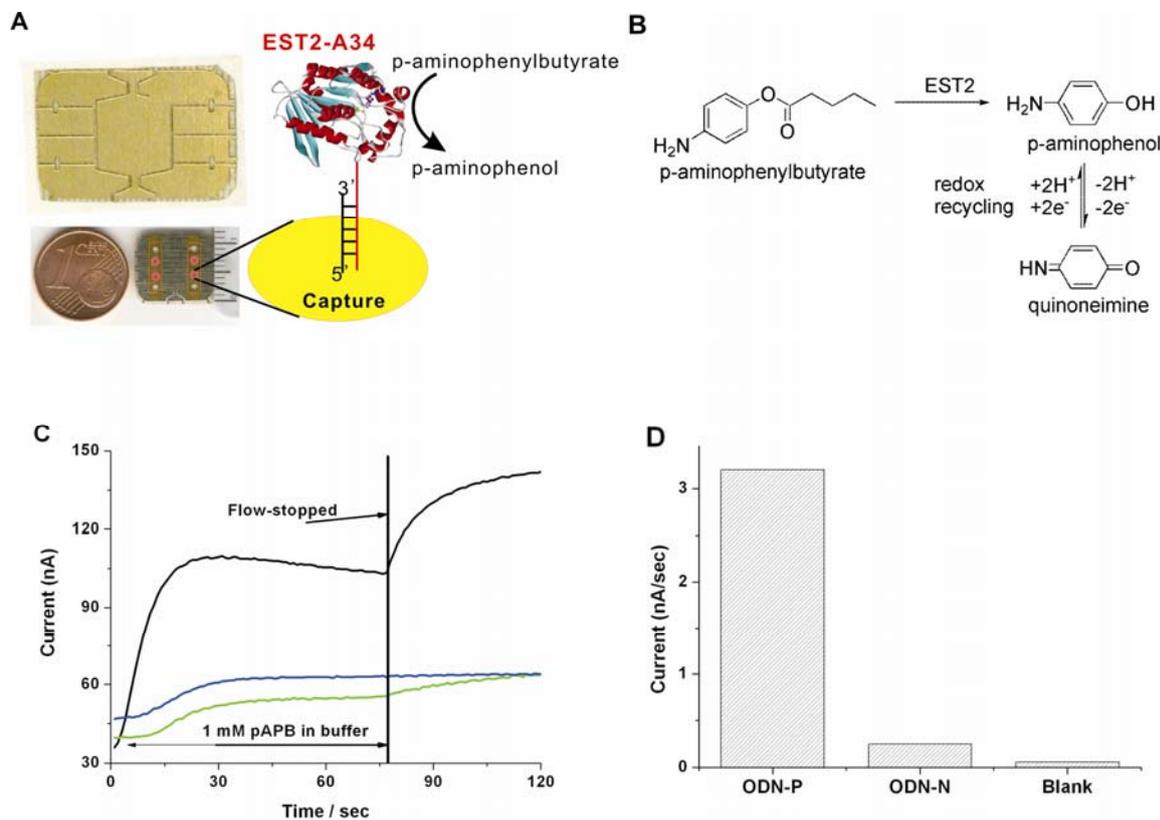
Fig. 3.16. Detection of EST2-A34 sensitivity. (A) Schematic diagram of DNA hybridization assay with EST2-A34 reporter. (B) The esterase immobilized on the electrode by DNA hybridization catalyzes the hydrolysis of p-aminophenylbutyrate (pAPB) to the electrochemical active p-aminophenol and results in redox recycling between p-aminophenol and quinoneimine. (C) Currents measured from the different capture modified position. At first 75 sec 1mM pAPB was continuously delivered to the electrode with a flow rate of 0.2 mL/min. Then the substrate flow was stopped. The slope of the burst from first 5 sec was used to compare the amount of the immobilized enzyme. Different curves represent signal presented from electrodes with perfectly matched (ODN-P ——), noncomplementary (ODN-N ——) and blank electrode (Blank ——) respectively. (D) Relative amounts of immobilized esterase as determined by the slope under stop-flow regime in (C).

Compared to capture ODN-P, which was complementary to EST2-A34, when a non-complementary capture, ODN-N, was placed on the electrode, only a marginal signal was detected. By omitting the capture completely, a very low, barely measurable signal was registered (Fig. 3.16C), which probably resulted from an unspecific interaction of EST2-A34 with the gold surface. Reports about noncovalent interactions between the DNA backbone and the gold surface support this interpretation (Kimura-Suda et al., 2003; Lao et al., 2005). As depicted in Fig. 3.16D, the slope of signals from the electrodes equipped with complementary

capture, non complementary capture and blank were 3.20, 0.25 and 0.06 nA/sec, respectively. This implies that EST2 immobilized exclusively on electrodes through Watson-Crick base pairs formed between the EST2-A34 and its corresponding capture.

The detection limit of the conjugate reporter was determined by serial dilution of the EST2-A34 in hybridization buffer, followed by hybridization with capture ODN-P (M&M 2.2.13.1). The lowest amount of EST2-A34 that could be detected under the used experimental arrangements with an analytical standard of signal-to-noise > 3, was estimated to be 1.5×10^{-18} mol (Fig. 3.17) corresponding to 0.5 µl of 3 pM EST2 or target ODNs.
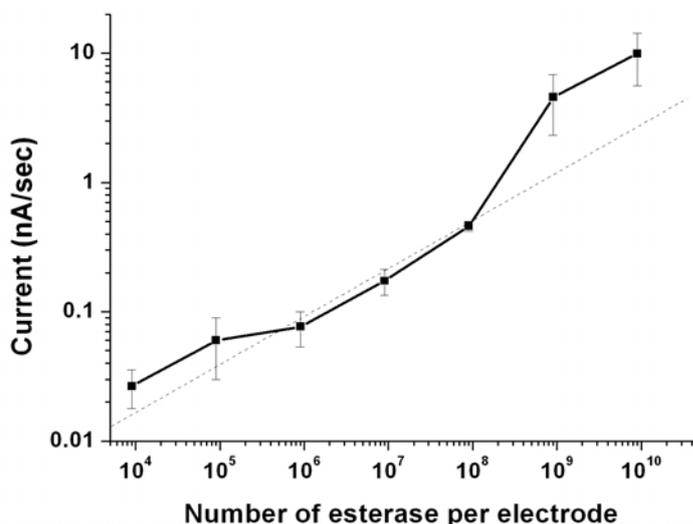
Fig. 3.17. Determination of detection limit of EST2-A34 conjugates on a gold electrode of 0.6 mm^2 area. Shown are mean values of replicates from three independent experiments

3.2.4 Selectivity of the detection

3.2.4.1 Directly detection of mismatched capture ODN

DNA hybridization on a solid support is usually used to detect a mismatch within nucleotides stretch in biosensor based systems. However, experiment methods are limited for comprehensive studies to hybridization conditions, such as temperature and necessary washing steps in order to achieve an optimal fidelity and stringency of DNA hybridization. In order to improve this situation, the hybridization behaviors obtained by two different types of EST2 reporters, a covalent EST2-A34 conjugate and an EST2-biotin•SA•biotin-34 complex were

compared (M&M 2.2.13.2). The latter was the outcome of EST2-biotin•SA binding to ODN biotin-34, which had hybridized to its surface-immobilized capture.

Experiments were carried out simultaneously on one chip containing an array of four working electrodes with immobilized different capture ODNs. Two different hybridization temperatures were compared using two sorts of esterase 2 conjugates. At 50 ℃ EST2-A34 was able to distinguish the perfect match and single mismatch (Fig. 3.18A), while EST2-biotin•SA•biotin-34 complex failed to do so (Fig. 3.18B). However, at 20 ℃, as shown in Fig. 3.18C&D, both EST2-A34 and EST2-biotin•SA•biotin-34 were able to detect the mismatch, despite the resolution shown in Fig. 3.18D is not as good as Fig. 3.18C. Clearly, the selectivity provided by covalent EST2-A34 conjugate is superior to the selectivity achieved via streptavidin/biotin conjugation. Additional washing steps with a low salt buffer did not improve the stringency of mismatch recognition (Fig. 3.18C&D).

It is known that base mismatches have influence on the stability of helices and exert a stronger effect on solid-phase hybridization (Hughes et al., 2001; Peterson et al., 2002). These effects were also observed in Fig. 3.18A&C when the hybridization was performed at 50 ℃ and 20 ℃.

In the case of short-length capture ODNs, mismatch discrimination can be achieved by rinsing the initially formed complex with low salt buffer, which leads to preferential dissociation of the less stable complex. In experiments presented in Fig. 3.18C&D with 24-mer captures, such an effect was not observed. Nevertheless, mismatch discrimination achieved by EST2-A34 without additional stringent washing was sufficient enough to detect the mismatch hybridization (Fig. 3.18A&C). The solid phase hybridization appears to have a barrier that prevents the mismatched ODN from binding to the capture (Peterson et al., 2002). And this energy barrier was overcome at 50 ℃ hybridization, thus increasing density of immobilized EST2-A34 and subsequently current response. However, the ability to discriminate mismatches is superior at 20 ℃.

There is a 10-fold increase in the signal intensity in Fig. 3.18A when compared with Fig. 3.16D. This is due to a lower capture density on the electrode surface, and a long thymidine spacer adopted in experiment depicted in Fig. 3.18. A low steric crowding effect on the electrode led to increases of hybridization efficiency (Peterson et al., 2001; Peterson et al., 2002; Lucarelli et al., 2004) and hence gives rise to a strong signal. Overall EST2-A34 gave a much stronger signal (Fig. 3.18A&C) than EST2-biotin•SA (Fig. 3.18 B&D). The molecular mass and dimension of streptavidin being 60 kDa and 8.4x8.4x4.65 nm respectively

(Scheuring et al., 1999), probably hindered the access of the reporter to the electrodes. The low signal intensity and mismatch selectivity observed with streptavidin/biotin mediated conjugation of ODN with EST2 (Fig. 3.18B&D) demonstrates the advantage of direct covalent conjugation of ODN with the reporter enzyme (Fig. 3.18A&C).
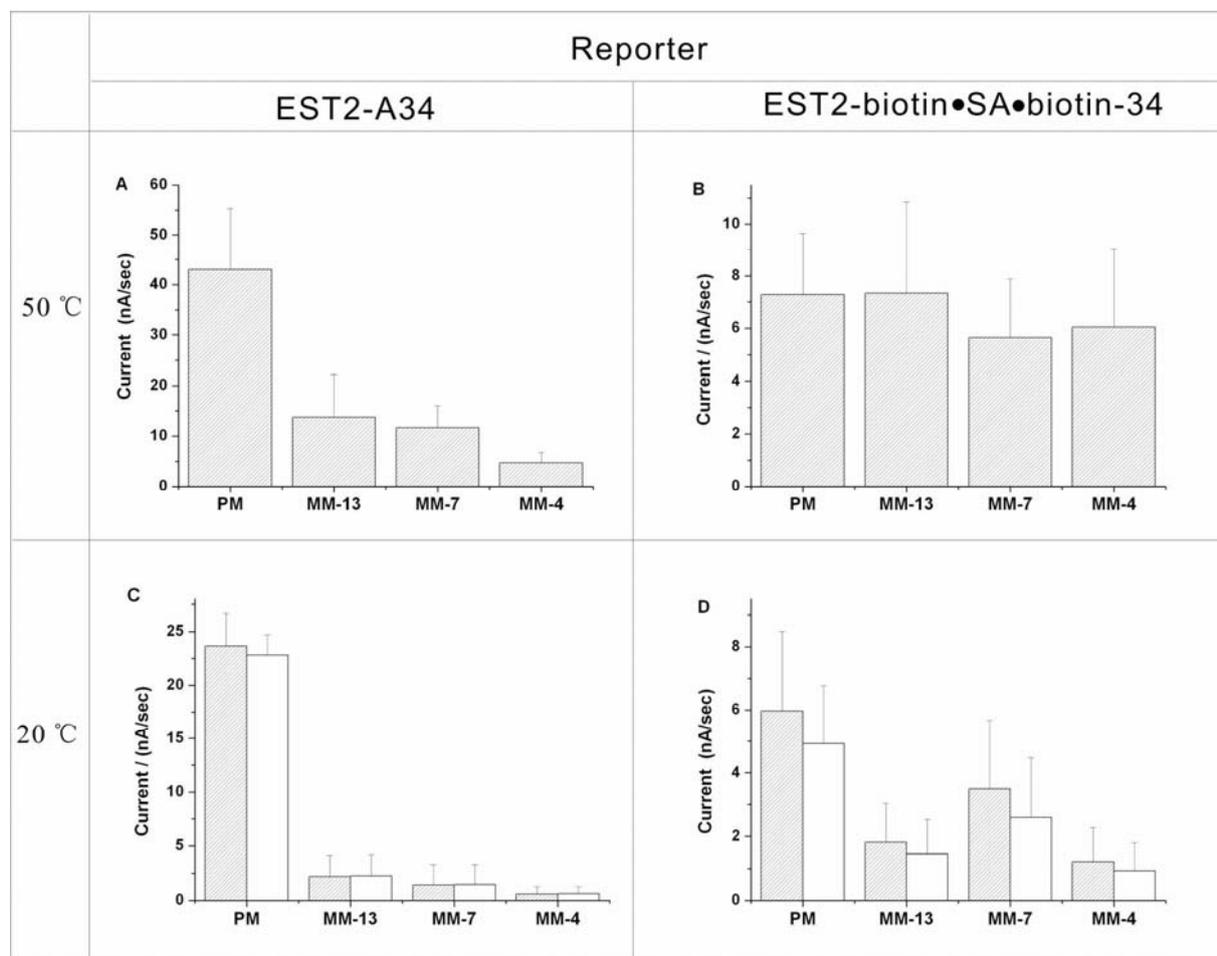
Fig. 3.18. Discrimination between immobilized, perfectly matched ODNs and single base mismatched ODNs. (A) and (C) hybridization of EST2-A34 at 50 ℃ and 20 ℃ respectively; (B) and (D) hybridization of biotin-34 at 50 ℃ and 20 ℃ respectively, followed by binding of EST2-biotin•SA conjugate. Empty bars in (C) and (D) shows the effect of an additional 20 min washing step repeated three times with 30 mM NaCl, 10 mM Tris-HCl, pH 8.0. PM is a perfectly matched capture to EST2-A34, while MM-13, MM-7 and MM-4 are mismatched captures that each containing one mismatch in number indicated position of 24 mer nucleotides. Reporter EST2-biotin•SA•biotin-34 is the result of ODN biotin-34 hybridization and afterwards binding with EST2-biotin•SA complex. Capture sequence see M&M 2.1.7.2.

3.2.4.2 Detection of 49-mer ODNs analyte

The main objective of this research is to detect a target ODN by hybridization on an electrical chip. As a model, a 49-mer analyte CM, has 22 nucleotides complementary with its

immobilized capture and the other part base-paired to EST2-A34 conjugate. ODN 1MM, 2MM and 3MM contain 1 to 3 mismatched nucleotide(s) corresponding to CM. As shown in Fig. 3.19, the ODNs containing, one, two and three mismatched nucleotide(s) present 24%, 12% and 11% signal compared to the fully complementary analyte CM, respectively. This indicates that the short analyte containing even only one mismatched nucleotide can be effectively identified.
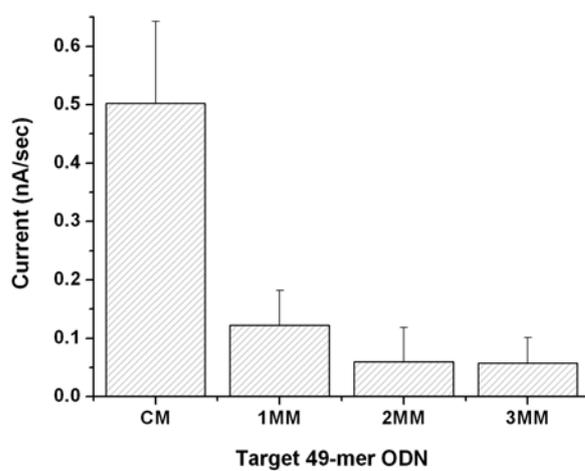
Fig. 3.19. EST2-A34 reporter distinguishes mismatched 49-mer ODNs. CM, 2MM, 3MM are 49-mer synthesized ODN harboring 0 to 3 mismatched nucleotide(s) respectively (Sequence see M&M 2.1.7.2.).

3.2.4.3 Detection of a mismatch in a single gene

High sensitivity, simple instrumentation, low price and a possibility of on-line applications are the main advantages of the electric detection systems. A 510-nucleotide sequence of EF-Ts gene was chosen as a model to investigate hybridization between perfectly matched and single-base mismatched DNA duplexes (M&M 2.2.13.4). The hybridization was performed in an array of four electrodes, each equipped with a different capture, and signals were collected in parallel under nearly simultaneous response of the current from all four electrodes. As demonstrated in Fig. 3.20A&B, the hybridization occurred at different regions of long ssDNA and signals could be determined by EST2-A34 reporter. To determine the ability for single mismatch identification, as shown in Fig. 3.20C, captures (C-TS2A, C-TS2C and C-TS2G) with single nucleotide variation gave less than 50% signal values as compared with that of perfectly matched capture, C-TS2.

Investigations using microarray technology show that secondary structures of long DNA can prevent target hybridize to ODNs microarray (Lane et al., 2004; Chien et al., 2004). In this

work, a significant position effect upon hybridization with different positions of a long DNA strand was also observed. In Fig. 3.20B, the relatively high signal provided by capture C-TS1 and low signal from C-TS4 were probably due to the effect of secondary structure. However, for point mutation detection, the repeated experiments presented in Fig. 3.20C shows the same qualitative result. Thus, point mutations can be identified by the method outlined in Fig.3.20.
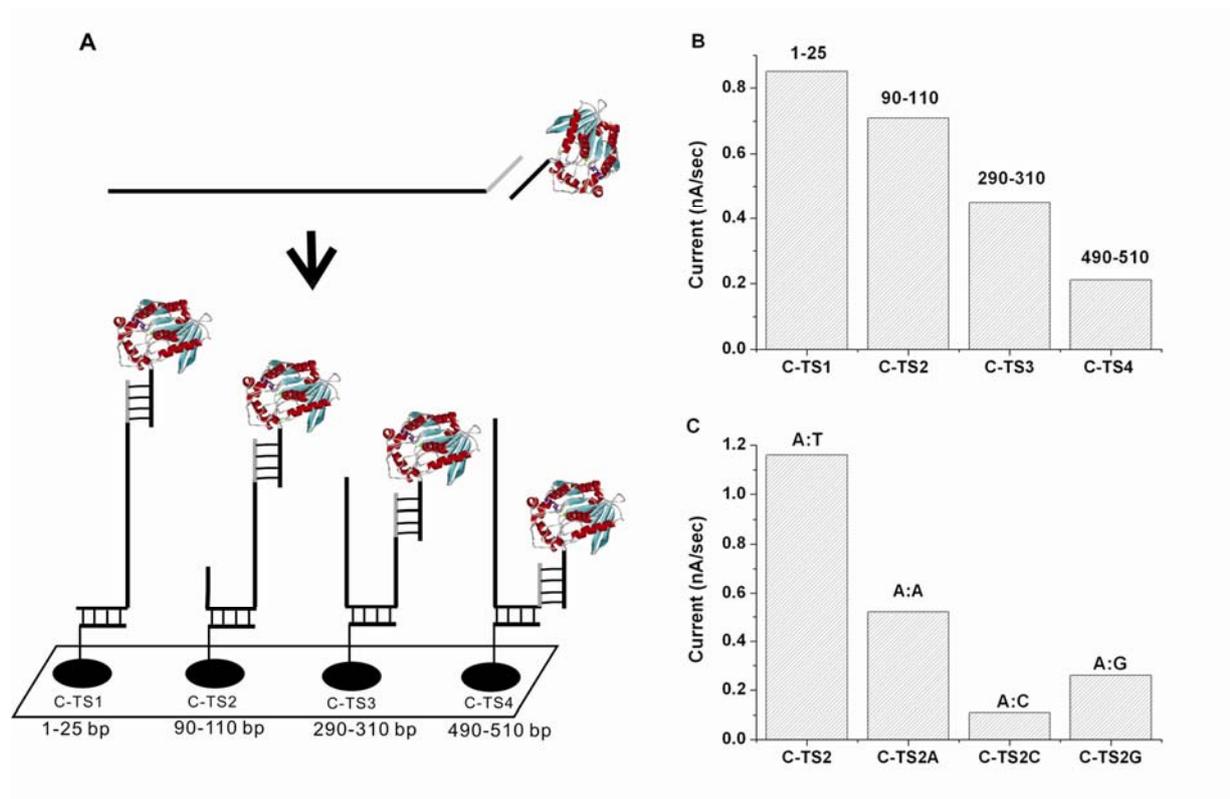
Fig. 3.20. Simultaneous amperometric measurement of immobilized EF-Ts ssDNA on an arrayed chip containing four electrodes. (A) Scheme of ssDNA preparation and hybridization. The sequences of captures list in M&M 2.1.7.2. (B) Diagram of current signals obtained by perfectly matched capture ODNs to different regions of ssDNA sample. (C) Diagram of current signals obtained from four types of mismatched base-pair in the 90-110 region of 510 nucleotides EF-Ts segment. Shown are the mean values of three independent experiments.

3.3 E-Chip based bacterial species identification

3.3.1 Comparison of 16S rRNA sequences of eight representative foodborne pathogens

Bacterial identification by hybridization assays is based on sequence difference. In order to carry out bacterial species identification, a study of sequence is required. Comparative sequence analysis of the 16S rRNA from eight representative bacteria species found in food

samples was created with software Vector NTI Suite 8.0 (Informax, Davidson, USA) (Fig. 3.21). The sequences of whole length 16S rRNA from eight bacteria were analyzed, but only a partial sequence, corresponding to 1017-1113 nucleotides of the *E. coli* 16S rRNA, was optimal for detection purpose. A stretch termed "capture region" exhibited large sequence diversity and was used for binding to specific capture ODN immobilized. For signal reporting, a rather universal probe was used to bind the so-called "detection region", corresponding to nucleotides 1082-1113 of the *E. coli* 16S rRNA. This universal sequence is conserved in all the eight bacteria and allows detection with only one reporter ODN conjugate.
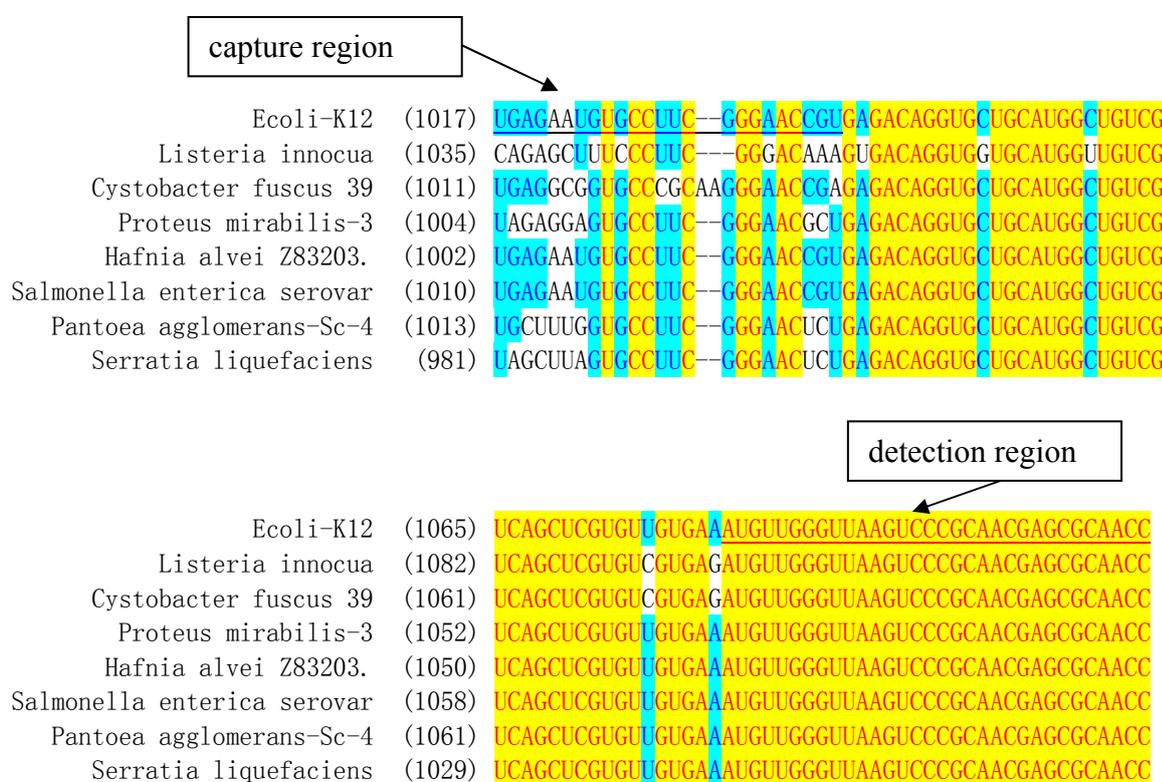
Fig. 3.21. 16S rRNA sequence alignment of eight bacteria in food sample. Shown are only partial sequences, corresponding to 1017-1113 nucleotides of the *E. coli* 16S rRNA. Positions conserved in all species are in yellow and position with 4-7 aligned sequence are shown in blue and less than four aligned are in normal. Sequence information come from: *E. coli*-K12 (Woese et al., 1980); *Listeria innocua* (Czajka et al., 1993); *Cystobacter fuscus* 39 (Sproer et al., 1999); *Proteus mirabilis*-3 (Mollet et al., 1997); *Hafnia alvei* Z83203 (Ridell et al., 1995); *Salmonella enterica* serovar (Chiu et al., 2005); *Pantoea agglomerans*-Sc-4 (Berg et al., 2006); *Serratia liquefaciens* (Olsson et al., 2004), respectively.

The designed conjugate EST2-U1082, indicates a complementary sequence to nucleotides 1082-1113 of the *E. coli* 16S rRNA (detection region in Fig. 3.21), and should be able to form a 32-bp double-stranded DNA/RNA duplex. It should be more stable than the duplex between

specific capture (23-25 nucleotides) and rRNA. Therefore the signal intensity of hybridization relies mainly on the selectivity of the specific capture to the 16S rRNA other than the duplex formed between EST2-U1082 and 16S rRNA.

3.3.2 Fragmentation of rRNA

Intact 16S rRNA is highly compact and the identified regions for binding to capture and reporter are usually not exposed. In order to obtain good hybridization efficiency, the highly compact structure must be unfolded. This can be either achieved through magnesium ion induced cleavage to produce relatively short fragments or introduction of helper ODN, which can bind to the segment between the capture ODN and the detection region of 16S rRNA (Fig. 3.21), helping to destabilize the local rRNA structure and rendering these two regions more accessible for hybridization binding.

The scheme of fragmentation of intact rRNA and subsequent hybridization is shown in Fig. 3.22A. *E. coli* total RNA mixed with different concentration of Mg^{2+} was incubated at 95 ℃ for 10 min (M&M 2.2.13.5). The fragmented rRNA was monitored by Agarose gel electrophoresis as shown in Fig. 3.22B. After 10 min incubation with 30 mM Mg^{2+}, as depicted in lane 4 of Fig 3.22B, almost all the intact 16S and 23S rRNA were digested, as judged by the disappearance of 16S and 23S rRNA bands.

To analyze the efficacy from the fragmentation assisted hybridization, capture ECOLI with sequence specific to *E. coli* 16S rRNA (sequence of ODNs related with bacteria species identification is in M&M 2.1.7.3) was immobilized on the electrodes and the E-Chip detection of fragmented rRNA was performed (M&M 2.2.13.5). The calculated electrical signal after different concentrations of magnesium ions treatment is shown in Fig. 3.22C. The experiment demonstrated that rRNA digested by 30 mM Mg^{2+}, which gave the highest signal, is the optimal fragmentation condition. Under this condition, the produced fragments were mainly around 200-600 nucleotides long with substantially reduced local rRNA secondary structure.

It is worth noting that, initial attempts to improve 16S rRNA hybridization with 30% formamide or 0.5 M guanidine thiocyanate in hybridization buffer failed, though these two agents were reported to be effective in DNA/RNA hybridization (Van and Chen, 1991; Kaabache et al., 1995). At 20 ℃, EST2 maintained about 50% enzymatic activity after incubation with either agent for 5 min, and increase of hybridization temperature led to

complete loss of EST2 activity. Therefore, the hybridization buffer for RNA detection was with an additional 0.05% Tween-20 and 2 mg/ml BSA compared with that of DNA hybridization. These two components help stabilizing the EST2 activity and minimizing non-specific adsorption on gold surface. Under this condition, incubation for 20 min at 65 ℃ did not significantly change the EST2 activity, but the hybridization efficiency was significantly improved.
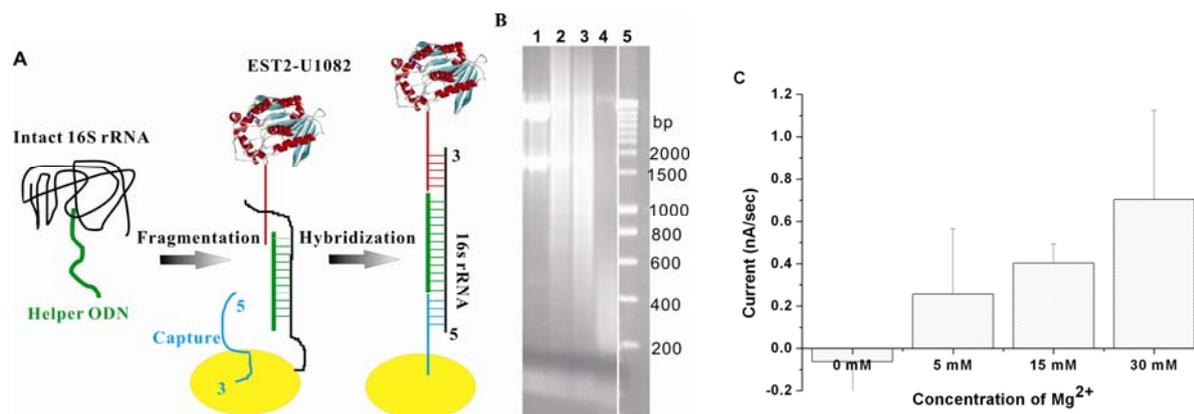
Fig. 3.22. Scheme and efficiency of *E.coli* Bl21(DE3) rRNA fragmentation and hybridization. (A) Scheme of fragmentation of intact rRNA and subsequent hybridization. (B) 2% Agarose gel analysis of fragmented rRNA. Lane 1, total rRNA without treatment; lane 2, total rRNA with 5 mM Mg^{2+} after 10 min at 95 ℃; lane 3, total rRNA with 15 mM Mg^{2+} after 10 min at 95 ℃; lane 4, total rRNA with 30 mM Mg^{2+} after 10 min at 95 ℃; lane 5, DNA ladder. (C) E-Chip detected signal intensity of rRNA fragmented by different concentrations of magnesium.

3.3.3 Bacterial species identification based on the 16S rRNA sequences

As a demonstration of bacteria species identification, rRNA hybridization was performed as described (M&M 2.2.13.5). Three different captures were immobilized on one chip at different electrode positions. Electrical signals upon hybridization of 400 nM of *E. coli* and 50 nM of *L. innocua* 16S rRNA are illustrated in Fig. 3.22 A and B, respectively. Captures LINNOC and ECOLI are specific to *L. innocua* and *E. coli* respectively, while EU943 is a universal capture that capable of binding with both bacteria rRNA at the region of 943-962 nucleotides. Both rRNAs were able to bind their corresponding capture specifically, almost no obvious current responses (under pAPB flow-stopped model) from control electrode positions were observed. Thus E-Chip detection using EST2-ODN conjugates as reporter is a feasible approach for bacterial species identification.

Low signal intensity from EU943 tethered electrode was probably due to a position effect. The distance between binding region of EU943 and EST2-U1082 is longer than that of the specific capture and EST2-U1082. The longer distance between capture and detection region led to a greater probability to be cleaved into two or more fragments.
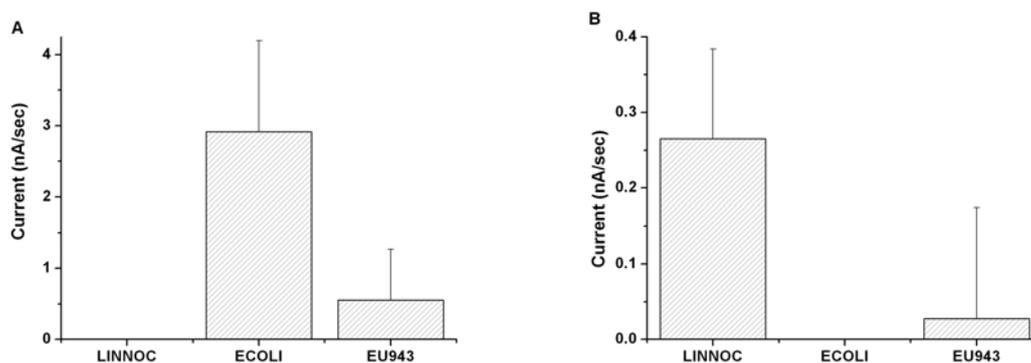
Fig. 3.23. Outcome of amperometric measurement of 16S rRNA from *E. coli* and *L. innocua*. Fragmented rRNA sample from (A) *E. coli* and (B) *L. innocua* were detected by E-Chip. LINNOC, ECOLI and EU943 in x-axis are the capture specific to *L. innocua*, *E. coli* and both.

E. coli BL21(DE3) cells with OD_{600} value of 0.6 contained 4.5×10^9 CFU/ml. To estimate the lower limit of 16S rRNA detection, a serial dilution of fragmented *E. coli* rRNA was prepared and measured by the hybridization procedure. The amperometric method allows the detection of 1 μl of 4 nM 16S rRNA. Based on the counted CFU and assuming 15,000 copies ribosome/cell, this quantity equals to approximately 7 ng of total rRNA or half a million cells. Under optimal conditions, this method should allow to detect much less cells provided that the total rRNA extraction method can be improved efficiently. As calculated from the CFU, only about 1-2% of rRNA yield of starting bacteria samples was obtained with the acidified-phenol extraction method (M&M 2.2.2.4).

In order to directly detect a low amount of bacteria, a mini-preparation scheme, which allows efficient preparation of rRNA from small amount *E. coli* cells, was developed (M&M 2.2.2.5). It directly showed that the E-Chip was able to determine around 1,000 *E. coli* Bl21(DE3) cells in 1 ml culture. The 1,000 cells/ml low-detection ability is one of the best detection ability reported hitherto.

3.4 Stem-loop structured ODN for oligodeoxynucleotide analyte detection

The amperometric 16S rRNA detection method described above shows promising application for EST2 reporting nucleic acids hybridization. This strategy requires two different regions of rRNA sequence simultaneously, one is sequence diversed capture region while the other is sequence conserved universal detection region. The selection of conserved detection region is dependent on target bacteria species. In order to make the analysis more independent of original sources, a biosensor, electrical chip based molecular beacon, which simply relies on the sequence diversity region was required.

Loop portion of the stem-loop structured ODN CMB442 is complementary to 16S rRNA of *E. coli* (442-459 of 1542 nucleotides), bearing 5'-thiol and 3'-biotin modifications. It was synthesized as described (M&M 2.2.15). The construction scheme of the molecular beacon on electrode of E-Chip (Fig. 2.3) requires first CMB442 to be immobilized onto the gold surface of the electrode, second a *tert*-dodecylmercaptan monolayer to be assembled to shield the biotin group and incubated with the analyte. Finally the EST2-biotin•SA conjugate was applied to label the available biotin group. In the presence of T442-Ex, an target analyte complementary to both loop and stem of the beacon, the signal increased for two folds (Signal/noise=3). The signal arisen from the absence of analyte was taken as noise. However, there is no signal enhancement above the background when applied with the T442 ODN, which is only complementary to loop portion.
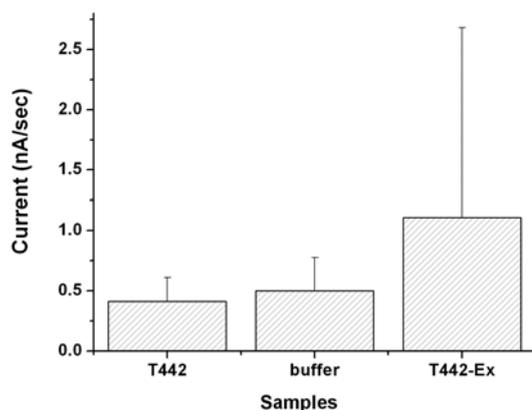
Fig. 3.24. Result of Amperometric measurement based on stem-loop structured molecular beacon detection of target ODN. The bar referring to buffer indicates the molecular beacon was treated with blank hybridization buffer without any analyte ODN. T442 is complementary to only loop region and T442-Ex can bind both stem and loop regions (Sequence see M&M 2.1.7.4.).

4. Discussion

4.1 Expression and purification of EST2

EST2 from *A. acidocaldarius* is a well studied thermostable protein. EST2WT was produced in a relatively low yield, barely detectable by Western blotting, using the original published pT7-SCⅡ-EST2 (Manco et al., 1998). Therefore a new construction based on plasmid pET-30a was chosen as an alternative for expression of EST2E118C. The pET System is one of the most powerful system yet developed for the expression of recombinant proteins in *E. coli* (Baneyx, 1999). Target genes are cloned in pET plasmids under control of strong bacteriophage T7 transcription signal; expression is induced by providing a source of T7 RNA polymerase in the host cell. T7 RNA polymerase is so selective and active that, when fully induced, almost all of the cell's resources are consumed for target gene expression; the desired product comprises more than half of the total cell protein a few hours after induction (Baneyx, 1999; Sorensen and Mortensen, 2005). Moreover, the strong ribosome binding site in pET system contributed to the increase of expression. In contrast, the construction of pT7-SCⅡ-EST2 was designed to express target gene that already carries its own prokaryotic ribosome binding site, while pET vectors contain the highly efficient ribosome binding site from the phage T7 major capsid protein and are used for the expression of target genes.

The published method for purification of EST2 is based on combined chromatography on ion-exchange Q Sepharose and hydrophobic Phenyl-Superose column (Manco et al., 1998). The EST2 specific activity after TFK-Sepharose purification was approximately 1,100 U/mg, which is better compared to the 500 U/mg specific activities from the published ion-exchange chromatography purification scheme. Compared with the conventional chromatography procedure (Manco et al., 1998), TFK ligand chromatography is simpler, labor-saving and able to produce EST2 with higher enzymatic activity. Affinity purification with a trifluoromethyl ketone ligand is more efficient for purification of *Bombyx mori* juvenile hormone esterase than DEAE ion exchange chromatography (Shiotsuki et al., 2000). The higher specific activity from TFK-Sepharose purification coincident with and supports this conclusion. Moreover, as a reporter enzyme, the higher specific activity enables to detect lower amount of analyte.

In the TFK purification scheme as shown in this study, EST2 was eluted at a condition that enzyme was denatured. Usually, strong inhibitors such as 3-*n*-octylthio-1,1,1-trifluoro-2-propanone, are used to elute protein from TFK-Sepharose (Shiotsuki et al., 1994; Wang et al.,

2000). However, it requires 3-5 days to completely remove inhibitor from enzymes via dialysis. Therefore, other effective methods to elute protein from ligand are required. Upon binding of TFK to active-serine of esterase, pKa of the formed ionized hemiketal intermediate (Fig. 1.4) is shifted to approximately 4.9 (Liang and Abeles, 1987; Brady et al., 1989). Solution of 8 M urea with pH 4.0 was applied in this study to release EST2 from TFK ligand successfully. This elution approach required 10 to 16 h to refold the EST2 through dialysis and did shorten the time period of purification and refolding. The most important criterion is the specific activity of EST2 from TFK purification scheme, which is much better than by using other methods. This is perhaps due to the single-step purification scheme and relatively short refolding processes.

The low purification yield (5.8%) obtained in the work is probably due to the small amount of matrix used and the loss of partially folded EST2 by centrifugation after the dialysis step. For EST2E118C purification procedure, one ml TFK-Sepharose resin was used. It is reasonable to speculate that the excess EST2E118C contained in S 100 lysate did not bind to the TFK-Sepharose in the column and caused the relatively low yield. The binding capacity was estimated to be approximately 20 mg EST2/ml TFK-Sepharose.

4.2 Factors affectting EST2 specific activity

Detergent can influence the EST2 activity significantly (Table 3.3). The investigated agents are commonly used in DNA/RNA hybridization experiments to improve hybridization specificity or accelerate hybridization kinetics. Triton X-100 has apparent inhibitory effect to some esterases (Allen et al., 1965), but in this study, it did promote the EST2 enzymatic activity. The prerequisite for utilization of EST2 as reporter enzyme is a maintenance of EST2 enzymatic activity under applied conditions. Therefore, Triton-X100 and Tween-20 can be utilized in nucleic acids hybridization to increase specificity and sensitivity, while inhibitory agents such as SDS and CTAB should be avoided.

A modest (2%, v/v) concentration of acetonitrile enhances EST2 activity (Fig. 3.8). The effect of miscible solvent on enzyme activity is complicated, and it can not be simply correlated either with polarity or denaturation capacity of the solvent (Khmelnitsky et al., 1991; Batra and Gupta, 1994). The solvent effects are enzyme specific. The fact that a modest concentration of acetonitrile can enhance enzymatic activity of trypsin, horse radish peroxidase and acid phosphatase has been determined experimentally (Batra and Gupta, 1994). It was concluded

that the enhancement of enzyme activity in modest aqueous-organic solvent mixtures may resemble the natural cellular microenvironments more closely than purely aqueous medium (Butler, 1979). The enhancements of EST2 activity can be explained as the miscible acetonitrile-water maintains the water-shell around the protein and thus preserve a high concentration of "free water" molecules near the protein (Khmelnitsky et al., 1991; Lozano et al., 1997). The more available biological active free-water near the catalytic center can accelerate the EST2 deacylation procedure (Fig. 1.13) that increases the EST2 catalytic efficiency.

The turnover number (k_{cat}) and catalytic efficiency (k_{cat}/K_m) observed at 70 ℃ (Manco et al., 1998), implies that the p-nitrophenylhexanoate has the highest activity among the tested p-nitrophenyl esters. However, as shown in Fig. 3.5, p-nitrophenylhexanoate did not fit the rule in this study. This change probably was due to the different working temperature utilized.

The stability of p-aminophenyl esters entirely relies on the rate of spontaneous hydrolysis of the esters bonds. Comparing with the mostly used p-aminophenylphosphate, the stability of p-aminophenylbutyrate is substantially improved. Solution of p-aminophenylphosphate in 100 mM Tris-HCl, pH 9.0 turned brown within a few min (Thompson et al., 1991), while p-aminophenylbutyrate solution will have brown color after an incubation time of at least 24 h. The color is due to the oxidization of p-aminophenol into quinonimine and subsequently converting into quinone, which displays color of brown to dark.

4.3 Comparison of the spectrophotometric and amperometric methods for detection of soluble EST2

As first reported by Agafonov et al., the spectrophotometric assay with p-nitrophenylacetate allows a detection of pmol amount of esterase, i.e. 10 nM EST2 in a 100 µl assay volume (Agafonov et al., 2005b). In this study, 15 pM soluble EST2 can be reliably detected in an amperometer, while 5 times higher concentration is required in a spectrophotometric assay. This detection limit is in the same range than the most sensitive labels, namely radioisotopes and fluorescence labeling (Sunkara et al., 2006). Previously, amperometric and spectrophotometric methods for alkaline phosphatase were compared. The amperometric method has a detection limit of 7 nM for the product of the enzymatic reaction, which is almost 20 times more sensitive than the spectrophotometric method (Thompson et al., 1991). The

amperometric method for monitoring of p-aminophenol has shown a better detection limit than that of the spectrophotometric with p-nitrophenylphosphate as the substrate.

EST2 has the best response to p-nitrophenyl esters with acyl chain of 4-5 carbons (Fig. 3.5) and p-aminophenyl esters with acyl chain of 4-6 carbons (Fig. 3.9 and Fig. 3.10). It is also noteworthy that at initial attempt, EST2 has no advantage compared to alkaline phosphatase under the same conditions. However, when p-nitrophenylacetate was replaced by p-nitrophenylbutyrate, the lowest detection limit was improved by nearly two orders of magnitude, from 10 nM (Agafonov et al., 2005b) to 72 pM EST2 (in this study). This is a very helpful hint for the development of optimal electrochemical substrate in the future.

However, the nature of the enzyme offers its substrate dependency. As could be shown in this way, p-aminophenylacetate provided a high signal response to acetylcholinesterase from *Electrophorus electricus* compared to *A. acidocaldarius* EST2. The lower detection limit of acetylcholinesterase by p-aminophenylacetate was 18 pM, this value is almost the same as the 15 pM detection limit of *A. acidocaldarius* EST2 with p-aminophenylbutyrate. Meanwhile, the p-aminophenylbutyrate has 30 times worse response to *Electrophorus electricus* acetylcholinesterase compared to p-aminophenylacetate. Acetylcholinesterase takes an important role in catalytic hydrolysis of neurotransmitter acetylcholine (Brodbeck et al., 1979; Gelb et al., 1985). Also it is one of the mostly used enzymes for monitoring pesticides. Both enzymes have the same type of serine-active catalytic triad centre and share the same inhibition mechanism to their inhibitors. Being monomeric, relatively small-sized, thermostable and easy for modification, EST2 has its advantage in construction of biosensor for detection of pesticide-like toxic agents.

The detection of esterase activity is meanwhile a routine analysis method. Influenza C virus is the only viral pathogen of the human upper respiratory tract presently known to produce an esterase. The acetylesterase of influenza C virus is located on the hemagglutinin molecule, a surface glycoprotein which also mediates attachment and penetration (Zimmer et al., 1992). Detection of such activity facilitates the differentiation between A, B and C viruses type (Wagaman et al., 1989). For this purpose, the p-aminophenylacetate could be a good substitute for p-nitrophenylacetate in detection of esterase in routine assay. In addition, a decrease in serum butyrylcholine esterase activity is observed in hepatic disease, carcinomas, and chronic debilitating diseases (Maekawa et al., 1997). With the whole series of stable substrate for esterase, p-aminophenyl esters with carbon chain length from 2 to 6 carbons, it provides an alternative to detect the level of esterase in blood samples with high accuracy and in short time.

4.4 Sensitivity of EST2-A34 conjugate for E-Chip detection of DNA

As the main purpose of this study, thermostable esterase 2 from *A. acidocaldarius* was established as a reporter enzyme to detect nucleic acids through solid-phase hybridization with electrode-immobilized capture ODNs. The detection limit with an EST2 reporter was tested and shows its promising practical application.

The non-specific adsorption of DNA to gold surface is a common phenomenon and in some cases the binding can be as strong as the specific thiol-gold interaction. Poly (adenine)-gold interaction was reported to be comparable to or even stronger than the specific covalent gold-thiol interaction (Demers et al., 2002; Ostblom et al., 2005).

The unspecific interaction of EST2-A34 conjugate with gold surface of electrode was also observed in this research (Fig. 3.16D), though the intensity is nearly negligible. The DNA strand contacting gold via gold-nucleobase interaction might be responsible for the adsorption. This type of interaction can not be completely eliminated even in the presence of 6-mercapto-1-hexanol monolayer, which was supposed to be capable of eliminating adsorption effect (Kimura-Suda et al., 2003; Lao et al., 2005). Moreover, the introduction of thiol functionalized monolayer on electrode surface reduced the sensitivity of chip detection (Nebling et al., 2004). Taken these factors into account, for this investigation, a short incubation time (30 min) was used to prepare low density capture monolayer without mercaptan agent and 0.05 % Tween 20 and 1 mg/ml BSA were used in hybridization step to reduce the possible non-specific adsorption.

The optimal sensitivity range was estimated to be 10^6-10^8 molecules EST2-ODN conjugate/0.6 mm^2 gold electrode overlaid with 0.5 μl solution (Fig. 3.17). Below this range ($<10^6$ molecules) the signal intensity is low and the signal-to-noise ratio decreases. The ultramicroelectrodes show an optimal hemispheric diffusion behavior that allows an enhanced lateral diffusion of electroactive molecules to the electrode surface and thus increase the signal to noise ratio. Moreover, only gaps between interdigitated electrodes below 1 μm (Fig. 1.2) can obtain a ten-fold amplification effect of the potentiometric readout, as the number of redox recycling and collection efficiency is closely related under this condition (Niwa, et al., 1990; Hintsche et al., 2005). In order to fall below the limit of detection, the surface of the electrode and the volume of the analyzed solution should be decreased, which can be reached by high density interdigitated gold array electrodes and application of microfluidics.

A traditional membrane-blot on nitrocellulose or high through-put microarray on glass as solid support usually requires overnight hybridization time to obtain a good signal. In contrast to this factor, a detection of 10^6 molecules of ODN in this study can be achieved within 30 min. This is mainly due to the enzymatic amplification effect of EST2, as well as the redox recycling readout. On the other hand, it was the contribution of the high density of capture covered on electrode surface. The coverage of between 10^{12} to 10^{13} capture ODNs/cm^2 equals a local concentration of 0.1-1 M (Levicky and Horgan, 2005), much higher than used for hybridization in bulk solution. The high concentration of capture ODNs contributed to high efficiency of binding even a trace amount of analyte in short time and provided distinct signal.

Incorporation of a thymidine spacer (T6 or T12) in the capture ODNs (M&M 2.1.7.2) also contributed to the sensitivity of detection and specificity of base-pairing in this work, as the asymmetric structure of a capture layer formed by binding capture ODN to solid-surface. The spacer helps to provide high flexibility, which results in better recognition strand loading. Thymidine was widely adopted because of its weak binding ability to gold as compared to other nucleotides (Ostblom et al., 2005). On the other hand, the impact of an asymmetric capture layer can be minimized using a thymidine spacer and while enabling a solid-phase hybridization behaviors more similar to that of bulk hybridization (Levicky and Horgan, 2005). As shown in Fig. 3.16D and Fig. 3.18A, PM with T12 depicts higher signal intensity than that of capture ODN-P with T6, though they have the same sequence information despite of length of spacer.

In summary, significant signal amplification was achieved and the detection limit was improved in this work compared with what have been described previously.

4.5 Capture ODN mismatch discrimination by the EST2-ODN conjugate and EST2-streptavidin conjugate

Another objective of the present investigation was to compare EST2 with the widely used alkaline phosphatase reporter enzyme constructs. Alkaline phosphatase is a dimer commonly used for spectrophotometric or amperometric detections (Gabig-Ciminska et al., 2004; Lucarelli et al., 2005). It is bound to biotin-modified ODN as a streptavidin-alkaline phosphatase fusion protein. For comparison of alkaline phosphatase and EST2, a similar designed EST2-streptavidin conjugate was prepared.

Mismatch discrimination by covalent EST2-A34 was superior to the biotin-mediated EST2-streptavidin reporter (Fig. 3.18). EST2-ODN conjugate (44 kDa) having a ball-stick like structure should exhibit much less steric crowding effect than the dumbbell-like streptavidin-enzyme conjugate (96 kDa). As analogue to EST2-streptavidin conjugate, the most common enzyme used in numerous assays previously, is streptavidin-alkaline phosphatase conjugated via glutaraldehyde cross-linking between ε-amino of lysine residues (Avrameas, 1969). Due to the random modification of all accessible ε-amino groups of lysine residues in streptavidin and alkaline phosphatase, a large number of different complexes can be formed which leads to strong steric hindrance. EST2 and alkaline phosphatase have molecular mass of 34 and 138 kDa, respectively. Though, the EST2-streptavidin reporter has a smaller size than streptavidin-alkaline phosphatase and thus should lead to less steric crowding, it still did not provide as good selectivity and signal intensity as the more precisely coupled EST2-ODN (Fig. 3.18). EST2-streptavidin showed 2-3 orders of magnitude lower detection limits than streptavidin-alkaline phosphatase (data not shown). The efficiency of detection is in order of EST2-ODN>EST2-streptavidin>streptavidin-alkaline phosphatase.

Moreover, the streptavidin is responsible for an increased adsorption on gold surface, because streptavidin as well as avidin is well known to rapidly form a monolayer on a gold surface (< 10 min) under a wide range of conditions (Ebersole et al., 1990). Reporting DNA hybridization with bulky streptavidin-alkaline phosphatase conjugates might be disguised by unspecific interaction of the protein with the electrode surface (Ebersole et al., 1990) or by steric hindrance for the access of the biotin modified ODNs (Scheuring et al., 1999). The steric hindrance and adsorption effect also exists in the case of EST2-streptavidin conjugate.

Application of a single chain enzyme as a reporter allows a controlled chemical modification and conjugation with an ODN, a predictable molecular structure of the reporter enzyme and defined enzymatic activity. The structure and dimension merits make EST2-ODN conjugate more accessible to target than a streptavidin coupled enzyme. Correspondingly, the reproducibility and the selectivity of hybridization had been expected to be improved in the case of ODN covalently linked to EST2 as compared to streptavidin conjugation. This was indeed observed in the present investigation. It is clear that the preparation of an esterase 2 reporter enzyme conjugated with ODN is feasible and superior over streptavidin.

What is not entirely understood is the temperature effect observed during hybridization with EST2-A34 conjugates as shown in Fig. 3.18. Based on thermodynamic calculation in bulk solution (SantaLucia, Jr., 1998), the predicted free energy penalty and melting temperature of

Fig. 3.18 was calculated and shown in Table 4.1. The free energy penalty for these three mismatched containing duplex differed only 3.2 to 5.7 kcal/mol compared with the perfectly matched duplex. All hybridization experiments were performed at 20 or 50 ℃, which are far lower than the predicted Tm. Generally, in membrane-blot experiments, hybridization temperature is kept 10 ℃ lower than the predicted Tm to increase the achieve hybridization selectivity. Clearly, in this study, at 20 or 50 ℃, it should not have achieved so distinct signals between hybridization with perfectly matched and mismatched capture ODNs, as the temperature is not so stringent that a duplex can be dissociated efficiently.

Still, the solid-phase hybridization on chip led to effective discrimination between the match and mismatch hybridization (Fig. 3.18). The observed experiments are better than could be expected from theoretical calculation. Reason for this surprising discrepancy was probably due to the distinct environment at the interface of solid-phase support and bulk solution. One of the most intriguing characters of the interface is the asymmetric structure of capture layer, as only one end of capture ODN was tethered onto solid-surface and the other end remained in bulk solution. The asymmetric capture layer exerts a strongly steric interaction between capture molecules close to the surface (Levicky and Horgan, 2005). It was speculated on theoretical grounds that the existence of an asymmetric structure of the capture layer mimicking an activation barrier that prevents target penetration to the probe film (Hagan and Chakraborty, 2004; Levicky and Horgan, 2005). This barrier probably contributes to high mismatch discrimination efficiency, as the hybridization duplex containing mismatched base-pairs are less stable than the perfect ones and are easy to be dissociated under this circumstance. Moreover, surface hybridization rates are also 20- to 40-fold slower than solution-phase rates for identical sequences and conditions (Gao et al., 2006). Perhaps the asymmetric structure and the steric hindrance resulting from the high density capture monolayer are responsible for this rate decrease.

Table 4.1 calculated nearest-neighbour parameter of A34 DNA duplex in 300 mM NaCl at 20 ℃

Capture name	ODN sequence (5'- 3')	ΔG (kcal/mol)	Tm (℃)
PM	GACAGGCGAGGAATACAGGTATTG	-52.3	91.1
MM-13	GACAGGCGAGGTATACAGGTATTG	-48.3	87.5
MM-7	GACAGGCGAGGAATACACGTATTG	-46.6	83.4
MM-4	GACAGGCGAGGAATACAGGTTTTG	-49.1	88.3

Interestingly, the selectivity at 50 ℃ in respect to single nucleotide mismatch was relatively low, compared with selectivity determined at 20 ℃ (Fig. 3.18). Differences in the thermodynamic stabilities of the perfectly matched and mismatched complexes should be actually larger at 50 ℃, which is near the melting temperature than at 20 ℃ condition. Perhaps, the low selectivity at 50 ℃ can be possibly explained by unspecific interaction of the protein or ODN with the gold electrode (Kimura-Suda et al., 2003; Lao et al., 2005). Temperature can accelerate both adsorption onto and desorption from surface, but the adsorption is always so predominant that protein or ODN are attached to surface. Desorption behaviours of nucleosides were observed only under a temperature from 100 to 210 ℃ (Ostblom et al., 2005). In summary, the possible explanation for the low selectivity at 50 ℃ was the stronger adsorption effect at 50 ℃ compared to that at 20 ℃.

4.6 Discrimination of single nucleotide mismatches

Mismatch detection is an important research topic of molecular biology and medicine. The ultimate goal is to develop an easily applicable platform for the detection of single nucleotide polymorphism (SNP) or point mutations (Tombelli et al., 2000; Marrazza et al., 2000; Nakamura et al., 2005).

In target analyte mismatch discrimination experiments, the 49-mer ODN with one mismatch presented about 20% signal (Fig. 3.19), while the 510-nucleotide ssDNA harboring one mismatch depicted 50% signal intensity (Fig. 3.20) compared to the completely matched analyte. In the case of 510-nucleotide DNA sample, the relatively high signal obtained from duplex containing one mismatch could be attributed to the cross-hybridization effect (Levicky and Horgan, 2005) and the unspecific adsorption of nucleobase-gold surface (Demers et al., 2002; Ostblom et al., 2005). Experimental observations have shown that the formation of hybridization duplex structures is more complicated than a simple one-to-one hybridization (Okahata et al., 1998; Peterson et al., 2002; Dai et al., 2002). As depicted in Fig. 1.17, a long target molecule can even bridge and hybridize across multiple capture ODNs and the mismatch within target might also facilitate bridging by destabilizing duplex formation at the location of the bridge (Levicky and Horgan, 2005). The 510-nucleotide ssDNA has a larger chance to bind several capture ODNs to neighboring positions and is also able to provide more nucleobase-

gold interactions on surface than that of 49-mer analyte could do. This perhaps is responsible for the relatively weak mismatch discrimination ability.

Despite the relatively low discrimination efficiency in 510-nucleotide ssDNA, however, under optimal condition, even a detection of a single nucleotide polymorphism is feasible by an electrode arrays equipped with capture ODNs complementary to successive DNA sequence segments.

In addition, there are various signal intensities obtained from hybridization with different regions of the 510-nucleotide ssDNA (Fig. 3.20A). This was likely due to the signal intensity from the hybridization, which critically depends on the secondary structure of the long DNA strand (Lane et al., 1997; Chien et al., 2004). Therefore, application of higher density electrode-arrays allowing parallel measurements and with internal controls may be, therefore, essential for this type of routine applications.

In order to prepare ssDNA from small amount of samples rapidly and efficiently, asymmetry PCR is commonly used. It was first developed for preparation of ssDNA in membrane-blot experiments (Gyllensten and Erlich, 1988). Single-stranded DNA can be produced in PCRs in which the concentration of one primer exceeds the other by a factor of 20-200. During the initial cycles of the PCR, double-stranded DNA is synthesized in a conventional exponential fashion. However, when the concentration of one primer becomes limiting, the reaction generates ssDNA that accumulates at an arithmetic rate. By the end of the reaction, the concentration of one strand of DNA is three to five times greater than the concentration of the other (Gyllensten and Erlich, 1988; Scully et al., 1990). The specific activity of the asymmetric probe is the same as that produced in the normal PCR, but the amount of DNA synthesized in the reaction will be much less. It is a simple, rapid and efficient way to prepare ssDNA directly by PCR amplification.

In this investigation, ssDNA analyte prepared by asymmetry PCR or the streptavidin coated magnetic beads method showed almost the same mismatch discrimination results (data not presented). Therefore, the important advantage of the combination of asymmetry PCR with EST2-ODN conjugates reporter, is that the isolated target analyte hybridization and reporter labeling processes can be combined into one operation. This combination can decrease the operation time and necessary manipulation steps, and thus offers the possibility to do faster and more automatic DNA detection based on a miniature "lab-on-chip". The latest continuous flow through thermal cycler microchip for DNA cycle sequencing allows preparing 500 bp DNA within 2 min while conventional chamber-type PCR still requires 1-2 hours (Hashimoto et al.,

2004; Wang et al., 2006). It is reasonable to speculate, that performing asymmetry PCR for DNA amplification with continuous flow PCR integrated on chip (Fig. 1.4) and labeling with EST2-ODN conjugates reporter offer a promising automatic and fast DNA detection implementation in the future.

4.7 Bacterial species identification through 16S rRNA sequence

The 16S rRNA sequence is highly conserved throughout evolution. Still, microorganisms can be identified by specific rRNA sequence on an electrochemical chip, if several factors are adjusted to fit each other. As illustrated in Fig. 3.21, the regions targeted by the capture sequences must show sufficient diversity to be distinguishable among different species, and the flanking regions should be highly conserved to allow the binding of universal EST2-ODN conjugate. As most 16S rRNAs are approximately 1500-nucleotide long and inevitable have extensive secondary structure motifs, the hybridization efficiency is strongly influenced by the accessibility of the target sequence as determined by the level of the local secondary structure (Chandler et al., 2003).

The RNA molecule has free 2'-hydroxy group on ribose. Mg^{2+} stimulates 2'-hydroxyl to attack 3'-phosphate and gives rise to a 2'3'-cyclic phosphate and a 5'-hydroxyl terminal (Scott et al., 1996; Soukup and Breaker, 1999). It was also observed in this study that the current signal increased upon addition of the Helper-ODN prior to fragmentation. This stabilization effect caused by helper-ODN was probably due to the forming of the DNA/RNA duplex that hindered the steric flexibility of 2'-hydroxyl and reduced the cleavage probability within this segment. The application of cleavage by divalent ion and protection of preferred RNA region enabled an improved detection of bacteria through 16S rRNA.

In order to establish a fast and effective bacteria species identification through the abundant 16S rRNA, fragmentation of rRNA in the presence of 30 mM Mg^{2+} for 5-10 min and performing hybridization at 65 ℃ for 20 min resulted in an optimal condition (Fig. 3.23). The already reported most significant factor affecting DNA/RNA hybridization specificity and improving hybridization efficiency was the presence of formamide (Small et al., 2001). The role of formamide is to reduce melting temperature and break RNA secondary structure. In an attempt to supplement 30% formamide in the hybridization solution at 20 ℃ resulted in no hybridization signal, while increased in the hybridization temperature, which could promote

the hybridization efficiency, led to irreversible inactivation of EST2. Therefore, without formamide, the three hybridization temperatures 20 ℃, 45 ℃ and 65 ℃ were investigated, and just the latter showed the highest signal intensity and specific signal response (data not presented). Temperature plays a more important role in binding of 16S rRNA to its capture ODNs than the effect of 30% formamide. It accelerates hybridization efficiency and probably also improves hybridization stringency.

As shown by this way, RNA target can be effectively detected at relatively high temperature hybridization conditions, while DNA target hybridization already can be performed simply at room temperature in 5 min. The abundant local secondary structures are responsible for the demanding stringent condition. As it was observed from both solution and solid phase hybridization, the presence of secondary structure in the single DNA strands also slows the DNA hybridization by factors of 20-40 folds (Sekar et al., 2005; Gao et al., 2006). To overcome the secondary structure problem, fragmentation of intact rRNA, increase of hybridization temperature and introduction of helper-ODNs led to substantial improvement of hybridization efficiency.

With the EST2-ODN conjugate reporter, we were able to directly detect approximately 1,000 *E. coli* cells in one ml sample with one electrode. In the past, an electrochemical RNA hybridization assay for detection of the fecal indicator bacterium *E. coli* enabled detection of 10^7 cells in 4 h (Lagier et al., 2005). Another direct detection of 16S rRNA in soil extracts by using oligodeoxynucleotide microarrays allowed detecting approximately 7.5×10^6 *G. chapellei* cells equivalents of RNA (Small et al., 2001). The observed detection limit of 1,000 *E. coli* cells is not surprising, as illustrated in Fig. 3.17, EST2-A34 conjugate has a detection limit of one million molecules. The 1,000 cells contained more than 10 million copies of 16S rRNA which is far above the EST2-ODN detection limits. This detection limit due to the use of esterase reporter is superior to the 10^4 cells/ml previously reported (Elsholz et al., 2006). The improvement can be attributed to the higher sensitivity of EST2 compared to alkaline phosphatase and the less steric hindrance of enzyme-ODN conjugates than that of streptavidin-enzyme.

4.8 Molecular beacon for oligodeoxynucleotide analyte detection

The pathogen identification is of importance in clinical samples or food contamination. However, if the analyte fall out of the defined detection category, most nucleic acids biosensor will inevitable fail to respond. The majority of available nucleic acids detection methods are designed or inherently confined to identify only few bacteria or pathogens (Mitterer et al., 2004; Nebling et al., 2004; Wang et al., 2007) or even only one analyte (Baeumner et al., 2004; Ko and Grant, 2006). For nucleic acids based biosensors, according to scheme of nucleic acid preparation, the identification can be simply classified into detection with or without PCR amplification of analyte. For the scheme requires PCR amplification, the obtaining of target DNA will become impossible if the unknown analyte in testing sample unfit for the designed PCR primers (Mitterer et al., 2004; Nebling et al., 2004). While the detection scheme without PCR amplification, for example, isolation of abundant 16S rRNA target, the method described in Fig. 3.21 is also not possible for a completely unknown analyte, because it requires the analyte to have both flexible capture region and universal detection region. Actually, a universal detection region for all potential pathogens is nearly impossible.

The conception of molecular beacon is promising, as it only requires a short stretch nucleic acids sequence. For those analyte analyses that can be done by directly analyzing the abundant rRNA, a high-density molecular beacon based biosensor equipped with different typical sequence information from known pathogens and will increase the unknown pathogene identification possibility.

A good performing of a molecular beacon biosensor should have a lower background signal and higher molecular beacon reactivity compared to other biosensor designs. However, results of E-Chip based detection of target ODN by means of a molecular beacon array, depicts that there is competition between the stability of stem-loop and conformation switch (Fig. 3.24). The reasons for the poor signal enhancement are likely found in a higher background signal and lower molecular beacon reactivity. In short, the stem structure of molecular beacon should remain stable enough to give low background, while rapidly become unstable upon hybridization with target a DNA sequence. This could be true in a solution-based application, but is difficult to realize in the case of immobilized on solid-surface (Wang et al., 2002; Du et al., 2003).

The target ODN T442 was unable to enhance signal when it is only complementary to the portion of loop part. The reason is still not fully understood.

In this study, the background signal from a blank buffer, in the absence of target, is relatively high. This might be due to the destabilization of stem-loop structure under the applied

conditions. There are four reasons that could contribute to the low stability of immobilized molecular beacon. First, some surface-immobilized molecular beacons are absorbed entirely on the surface, thus destabilizing the molecular beacon stem-and-loop structure. Secondly, there are still some surface effects which destabilize the stem structure of the molecular beacon, especially in the case of hydrophobic biotin label. Thirdly, steric effects caused by high immobilization density retard the formation of the stem structure and lower the quench efficiency (Wang et al., 2002; Yao and Tan, 2004). Finally, the length between the biotin group and the last base is about 15 nm, which makes the biotin functional group flexible even under the shield of the *tert*-mercaptan monolayer.

To further minimize the background and stabilize the stem-loop structure, optimization of the Mg^{2+} concentration, as by the addition of 100 mM Mg^{2+} has been reported to show maximal stem stability (Wang et al., 2002). Effects of the pH on the molecular beacon also seem to be an important factor as well (Yao and Tan, 2004). Larger reporter group maybe will help to reduce background at the cost of lost signal (Bockisch et al., 2005).

Notes

The error bars of results obtained from E-Chip hybridization experiments are relatively large. There are two potential reasons for this. All samples have to be handled manually, and thus there was a reproducibility problem. The other reason could be that the immobilization and hybridization on the electrode surface could produce irreproducibility between different chips (Mehlmann et al., 2005). High density array will help to produce result with low error bar.

5. Summary

Electrical Chip (E-Chip) system offers a fast, sensitive and cost-effective way to detect analyte. To improve its application of nucleic acids detection, a suitable enzyme reporter is expected. Esterase 2 (EST2) from *Alicyclobacillus acidocaldarius* was introduced and mutated to have an accessible cysteine residue at 118th codon. This esterase was purified by a single-step affinity chromatography with trifluoromethyl ketone as a ligand and covalently conjugated to a 5'-amino modified oligodeoxynucleotide. The purified conjugate served as a reporter enzyme for electrochemical detection of nucleic acids.

Being an optimal substrate, p-aminophenylbutyrate exerts maximal signal response to EST2 in E-Chip, as determined by comparison of p-aminophenyl esters with acyl chain length from two to eight carbons. An assay of 15 pM of soluble esterase 2 in 1 ml was obtained exploiting p-aminophenylbutyrate.

E-Chip detection of nucleic acids requires three essential steps: immobilization of thiol-modified capture oligodeoxynucleotides onto electrode, recruiting EST2 to electrode vicinity by means of nucleic acids hybridization, and amperometric determination of p-aminophenol produced by EST2 catalytic hydrolysis of p-aminophenylbutyrate. Generally, EST2 reporter allows a detection of approximately one million molecules/0.6 mm^2 electrode. EST2 covalently attached by an oligodeoxynucleotide significantly increased the ability of mismatch discrimination as compared to the streptavidin conjugated EST2. Moreover, single nucleotide mismatch in analyte could be reliably discriminated in the set-up, as demonstrated by single nucleotide mismatch in a 49-mer oligodeoxynucleotide as well as in a 510-nucleotide ssDNA.

Application of E-Chip to bacterial species identification through 16S rRNA was demonstrated. *Escherichia coli* and *Listeria innocua* were easily identified as judged by signals given by rRNA hybridization with species-specific capture ODNs. This system allows a detection of 10^3 *Escherichia coli* cells.

As a further optimization, a stem-loop structured molecular beacon with 5'-thiol and 3'-biotin modifications was synthesized and tested on the chip using EST2-streptavidin as reporter. The presence of target oligodeoxynucleotides complementary to the whole stem-loop sequence enhanced signal for a moderate 2-fold.

The future work should focus on combination of continuous flow PCR with EST2-oligodeoxynucleotide conjugate reporter to do faster and more automatic disease related DNA analysis, as well as construction of EST2 based biosensor for toxic agents detection.

6. Zusammenfassung

Ein elektrischer Biochip (E-Chip) ermöglicht eine schnelle, sensitive und kostengünstige Detektion von Analyten. Die Anwendung bei Nucleinsäure-Hybridisierungen bedarf aber eines geeigneten Reportersystems. Hierfür wurde Esterase 2 (EST2) von *Alicyclobacillus acidocaldarius* in der vorliegenden Arbeit eingeführt und für die Anwendung mutiert um ein Oberflächen-zugängliches Cystein an Position 118 zu schaffen. Das mutante EST2 Protein konnte durch Ein-Schritt-Affinitätschromatographie mit Trifluoromethylketon als Liganden gereinigt und nach kovalenter Kopplung eines Oligonukleotides an Cys118 als Reporterenzym für die elektrochemische Detektion von Nukleinsäurenhybridisierungen genutzt werden.

Im Vergleich von p-Aminophenylestern mit Kettenlänge des Acylrests von zwei bis acht Kohlenstoffatomen erwies sich p-Aminophenylbutyrat als optimales Substrat, das hohe Signalstärken erzeugte. Es konnten 15 pM/1 ml EST2 nachgewiesen werden.

Der Nachweis von Nucleinsäuren über einen E-Chip bedarf dreier Schritte: Immobilisierung eines Thiol-modifizierten Fänger-Oligonukleotides auf der Gold-Elektrode. Fixierung der für die enzymatische Generierung der elektrochemisch aktiven Spezies benötigten EST2 auf der Elektrode, durch Hybridisierung an die Probensequenz die wiederum an die Fängersequenz bindet. Anschließend erfolgt die amperometrische Bestimmung des durch Enzymkatalyse gebildeten p-Aminophenols aus p-Aminophenolbutyrat.

Allgemein ermöglichte EST2 als Reportergruppe die Detektion von ungefähr einer Million Molekülen je 0.6 mm^2 Elektode. Das EST2-Oligonucleotidekonjugat erhöhte zudem die Detektionsschwelle einer Basenfehlpaarung im Vergleich zu einer häufiger verwendeten, aber unspezifischeren Streptavidin-konjugierten EST2. Zuverlässig wurde eine einzelne Fehlpaarung in einem 49mer wie auch einem 510-Nucleotiden langen DNA Stück nachgewiesen.

Die Anwendbarkeit der in dieser Arbeit entwickelten E-Chip Methodik konnte bei der bakterielle Speziesbestimmung durch Hybridiserung an 16S rRNA-spezifischen Fängern gezeigt werden. *Escherichia coli* und *Listeria innocua* ließen sich einfach durch die Höhe des amperometrischen Signales voneinander unterscheiden. Hierzu reichten bereits 10^3 *Eschericia coli* Zellen aus. Als weitere Optimierung wurde eine Haarnadelschleife als ‚Molecular Beacon' mit einer 5'-Thiol und einer 3'-Biotingruppe synthetisiert und mit EST2-Streptavidin als Reporter getestet. In Gegenwart der zur Haarnadelschleife komplementären Zielsequenz erhöhte das elektrochemische Signal allerdings nur moderat um den Faktor 2.

Zukünftige Arbeiten sollten die Kombination einer kontinuierlichen PCR zur Proben-Amplifikation im Chipsystem mit den EST2-Oligonucleotid-Reportern ermöglichen, um eine schnellere, voll-automatische DNA-Analyse zu ermöglichen. Ebenso wären EST2 basierte Biosensoren gegen toxische Verbindungen denkbar.

7. Acknowledgement

8. References

Abdullah-Sayani, A., Bueno-de-Mesquita, J.M., and Van de Vijver, M.J. 2006. Technology insight: tuning into the genetic orchestra using microarrays - limitations of DNA microarrays in clinical practice. Nat. Clin. Pract.Oncol. 3, 501-516.

Agafonov, D.E., Huang, Y., Grote, M., and Sprinzl, M., 2005a. Efficient suppression of the amber codon in E. coli in vitro translation system. FEBS Lett. 579, 2156-2160.

Agafonov, D.E., Rabe, K.S., Grote, M., Huang, Y., and Sprinzl, M., 2005b. The esterase from Alicyclobacillus acidocaldarius as a reporter enzyme and affinity tag for protein biosynthesis. FEBS Lett. 579, 2082-2086.

Agafonov, D.E., Rabe, K.S., Grote, M., Voertler, C.S., and Sprinzl, M., 2006. C-terminal modifications of a protein by UAG-encoded incorporation of puromycin during in vitro protein synthesis in the absence of release factor 1. Chembiochem. 7, 330-336.

Allen, K.N. and Abeles, R.H., 1989. Inhibition kinetics of acetylcholinesterase with fluoromethyl ketones. Biochemistry 28, 8466-8473.

Allen, S.L., Allen, J.M., and Licht, B.M., 1965. Effects of Triton X-100 upon the activity of some electrophoretically separated acid phosphatases and esterases. J. Histochem. Cytochem. 13, 434-440.

Arpigny, J.L. and Jaeger, K.E., 1999. Bacterial lipolytic enzymes: classification and properties. Biochem. J. 343 Pt 1, 177-183.

Avrameas, S., 1969. Coupling of enzymes to proteins with glutaraldehyde. Use of the conjugates for the detection of antigens and antibodies. Immunochemistry. 6, 43-52.

Baeumner, A.J., Leonard, B., McElwee, J., and Montagna, R.A., 2004. A rapid biosensor for viable B. anthracis spores. Anal. Bioanal. Chem. 380, 15-23.

Baneyx, F., 1999. Recombinant protein expression in Escherichia coli. Curr. Opin. Biotechnol. 10, 411-421.

Batra, R. and Gupta, M.N., 1994. Enhancement of Enzyme-Activity in Aqueous-Organic Solvent Mixtures. Biotechnology Letters 16, 1059-1064.

Bdel-Aal, Y.A. and Hammock, B.D., 1985. Apparent multiple catalytic sites involved in the ester hydrolysis of juvenile hormones by the hemolymph and by an affinity-purified esterase from Manduca sexta Johannson (Lepidoptera: Sphingidae). Arch. Biochem. Biophys. 243, 206-219.

Berg, G., Opelt, K., Zachow, C., Lottmann, J., Gotz, M., Costa, R., and Smalla, K., 2006. The rhizosphere effect on bacteria antagonistic towards the pathogenic fungus Verticillium differs depending on plant species and site. FEMS Microbiol. Ecol. 56, 250-261.

Blow, D.M., 1976. Structure and Mechanism of Chymotrypsin. Accounts of Chemical Research 9, 145-152.

Bockisch, B., Grunwald, T., Spillner, E., and Bredehorst, R., 2005. Immobilized stem-loop structured probes as conformational switches for enzymatic detection of microbial 16S rRNA. Nucleic Acids Res. 33, e101.

Bonnet, G., Tyagi, S., Libchaber, A., and Kramer, F.R., 1999. Thermodynamic basis of the enhanced specificity of structured DNA probes. Proc. Natl. Acad. Sci. U. S. A 96, 6171-6176.

Boon, E.M., Ceres, D.M., Drummond, T.G., Hill, M.G., and Barton, J.K., 2000. Mutation detection by electrocatalysis at DNA-modified electrodes. Nat. Biotechnol. 18, 1096-1100.

Bradford, M.M., 1976. A rapid and sensitive method for the quantitation of microgram quantities of protein utilizing the principle of protein-dye binding. Anal. Biochem. 72, 248-254.

Brady, K., Liang, T.C., and Abeles, R.H., 1989. pH dependence of the inhibition of chymotrypsin by a peptidyl trifluoromethyl ketone. Biochemistry 28, 9066-9070.

Brenner, S., 1988. The molecular evolution of genes and proteins: a tale of two serines. Nature 334, 528-530.

Breslauer, K.J., Frank, R., Blocker, H., and Marky, L.A., 1986. Predicting DNA duplex stability from the base sequence. Proc. Natl. Acad. Sci. U. S. A 83, 3746-3750.

Brodbeck, U., Schweikert, K., Gentinetta, R., and Rottenberg, M., 1979. Fluorinated aldehydes and ketones acting as quasi-substrate inhibitors of acetylcholinesterase. Biochim. Biophys. Acta 567, 357-369.

Butler, L.G., 1979. Enzymes in non-aqueous solvents. Enzyme Microb. Technol. 1, 253-259.

Cammarano, P., Teichner, A., and Londei, P., 1986. Intralineage Heterogeneity of Archaebacterial Ribosomes, Evidence for 2 Physicochemically Distinct Ribosome Classes Within the 3Rd Urkindgom. Systematic and Applied Microbiology 7, 137-146.

Cannon, W.R. and Benkovic, S.J., 1998. Solvation, reorganization energy, and biological catalysis. J. Biol. Chem. 273, 26257-26260.

Caruana, D.J. and Heller, A., 1999. Enzyme-Amplified Amperometric Detection of Hybridization and of a Single Base Pair Mutation in an 18-Base Oligonucleotide on a 7-m-Diameter Microelectrode. J. Am. Chem. Soc. 121, 697-774.

Casey, J. and Davidson, N., 1977. Rates of formation and thermal stabilities of RNA:DNA and DNA:DNA duplexes at high concentrations of formamide. Nucleic Acids Res. 4, 1539-1552.

Chan, V., Graves, D.J., and McKenzie, S.E., 1995. The biophysics of DNA hybridization with immobilized oligonucleotide probes. Biophys. J. 69, 2243-2255.

Chandler, D.P., Newton, G.J., Small, J.A., and Daly, D.S., 2003. Sequence versus structure for the direct detection of 16S rRNA on planar oligonucleotide microarrays. Appl. Environ. Microbiol. 69, 2950-2958.

Chien, F.C., Liu, S.H., Su, H.J., Kao, L.A., Chiou, C.F., Chen, W.Y., and Chen, S.J., 2004. An investigation into the influence of secondary structures on DNA hybridization using surface plasmon resonance biosensing. Chem. Phys. Lett. 397, 429-434.

Chiu, C.H., Tang, P., Chu, C., Hu, S., Bao, Q., Yu, J., Chou, Y.Y., Wang, H.S., and Lee, Y.S., 2005. The genome sequence of Salmonella enterica serovar Choleraesuis, a highly invasive and resistant zoonotic pathogen. Nucleic Acids Res. 33, 1690-1698.

Czajka, J., Bsat, N., Piani, M., Russ, W., Sultana, K., Wiedmann, M., Whitaker, R., and Batt, C.A., 1993. Differentiation of Listeria monocytogenes and Listeria innocua by 16S rRNA genes and intraspecies discrimination of Listeria monocytogenes strains by random amplified polymorphic DNA polymorphisms. Appl. Environ. Microbiol. 59, 304-308.

Dai, H., Meyer, M., Stepaniants, S., Ziman, M., and Stoughton, R., 2002. Use of hybridization kinetics for differentiating specific from non-specific binding to oligonucleotide microarrays. Nucleic Acids Res. 30, e86.

De Simone, G., Galdiero, S., Manco, G., Lang, D., Rossi, M., and Pedone, C., 2000. A snapshot of a transition state analogue of a novel thermophilic esterase belonging to the subfamily of mammalian hormone-sensitive lipase. J. Mol. Biol. 303, 761-771.

De Simone, G., Mandrich, L., Menchise, V., Giordano, V., Febbraio, F., Rossi, M., Pedone, C., and Manco, G., 2004. A substrate-induced switch in the reaction mechanism of a thermophilic esterase: kinetic evidences and structural basis. J. Biol. Chem. 279, 6815-6823.

Demers, L.M., Ostblom, M., Zhang, H., Jang, N.H., Liedberg, B., and Mirkin, C.A., 2002. Thermal desorption behavior and binding properties of DNA bases and nucleosides on gold. J. Am. Chem. Soc. 124, 11248-11249.

Derewenda, Z.S., 1994. Structure and function of lipases. Adv. Protein Chem. 45, 1-52.

Derewenda, Z.S. and Sharp, A.M., 1993. News from the interface: the molecular structures of triacylglyceride lipases. Trends Biochem. Sci. 18, 20-25.

Doll, B., Pleschka, S., Zimmer, G., and Herrler, G., 1993. Surface glycoprotein of influenza C virus: inactivation and restoration of the acetylesterase activity on nitrocellulose. Virus Res. 30, 105-110.

Drummond, T.G., Hill, M.G., and Barton, J.K., 2003. Electrochemical DNA sensors. Nat. Biotechnol 21, 1192-1199.

Du, H., Disney, M.D., Miller, B.L., and Krauss, T.D., 2003. Hybridization-based unquenching of DNA hairpins on au surfaces: prototypical "molecular beacon" biosensors. J. Am. Chem. Soc. 125, 4012-4013.

Ebersole, R.C., Miller, J.A., Moran, J.R., and Ward, M.D., 1990. Spontaneously Formed Functionally Active Avidin Monolayers on Metal-Surfaces - A Strategy for Immobilizing Biological Reagents and Design of Piezoelectric Biosensors. Journal of the American Chemical Society 112, 3239-3241.

Ehresmann, B., Imbault, P., and Weil, J.H., 1973. Spectrophotometric determination of protein concentration in cell extracts containing tRNA's and rRNA's. Anal. Biochem. 54, 454-463.

Elsholz, B., Worl, R., Blohm, L., Albers, J., Feucht, H., Grunwald, T., Jurgen, B., Schweder, T., and Hintsche, R., 2006. Automated detection and quantitation of bacterial RNA by using electrical microarrays. Anal. Chem. 78, 4794-4802.

Fan, C., Plaxco, K.W., and Heeger, A.J., 2003. Electrochemical interrogation of conformational changes as a reagentless method for the sequence-specific detection of DNA. Proc. Natl. Acad. Sci. U. S. A 100, 9134-9137.

Gabig-Ciminska, M., Holmgren, A., Andresen, H., Bundvig, B.K., Wumpelmann, M., Albers, J., Hintsche, R., Breitenstein, A., Neubauer, P., Los, M., Czyz, A., Wegrzyn, G., Silfversparre, G., Jurgen, B., Schweder, T., and Enfors, S.O., 2004. Electric chips for rapid detection and quantification of nucleic acids. Biosens. Bioelectron. 19, 537-546.

Gao, Y., Wolf, L.K., and Georgiadis, R.M., 2006. Secondary structure effects on DNA hybridization kinetics: a solution versus surface comparison. Nucleic Acids Res. 34, 3370-3377.

Gelb, M.H., Svaren, J.P., and Abeles, R.H., 1985. Fluoro ketone inhibitors of hydrolytic enzymes. Biochemistry 24, 1813-1817.

Ghosh, U., Ganessunker, D., Sattigeri, V.J., Carlson, K.E., Mortensen, D.J., Katzenellenbogen, B.S., and Katzenellenbogen, J.A., 2003. Estrogenic diazenes: heterocyclic non-steroidal estrogens of unusual structure with selectivity for estrogen receptor subtypes. Bioorg. Med. Chem. 11, 629-657.

Giordano, B.C., Ferrance, J., Swedberg, S., Huhmer, A.F., and Landers, J.P., 2001. Polymerase chain reaction in polymeric microchips: DNA amplification in less than 240 seconds. Anal. Biochem 291, 124-132.

Gooding, J.J., 2002. Electrochemical DNA hyhridization biosensors. Electroanalysis 14, 1149-1156.

Gyllensten, U.B. and Erlich, H.A., 1988. Generation of single-stranded DNA by the polymerase chain reaction and its application to direct sequencing of the HLA-DQA locus. Proc. Natl. Acad. Sci. U. S. A 85, 7652-7656.

Hagan, M.F. and Chakraborty, A.K., 2004. Hybridization dynamics of surface immobilized DNA. J. Chem. Phys. 120, 4958-4968.

Haki, G.D. and Rakshit, S.K., 2003. Developments in industrially important thermostable enzymes: a review. Bioresour. Technol. 89, 17-34.

Hanzlik, T.N. and Hammock, B.D., 1987. Characterization of affinity-purified juvenile hormone esterase from Trichoplusia ni. J. Biol. Chem. 262, 13584-13591.

Hashimoto, M., Chen, P.C., Mitchell, M.W., Nikitopoulos, D.E., Soper, S.A., and Murphy, M.C., 2004. Rapid PCR in a continuous flow device. Lab Chip. 4, 638-645.

Held, G.A., Grinstein, G., and Tu, Y., 2003. Modeling of DNA microarray data by using physical properties of hybridization. Proc. Natl. Acad. Sci. U. S. A 100, 7575-7580.

Hemila, H., Koivula, T.T., and Palva, I., 1994. Hormone-sensitive lipase is closely related to several bacterial proteins, and distantly related to acetylcholinesterase and lipoprotein lipase: identification of a superfamily of esterases and lipases. Biochim. Biophys. Acta 1210, 249-253.

Higerd, T.B. and Spizizen, J., 1973. Isolation of two acetyl esterases from extracts of Bacillus subtilis. J. Bacteriol. 114, 1184-1192.

Hintsche, R., Albers, J., Bernt, H., and Eder, A.E., 2000. Multiplexing of microelectrode arrays in voltammetric measurements. Electroanalysis 12, 660-665.

Hintsche, R., Elsholz, B., Piechotta, R., Woerl, R., Schabmueller, C.C.J., Albers, J., Dharuman, V., Nebling, E., Hanisch, A., Blohm, L., Hofmann, F., Holzapfl, B., Frey, A., Paulus, C., Schienle, M., and Thewes, R., Fully electrical microarrays. In: Palecek, E., Scheller, F., and Wang, J. (Eds.), Electrochemistry of nucleic acids and proteins, Elsevier B.V., Amsterdam, 2005, pp. 247-279.

Hintsche, R., Gumbrecht, W., and Thewes, R., 2004. http://www.deutscher-zukunftspreis.de/. Deutscher Zukunftspreis - Preis des Bunderspräsidenten für Technik und Innovation.

Holm, C., Kirchgessner, T.G., Svenson, K.L., Lusis, A.J., Belfrage, P., and Schotz, M.C., 1988. Nucleotide sequence of rat adipose hormone sensitive lipase cDNA. Nucleic Acids Res. 16, 9879.

Hotta, Y., Ezaki, S., Atomi, H., and Imanaka, T., 2002. Extremely stable and versatile carboxylesterase from a hyperthermophilic archaeon. Appl Environ. Microbiol. 68, 3925-3931.

Hudson, K.L., 2006. Genetic testing oversight. Science 313, 1853.

Hughes, T.R., Mao, M., Jones, A.R., Burchard, J., Marton, M.J., Shannon, K.W., Lefkowitz, S.M., Ziman, M., Schelter, J.M., Meyer, M.R., Kobayashi, S., Davis, C., Dai, H., He, Y.D., Stephaniants, S.B., Cavet, G., Walker, W.L., West, A., Coffey, E., Shoemaker, D.D., Stoughton, R., Blanchard, A.P., Friend, S.H., and Linsley, P.S., 2001. Expression profiling using microarrays fabricated by an ink-jet oligonucleotide synthesizer. Nat. Biotechnol. 19, 342-347.

Hwang, S., Kim, E., and Kwak, J., 2005. Electrochemical detection of DNA hybridization using biometallization. Anal. Chem. 77, 579-584.

Inoue, H., Nojima, H., and Okayama, H., 1990. High efficiency transformation of Escherichia coli with plasmids. Gene 96, 23-28.

Jaeger, K.E., Dijkstra, B.W., and Reetz, M.T., 1999. Bacterial biocatalysts: molecular biology, three-dimensional structures, and biotechnological applications of lipases. Annu. Rev. Microbiol. 53, 315-351.

Jaeger, K.E. and Reetz, M.T., 1998. Microbial lipases form versatile tools for biotechnology. Trends Biotechnol. 16, 396-403.

Kaabache, T., Barraud, B., Feldmann, G., Bernuau, D., and Lardeux, B., 1995. Direct solution hybridization of guanidine thiocyanate-solubilized cells for quantitation of mRNAs in hepatocytes. Anal. Biochem. 232, 225-230.

Khmelnitsky, Y.L., Mozhaev, V.V., Belova, A.B., Sergeeva, M.V., and Martinek, K., 1991. Denaturation capacity: a new quantitative criterion for selection of organic solvents as reaction media in biocatalysis. Eur. J. Biochem. 198, 31-41.

Kimura-Suda, H., Petrovykh, D.Y., Tarlov, M.J., and Whitman, L.J., 2003. Base-dependent competitive adsorption of single-stranded DNA on gold. J. Am. Chem. Soc. 125, 9014-9015.

Ko, S. and Grant, S.A., 2006. A novel FRET-based optical fiber biosensor for rapid detection of Salmonella typhimurium. Biosens. Bioelectron. 21, 1283-1290.

Kopp, M.U., Mello, A.J., and Manz, A., 1998. Chemical amplification: continuous-flow PCR on a chip. Science 280, 1046-1048.

Kraut, J., 1977. Serine proteases: structure and mechanism of catalysis. Annu. Rev. Biochem. 46, 331-358.

Krejci, E., Duval, N., Chatonnet, A., Vincens, P., and Massoulie, J., 1991. Cholinesterase-like domains in enzymes and structural proteins: functional and evolutionary relationships and identification of a catalytically essential aspartic acid. Proc. Natl. Acad. Sci. U. S. A 88, 6647-6651.

Kricka, L.J. and Wilding, P., 2003. Microchip PCR. Anal. Bioanal. Chem. 377, 820-825.

Kukolka, F. and Niemeyer, C.M., 2004. Synthesis of fluorescent oligonucleotide-EYFP conjugate: Towards supramolecular construction of semisynthetic biomolecular antennae. Org. Biomol. Chem. 2, 2203-2206.

Laemmli, U.K., 1970. Cleavage of structural proteins during the assembly of the head of bacteriophage T4. Nature 227, 680-685.

Lagier, M.J., Scholin, C.A., Fell, J.W., Wang, J., and Goodwin, K.D., 2005. An electrochemical RNA hybridization assay for detection of the fecal indicator bacterium Escherichia coli. Mar. Pollut. Bull. 50, 1251-1261.

Lane, M.J., Paner, T., Kashin, I., Faldasz, B.D., Li, B., Gallo, F.J., and Benight, A.S., 1997. The thermodynamic advantage of DNA oligonucleotide 'stacking hybridization' reactions: energetics of a DNA nick. Nucleic Acids Res. 25, 611-617.

Lane, S., Evermann, J., Loge, F., and Call, D.R., 2004. Amplicon secondary structure prevents target hybridization to oligonucleotide microarrays. Biosens. Bioelectron. 20, 728-735.

Lao, R., Song, S., Wu, H., Wang, L., Zhang, Z., He, L., and Fan, C., 2005. Electrochemical interrogation of DNA monolayers on gold surfaces. Anal. Chem. 77, 6475-6480.

Leberman, R., Antonsson, B., Giovanelli, R., Guariguata, R., Schumann, R., and Wittinghofer, A., 1980. A simplified procedure for the isolation of bacterial polypeptide elongation factor EF-Tu. Anal. Biochem. 104, 29-36.

Levicky, R., Herne, T.M., Tarlov, M.J., and Satija, S.K., 1998. Using self-assembly to control the structure of DNA monolayers on gold: A neutron reflectivity study. Journal of the American Chemical Society 120, 9787-9792.

Levicky, R. and Horgan, A., 2005. Physicochemical perspectives on DNA microarray and biosensor technologies. Trends Biotechnol 23, 143-149.

Liang, R.Q., Li, W., Li, Y., Tan, C.Y., Li, J.X., Jin, Y.X., and Ruan, K.C., 2005. An oligonucleotide microarray for microRNA expression analysis based on labeling RNA with quantum dot and nanogold probe. Nucleic Acids Res. 33, e17.

Liang, T.C. and Abeles, R.H., 1987. Complex of alpha-chymotrypsin and N-acetyl-L-leucyl-L-phenylalanyl trifluoromethyl ketone: structural studies with NMR spectroscopy. Biochemistry 26, 7603-7608.

Liu, R.H., Yang, J., Lenigk, R., Bonanno, J., and Grodzinski, P., 2004. Self-contained, fully integrated biochip for sample preparation, polymerase chain reaction amplification, and DNA microarray detection. Anal. Chem. 76, 1824-1831.

Livache, T., Maillart, E., Lassalle, N., Mailley, P., Corso, B., Guedon, P., Roget, A., and Levy, Y., 2003. Polypyrrole based DNA hybridization assays: study of label free detection processes versus fluorescence on microchips. J. Pharm. Biomed. Anal. 32, 687-696.

Lozano, P., deDiego, T., and Iborra, J.L., 1997. Hydrophobicity and water activity relationships of water-miscible aprotic solvents on kyotorphin synthesis catalyzed by alpha-chymotrypsin. Biotechnology Letters 19, 1005-1009.

Lucarelli, F., Marrazza, G., and Mascini, M., 2005. Enzyme-based impedimetric detection of PCR products using oligonucleotide-modified screen-printed gold electrodes. Biosens. Bioelectron. 20, 2001-2009.

Lucarelli, F., Marrazza, G., Turner, A.P., and Mascini, M., 2004. Carbon and gold electrodes as electrochemical transducers for DNA hybridisation sensors. Biosens. Bioelectron. 19, 515-530.

Maekawa, M., Sudo, K., Dey, D.C., Ishikawa, J., Izumi, M., Kotani, K., and Kanno, T., 1997. Genetic mutations of butyrylcholine esterase identified from phenotypic abnormalities in Japan. Clin. Chem. 43, 924-929.

Manco, G., Adinolfi, E., Pisani, F.M., Carratore, V., and Rossi, M., 1997. Identification of an esterase from Bacillus acidocaldarius with sequence similarity to a hormone sensitive lipase subfamily. Protein and Peptide Letters 4, 375-382.

Manco, G., Adinolfi, E., Pisani, F.M., Ottolina, G., Carrea, G., and Rossi, M., 1998. Overexpression and properties of a new thermophilic and thermostable esterase from Bacillus acidocaldarius with sequence similarity to hormone-sensitive lipase subfamily. Biochem. J. 332 (Pt 1), 203-212.

Manco, G., Giosue, E., D'Auria, S., Herman, P., Carrea, G., and Rossi, M., 2000. Cloning, overexpression, and properties of a new thermophilic and thermostable esterase with sequence similarity to hormone-sensitive lipase subfamily from the archaeon Archaeoglobus fulgidus. Arch. Biochem. Biophys. 373, 182-192.

Marrazza, G., Chiti, G., Mascini, M., and Anichini, M., 2000. Detection of human apolipoprotein E genotypes by DNA electrochemical biosensor coupled with PCR. Clin. Chem. 46, 31-37.

Massiah, M.A., Viragh, C., Reddy, P.M., Kovach, I.M., Johnson, J., Rosenberry, T.L., and Mildvan, A.S., 2001. Short, strong hydrogen bonds at the active site of human acetylcholinesterase: proton NMR studies. Biochemistry 40, 5682-5690.

Mehlmann, M., Townsend, M.B., Stears, R.L., Kuchta, R.D., and Rowlen, K.L., 2005. Optimization of fragmentation conditions for microarray analysis of viral RNA. Anal. Biochem. 347, 316-323.

Millan, K.M. and Mikkelsen, S.R., 1993. Sequence-Selective Biosensor for Dna-Based on Electroactive Hybridization Indicators. Analytical Chemistry 65, 2317-2323.

Millan, K.M., Saraullo, A., and Mikkelsen, S.R., 1994. Voltammetric DNA biosensor for cystic fibrosis based on a modified carbon paste electrode. Anal. Chem. 66, 2943-2948.

Mitterer, G., Huber, M., Leidinger, E., Kirisits, C., Lubitz, W., Mueller, M.W., and Schmidt, W.M., 2004. Microarray-based identification of bacteria in clinical samples by solid-phase PCR amplification of 23S ribosomal DNA sequences. J. Clin. Microbiol. 42, 1048-1057.

Mollet, C., Drancourt, M., and Raoult, D., 1997. rpoB sequence analysis as a novel basis for bacterial identification. Mol. Microbiol. 26, 1005-1011.

Morana, A., Di, P.N., Aurilia, V., Rossi, M., and Cannio, R., 2002. A carboxylesterase from the hyperthermophilic archaeon Sulfolobus solfataricus: cloning of the gene, characterization of the protein. Gene 283, 107-115.

Morrison, L.E. and Stols, L.M., 1993. Sensitive fluorescence-based thermodynamic and kinetic measurements of DNA hybridization in solution. Biochemistry 32, 3095-3104.

Nakamura, T., Sakaeda, T., Takahashi, M., Hashimoto, K., Gemma, N., Moriya, Y., Komoto, C., Nishiguchi, K., Okamura, N., and Okumura, K., 2005. Simultaneous determination of single nucleotide polymorphisms of MDR1 genes by electrochemical DNA chip. Drug Metab Pharmacokinet. 20, 219-225.

Nebling, E., Grunwald, T., Albers, J., Schafer, P., and Hintsche, R., 2004. Electrical detection of viral DNA using ultramicroelectrode arrays. Anal. Chem. 76, 689-696.

Niwa, O., Morita, M., and Tabei, H., 1990. Electrochemical-Behavior of Reversible Redox Species at Interdigitated Array Electrodes with Different Geometries - Consideration of Redox Cycling and Collection Efficiency. Analytical Chemistry 62, 447-452.

Niwa, O., Xu, Y., Halsall, H.B., and Heineman, W.R., 1993. Small-volume voltammetric detection of 4-aminophenol with interdigitated array electrodes and its application to electrochemical enzyme immunoassay. Anal. Chem. 65, 1559-1563.

Okahata, Y., Kawase, M., Niikura, K., Ohtake, F., Furusawa, H., and Ebara, Y., 1998. Kinetic measurements of DNA hybridization on an oligonucleotide-immobilized 27-MHz quartz crystal microbalance. Anal. Chem. 70, 1288-1296.

Olsson, C., Ahrne, S., Pettersson, B., and Molin, G., 2004. DNA based classification of food associated Enterobacteriaceae previously identified by Biolog GN Microplates. Syst. Appl. Microbiol. 27, 219-228.

Ostblom, M., Liedberg, B., Demers, L.M., and Mirkin, C.A., 2005. On the structure and desorption dynamics of DNA bases adsorbed on gold: a temperature-programmed study. J. Phys. Chem. B Condens. Matter Mater. Surf. Interfaces. Biophys. 109, 15150-15160.

Paeschke, M., Dietrich, F., Uhlig, A., and Hintsche, R., 1996. Voltammetric multichannel measurements using silicon fabricated microelectrode arrays. Electroanalysis 8, 891-898.

Paeschke, M., Wollenberger, U., Kohler, C., Lisec, T., Schnakenberg, U., and Hintsche, R., 1995. Properties of Interdigital Electrode Arrays with Different Geometries. Analytica Chimica Acta 305, 126-136.

Palecek, E., 1960. Oscillographic polarography of highly polymerized deoxyribonucleic acid. Nature 188, 656-657.

Palecek, E., Fojta, M., and Jelen, F., 2002. New approaches in the development of DNA sensors: hybridization and electrochemical detection of DNA and RNA at two different surfaces. Bioelectrochemistry. 56, 85-90.

Pariente, F., Hernandez, L., and Lorenzo, E., 1993. 4-Aminophenyl acetate as a substrate for amperometric esterase sensors. Analytica Chimica Acta 273, 399-407.

Park, S.J., Taton, T.A., and Mirkin, C.A., 2002. Array-based electrical detection of DNA with nanoparticle probes. Science 295, 1503-1506.

Patel, D.J., Pardi, A., and Itakura, K., 1982. DNA conformation, dynamics, and interactions in solution. Science 216, 581-590.

Perlette, J. and Tan, W., 2001. Real-time monitoring of intracellular mRNA hybridization inside single living cells. Anal. Chem. 73, 5544-5550.

Peterson, A.W., Heaton, R.J., and Georgiadis, R.M., 2001. The effect of surface probe density on DNA hybridization. Nucleic Acids Res. 29, 5163-5168.

Peterson, A.W., Wolf, L.K., and Georgiadis, R.M., 2002. Hybridization of mismatched or partially matched DNA at surfaces. J. Am. Chem. Soc. 124, 14601-14607.

Piatek, A.S., Telenti, A., Murray, M.R., El-Hajj, H., Jacobs, W.R., Jr., Kramer, F.R., and Alland, D., 2000. Genotypic analysis of Mycobacterium tuberculosis in two distinct populations using molecular beacons: implications for rapid susceptibility testing. Antimicrob. Agents Chemother. 44, 103-110.

Piunno, P.A., Krull, U.J., Hudson, R.H., Damha, M.J., and Cohen, H., 1995. Fiber-optic DNA sensor for fluorometric nucleic acid determination. Anal. Chem. 67, 2635-2643.

Prestwich, G.D., Eng, W.S., Roe, R.M., and Hammock, B.D., 1984. Synthesis and bioassay of isoprenoid 3-alkylthio-1,1,1-trifluoro-2-propanones: potent, selective inhibitors of juvenile hormone esterase. Arch. Biochem. Biophys. 228, 639-645.

Prestwich, G.D. and Hammock, B.D., 1985. Rapid purification of cytosolic epoxide hydrolase from normal and clofibrate-treated animals by affinity chromatography. Proc. Natl. Acad. Sci. U. S. A 82, 1663-1667.

Ram, S. and Ehrenkaufer, R.E., 1984. A General Procedure for Mild and Rapid Reduction of Aliphatic and Aromatic Nitro-Compounds Using Ammonium Formate As A Catalytic Hydrogen Transfer Agent. Tetrahedron Letters 25, 3415-3418.

Rhee, J.K., Ahn, D.G., Kim, Y.G., and Oh, J.W., 2005. New thermophilic and thermostable esterase with sequence similarity to the hormone-sensitive lipase family, cloned from a metagenomic library. Appl. Environ. Microbiol. 71, 817-825.

Ridell, J., Siitonen, A., Paulin, L., Lindroos, O., Korkeala, H., and Albert, M.J., 1995. Characterization of Hafnia alvei by biochemical tests, random amplified polymorphic DNA PCR, and partial sequencing of 16S rRNA gene. J. Clin. Microbiol. 33, 2372-2376.

SantaLucia, J., Jr., 1998. A unified view of polymer, dumbbell, and oligonucleotide DNA nearest-neighbor thermodynamics. Proc. Natl. Acad. Sci. U. S. A 95, 1460-1465.

Schaffer, N.K., Michel, H.O., and Bridges, A.F., 1973. Amino acid sequence in the region of the reactive serine residue of eel acetylcholinesterase. Biochemistry 12, 2946-2950.

Scheuring, S., Mueller, D.J., Ringler, P., Heymann, J.B., and Engel, A., 1999. Imaging streptavidin 2D crystals on biotinylated lipid monolayers at high resolution with the atomic force microscope. J. Microscopy 193, 28-35.

Scott, W.G., Murray, J.B., Arnold, J.R., Stoddard, B.L., and Klug, A., 1996. Capturing the structure of a catalytic RNA intermediate: the hammerhead ribozyme. Science 274, 2065-2069.

Scully, S.P., Joyce, M.E., Abidi, N., and Bolander, M.E., 1990. The use of polymerase chain reaction generated nucleotide sequences as probes for hybridization. Mol. Cell Probes 4, 485-495.

Sekar, M.M., Bloch, W., and St John, P.M., 2005. Comparative study of sequence-dependent hybridization kinetics in solution and on microspheres. Nucleic Acids Res. 33, 366-375.

Service, R.F., 1998. Microchip arrays put DNA on the spot. Science 282, 396-399.

Shiotsuki, T., Bonning, B.C., Hirai, M., Kikuchi, K., and Hammock, B.D., 2000. Characterization and affinity purification of juvenile hormone esterase from Bombyx mori. Biosci. Biotechnol Biochem 64, 1681-1687.

Shiotsuki, T., Huang, T.L., Uematsu, T., Bonning, B.C., Ward, V.K., and Hammock, B.D., 1994. Juvenile hormone esterase purified by affinity chromatography with 8-mercapto-1,1,1-trifluoro-2-octanone as a rationally designed ligand. Protein Expr. Purif. 5, 296-306.

Simons, J.W., Boots, J.W., Kats, M.P., Slotboom, A.J., Egmond, M.R., and Verheij, H.M., 1997. Dissecting the catalytic mechanism of staphylococcal lipases using carbamate substrates: chain length selectivity, interfacial activation, and cofactor dependence. Biochemistry 36, 14539-14550.

Small, J., Call, D.R., Brockman, F.J., Straub, T.M., and Chandler, D.P., 2001. Direct detection of 16S rRNA in soil extracts by using oligonucleotide microarrays. Appl. Environ. Microbiol. 67, 4708-4716.

Sorensen, H.P. and Mortensen, K.K., 2005. Advanced genetic strategies for recombinant protein expression in Escherichia coli. J. Biotechnol. 115, 113-128.

Soukup, G.A. and Breaker, R.R., 1999. Relationship between internucleotide linkage geometry and the stability of RNA. RNA. 5, 1308-1325.

Sproer, C., Reichenbach, H., and Stackebrandt, E., 1999. The correlation between morphological and phylogenetic classification of myxobacteria. Int. J. Syst. Bacteriol. 49 Pt 3, 1255-1262.

Steel, A.B., Herne, T.M., and Tarlov, M.J., 1998. Electrochemical quantitation of DNA immobilized on gold. Anal. Chem. 70, 4670-4677.

Stevens, P.W., Henry, M.R., and Kelso, D.M., 1999. DNA hybridization on microparticles: determining capture-probe density and equilibrium dissociation constants. Nucleic Acids Research 27, 1719-1727.

Sun, C.P., Liao, J.C., Zhang, Y.H., Gau, V., Mastali, M., Babbitt, J.T., Grundfest, W.S., Churchill, B.M., McCabe, E.R., and Haake, D.A., 2005. Rapid, species-specific detection of uropathogen 16S rDNA and rRNA at ambient temperature by dot-blot hybridization and an electrochemical sensor array. Mol. Genet. Metab 84, 90-99.

Sunkara, V., Hong, B.J., and Park, J.W., 2006. Sensitivity enhancement of DNA microarray on nano-scale controlled surface by using a streptavidin-fluorophore conjugate. Biosens. Bioelectron. 22, 1532-1537.

Takahashi, L.H., Radhakrishnan, R., Rosenfield, R.E., Jr., Meyer, E.F., Jr., Trainor, D.A., and Stein, M., 1988. X-ray diffraction analysis of the inhibition of porcine pancreatic elastase by a peptidyl trifluoromethylketone. J. Mol. Biol. 201, 423-428.

Takenaka, S., Yamashita, K., Takagi, M., Uto, Y., and Kondo, H., 2000. DNA sensing on a DNA probe-modified electrode using ferrocenylnaphthalene diimide as the electrochemically active ligand. Analytical Chemistry 72, 1334-1341.

Tan, W., Fang, X., Li, J., and Liu, X., 2000. Molecular beacons: a novel DNA probe for nucleic acid and protein studies. Chemistry 6, 1107-1111.

Tartagni, A., Altomare, R., Guerrieri, R., Fuchs, A., Manaresi, N., Medoro, G., and Thewes, B., 2004. Microelectronic chips for molecular and cell biology. Sensors update 13, 155-200.

Thompson, R.Q., Barone, G.C., III, Halsall, H.B., and Heineman, W.R., 1991. Comparison of methods for following alkaline phosphatase catalysis: spectrophotometric versus amperometric detection. Anal. Biochem. 192, 90-95.

Thorp, H.H., 1998. Cutting out the middleman: DNA biosensors based on electrochemical oxidation. Trends in Biotechnology 16, 117-121.

Tillib, S.V., Strizhkov, B.N., and Mirzabekov, A.D., 2001. Integration of multiple PCR amplifications and DNA mutation analyses by using oligonucleotide microchip. Anal. Biochem 292, 155-160.

Tombelli, S., Mascini, M., Braccini, L., Anichini, M., and Turner, A.P., 2000. Coupling of a DNA piezoelectric biosensor and polymerase chain reaction to detect apolipoprotein E polymorphisms. Biosens. Bioelectron. 15, 363-370.

Tyagi, S. and Kramer, F.R., 1996. Molecular beacons: Probes that fluoresce upon hybridization. Nature Biotechnology 14, 303-308.

Van, N.J. and Chen, L., 1991. The use of oligodeoxynucleotide probes in chaotrope-based hybridization solutions. Nucleic Acids Res. 19, 5143-5151.

Van, T.O., Beijnen, J.H., Verweij, J., Scherrenburg, E.J., Nooijen, W.J., and Sparreboom, A., 1999. Rapid esterase-sensitive breakdown of polysorbate 80 and its impact on the plasma pharmacokinetics of docetaxel and metabolites in mice. Clin. Cancer Res. 5, 2918-2924.

Vet, J.A., Majithia, A.R., Marras, S.A., Tyagi, S., Dube, S., Poiesz, B.J., and Kramer, F.R., 1999. Multiplex detection of four pathogenic retroviruses using molecular beacons. Proc. Natl. Acad. Sci. U. S. A 96, 6394-6399.

Wagaman, P.C., Spence, H.A., and O'Callaghan, R.J., 1989. Detection of influenza C virus by using an in situ esterase assay. J. Clin. Microbiol. 27, 832-836.

Wang, D., Zhu, L., Jiang, D., Ma, X., Zhou, Y., and Cheng, J., 2004. Direct detection of 16S rRNA using oligonucleotide microarrays assisted by base stacking hybridization and tyramide signal amplification. J. Biochem Biophys. Methods 59, 109-120.

Wang, G.Y., Michailides, T.J., Hammock, B.D., Lee, Y.M., and Bostock, R.M., 2000. Affinity Purification and Characterization of a Cutinase from the Fungal Plant Pathogen Mo*nilinia fructicola (W*int.) Honey. Arch. Biochem. Biophys. 382, 31-38.

Wang, H., Chen, J., Zhu, L., Shadpour, H., Hupert, M.L., and Soper, S.A., 2006. Continuous flow thermal cycler microchip for DNA cycle sequencing. Anal. Chem. 78, 6223-6231.

Wang, H., Li, J., Liu, H., Liu, Q., Mei, Q., Wang, Y., Zhu, J., He, N., and Lu, Z., 2002. Label-free hybridization detection of a single nucleotide mismatch by immobilization of molecular beacons on an agarose film. Nucleic Acids Res. 30, e61.

Wang, J., 2000. From DNA biosensors to gene chips. Nucleic Acids Res. 28, 3011-3016.

Wang, J., Electrochemical nucleic acid biosensors. In: Palecek, E., Scheller, F., and Wang, J. (Eds.), Electrochemistry of nucleic acids and proteins, Elsevier B.V., Amsterdam, 2005, pp. 175-194.

Wang, J., Cai, X.H., Tian, B.M., and Shiraishi, H., 1996. Microfabricated thick-film electrochemical sensor for nucleic acid determination. Analyst 121, 965-969.

Wang, Y., Stanzel, M., Gumbrecht, W., Humenik, M., and Sprinzl, M., 2007. Esterase 2-oligodeoxynucleotide conjugates as sensitive reporter for electrochemical detection of nucleic acid hybridization. Biosens. Bioelectron. 22, 1798-1806.

Watterson, J.H., Piunno, P.A.E., Wust, C.C., and Krull, U.J., 2000. Effects of oligonucleotide immobilization density on selectivity of quantitative transduction of hybridization of immobilized DNA. Langmuir 16, 4984-4992.

Wei, Y., Contreras, J.A., Sheffield, P., Osterlund, T., Derewenda, U., Kneusel, R.E., Matern, U., Holm, C., and Derewenda, Z.S., 1999. Crystal structure of brefeldin A esterase, a bacterial homolog of the mammalian hormone-sensitive lipase. Nat. Struct. Biol. 6, 340-345.

Woese, C.R., 1987. Bacterial evolution. Microbiol. Rev. 51, 221-271.

Woese, C.R., Magrum, L.J., Gupta, R., Siegel, R.B., Stahl, D.A., Kop, J., Crawford, N., Brosius, J., Gutell, R., Hogan, J.J., and Noller, H.F., 1980. Secondary structure model for bacterial 16S ribosomal RNA: phylogenetic, enzymatic and chemical evidence. Nucleic Acids Res. 8, 2275-2293.

Wolfenden, R., Ridgway, C., and Young, G., 1998. Spontaneous hydrolysis of ionized phosphate monoesters and diesters and the proficiencies of phosphatases and phosphodiesterases as catalysts. Journal of the American Chemical Society 120, 833-834.

Wu, P., Nakano, S., and Sugimoto, N., 2002. Temperature dependence of thermodynamic properties for DNA/DNA and RNA/DNA duplex formation. Eur. J. Biochem. 269, 2821-2830.

Yao, G. and Tan, W., 2004. Molecular-beacon-based array for sensitive DNA analysis. Anal. Biochem. 331, 216-223.

Zhang, Y., Kim, H.H., and Heller, A., 2003. Enzyme-amplified amperometric detection of 3000 copies of DNA in a 10-microL droplet at 0.5 fM concentration. Anal. Chem. 75, 3267-3269.

Zhang, Y., Kim, H.H., Mano, N., Dequaire, M., and Heller, A., 2002. Simple enzyme-amplified amperometric detection of a 38-base oligonucleotide at 20 pmol L^{-1} concentration in a 30- microL droplet. Anal. Bioanal. Chem. 374, 1050-1055.

Zhang, Y., Pothukuchy, A., Shin, W., Kim, Y., and Heller, A., 2004. Detection of approximately 10(3) copies of DNA by an electrochemical enzyme-amplified sandwich assay with ambient O(2) as the substrate. Anal. Chem. 76, 4093-4097.

Zhou, X.C., Huang, L.Q., and Li, S.F., 2001. Microgravimetric DNA sensor based on quartz crystal microbalance: comparison of oligonucleotide immobilization methods and the application in genetic diagnosis. Biosens. Bioelectron. 16, 85-95.

Zimmer, G., Reuter, G., and Schauer, R., 1992. Use of influenza C virus for detection of 9-O-acetylated sialic acids on immobilized glycoconjugates by esterase activity. Eur. J. Biochem. 204, 209-215.

Zor, T. and Selinger, Z., 1996. Linearization of the Bradford protein assay increases its sensitivity: theoretical and experimental studies. Anal. Biochem. 236, 302-308.

9. Erklärung

Hiermit erkläre ich, daß ich die Arbeit selbständig verfaßt und keine anderen als die angegebenen Quellen und Hilfsmittel benutzt habe.

Ferner erkläre ich, daß ich anderweitig mit oder ohne Erfolg nicht versucht habe, eine Dissertation oder mich der Doktorprüfung zu unterziehen.

Bayreuth, March 6, 2007

Yiran Wang

10. Curriculum Vitae

Yiran Wang

Department of Biochemistry, University Bayreuth, Universitätsstrasse 30, D-95440 Bayreuth

Phone: (0921) 55 4353   E-mail: yiran.wang@uni-bayreuth.de; wang.yiran@gmail.com

Education

PhD in **Biochemistry**, University Bayreuth, Bayreuth, Germany   2003 – 2007

MS in **Biochemistry and Molecular Biology,** Fudan University, Shanghai, China   2000 – 2003

BE in **Biochemical Engineering,** Tianjin University, Tianjin, China   1994 – 1998

Work experience

Fudan Biological Engineering Company, Shanghai, China   2001 - 2003

Hangzhou East China Pharmaceutical Group Co. Ltd, Hangzhou, Zhejiang, China   1998 - 1999

Publications

1. **Wang, Y.**, Stanzel, M., Gumbrecht, W., Humenik, M., Sprinzl, M., Esterase 2-oligodeoxynucleotide conjugates as sensitive reporter for electrochemical detection of nucleic acid hybridization, 2006, Biosens. Bioelectron. 22, 1798-1806..

2. Humenik, M., Huang, Y., **Wang, Y.**, Sprinzl, M., C-Terminal Incorporation of Bio-Orthogonal Azide Group into the Protein and Preparation of Protein-Oligodeoxynucleotide Conjugates via Cu^I-Catalyzed Cycloaddition, submitted.

3. **Wang, Y.**, Hong, J., Ming, M., Ding, J., Li, Q., Huang, W., Rapid cloning of an archaerhodopsin gene from Halobacterium species xz515 by ligation-mediated PCR amplification, 2003, Journal of Fudan University, 42, 576-583.

4. Deng, Y., Wang, Z., Ying, K., Gu, S., Ji, C, Huang, Y., Gu, X., **Wang, Y.**, Xu, Y., Li, Y., Xie, Y., Mao, Y., NADPH-dependent GMP reductase isoenzyme of human (GMPR2)-expression, purification and kinetic properties, 2002, Int J Biochem Cell Biol 34, 1035-1050.